工業化学　轟 眞市

論文題目:

**STUDIES ON LOCAL STRUCTURE AROUND RARE EARTH IONS IN GLASSES**
**(ガラス中の希土類イオンの局所構造に関する研究)**

# 緒言

本論文は，希土類イオンを含有する酸化物ガラスおよびフッ化物ガラスを作成しその局所構造について研究したものである．

ガラスはレンズやプリズムのような，光を吸収することの無い受動的な素子として広く用いられてきた．近年，光情報処理の観点から，光と積極的に相互作用するような動能的な素子が求められている．希土類含有ガラスは，希土類とガラスの両方の長所を兼ね備えた材料として注目されている．ガラス材料は，光活性イオンをとり囲む構造の微視的不規則性のために，発光及び吸収スペクトルの不均一な広がりが大きいという短所があるが，高い成型性による大型化，ファイバー化によってその短所が補われたり，ホールバーニングのような不均一な広がりそのものを活用する素子が考案されている．

このような素子の開発のためには，ガラス中の希土類イオンの局所構造に関する知見を得ることが重要である．現在までの研究では，希土類イオンの第一配位圏に関する情報しか選られていない．

本研究では，種々の酸化物ガラス中にドープした $Eu^{3+}$ イオンのまわりの局所構造を，分光学的手法を用いて評価し，希土類イオンの第二配位圏内に関する情報を得ることにより，ガラス網目構造の局所的な変化について考察した．またこれに基づいて，スペクトルの不均一な線幅の組成依存性を，定性的に説明した．また，局所振動状態，およびスペクトルの不均一な広がりが光機能特性を支配する現象である，アップコンバージョン蛍光およびホールバーニングを取り上げ，フッ化物ガラス中の希土類イオンの局所構造との関係を研究した．

# 目次



# 総括

本論文では，無機ガラス系，特に酸化物ガラスにドープした希土類イオンの局所構造を，蛍光，およびメスバウアー分光学的測定により系統的に研究した．実験結果に基づき，希土類イオンのまわりのガラス網目構造を明らかにし，またスペクトルの不均一な線幅が，希土類をとり囲むガラス網目の柔軟性に密接にかかわっていることを示した．さらに，希土類イオンの局所構造に影響される現象として，希土類含有フッ化物ガラスのアップコンバージョンとホールバーニングについて研究した．

第一章では，種々の酸化物ガラス ($Na_2O$ との 2 成分系) 中の $Eu^{3+}$ イオンのまわりの局所振動状態を調べた．励起スペクトル中に現れるフォノンサイドバンド (PSB) から， $Eu^{3+}$ イオンのエネルギー緩和に用いられるフォノンのエネルギーを見積もり， $Eu^{3+}$ イオンの第二配位圏の構造に関する知見を得た．$Eu^{3+}$ イオンのまわりの構造単位の振動エネルギーは，質量の大きい希土類イオンの局所振動への寄与のために，相当するガラ

スマトリックス中の構造単位の振動エネルギーよりも小さくなることがわかった．ケイ酸塩ガラスでは， $Q^n$ 構造単位 ($n$=3, 2, 1; $n$ は $SiO_{4/2}$ 四面体中の架橋酸素 (BO) の数) の振動の寄与を見積もることができた．この結果から，低アルカリ組成において $Eu^{3+}$ イオンに非架橋酸素 (NBO) が優先配位する傾向が認められた．これは， $Eu^{3+}$ イオンのもつ正電荷を中和するための局所的な構造変化が原因と考えらる．また，ゲルマン酸塩ガラスやアルミノケイ酸塩ガラスにおいても，NBO の寄与が大きく，負電荷を有する $GeO_{6/2}^{2-}$ 八面体や $AlO_{n/2}^{(n-3)-}$ 多面体に相当するピークは PSB に現れなかった．これは $Eu^{3+}$ イオンの正電荷の補償にこれらの基が関与しておらず，$Eu^{3+}$ との電気的相互作用が NBO より小さいためと考えられる．すなわち，$Eu^{3+}$ イオンは網目修飾カチオンとして NBO を生成させており，$GeO_{6/2}^{2-}$ や $AlO_{n/2}^{(n-3)-}$ のようなマクロアニオンの生成に関与していないと思われる．

第二章では，種々の酸化物ガラス中の $Eu^{3+}$ サイトの局所的塩基度を調べた．$^{151}Eu$ のメスバウアースペクトルを測定し，そのアイソマーシフトの値から $Eu^{3+}$ サイトの局所的塩基度，すなわち配位子の電子供与性を評価し，理論的光学的塩基度との相関から局所的構造変化を見積もった．ホウ酸塩ガラス及びゲルマン酸塩ガラスにおいては， 局所的塩基度が網目形成カチオンの配位数変化に対応して変化した．ケイ酸塩ガラス及びアミノケイ酸塩ガラスでは，局所的塩基度が光学的塩基度との良い相関性が見られなかった．これは，$Eu^{3+}$ イオンが NBO に優先配位されているためと思われる．ケイ酸塩ガラス中の $Eu^{3+}$ イオンは一定量の NBO–Na 対に配位されており，その量は Na 含有量には依存しないが，Al 含有量の増加とともに減少すると考えられる．

第三章では，酸化物ガラス中の $Eu^{3+}$ イオンのスペクトルの不均一な線幅, $\Delta\nu_{IH}$, の起源を，前章で明らかになった局所構造に基づいて考察した．ケイ酸塩ガラスの $\Delta\nu_{IH}$ の値は，$Na_2O$ 含有量の減少につれて増大した．サイト選択スペクトルの測定からもとめた，$^7F_1$ 準位のシュタルク分裂の組成依存性から，アルカリ含有量の減少とともに低配位数の $Eu^{3+}$ サイトが多くなることが示された．これらのことより，不均一な線幅は，ガラス網目の柔軟性，すなわち $Eu^{3+}$ のまわりの酸素多面体間の結合数及び NBO 濃度に関係すると考えられる．すなわち，柔軟性の低下が，相対的に不安定な低配位数サイトを増やし，不均一幅が増大する．この仮定は $GeO_{6/2}^{2-}$, $AlO_{n/2}^{(n-3)-}$, $BO_{4/2}^{-}$ のようなマクロアニオンを含む他の酸化物ガラスにもあてはまる．マクロアニオンの生成により，NBOが消費され，

酸素多面体間の結合点が増えるので，ガラス網目の柔軟性は低下し，不均一な線幅が増大する．

第四章では，二重結合酸素 (DBO) を含むガラス系である，リン酸塩ガラス中の $Eu^{3+}$ イオンのスペクトルの不均一な線幅について研究した．DBO を有する試料の $\Delta\nu_{IH}$ は，本研究で取り扱ったすべての酸化物ガラスの中で最少の値を示した．PSB から見積 もられる $Eu^{3+}$ に配位した DBO 量の減少とともに，$\Delta\nu_{IH}$ は増加した．さらに，ホウリン酸塩ガラス中の $Eu^{3+}$ イオンは，局所的電荷補償のために，$PO_{4/2}$ 四面体中の NBO に優先配位されていることがわかった．

結論として，$Eu^{3+}$ の蛍光の線幅は，ガラス網目構造の局所的柔軟性，すなわち，$Eu^{3+}$ イオンのまわりの，NBO 濃度及び酸素多面体間の結合点数に依存することがわかった．

第五章では，フッ化物ガラス中の希土類イオンの局所振動状態を調べ，$Er^{3+}$ イオンのアップコンバージョンへの影響について考察した．$Er^{3+}$ イオンの 800nm 励起による 550nm のアップコンバージョン蛍光強度は，$\hbar\omega$ の減少と共に増加した．また，$\hbar\omega$ は IR スペクトルで求められたガラスマトリックスの最大振動数より小さくなることがわかった．これは，PSB に反映されている振動は希土類イオンを含んだ有効質量の大きい振動系であるためと考えられた．これを実証するために，質点モデルによる連成振動計算，及び分子動力学計算によって合成したフッ化物ガラスの振動状態の解析を行い，局所振動のみかけの弱化を説明した．

第六章では， $Sm^{2+}$ 含有フッ化物ガラスを作製し，室温においてホールバーニング (HB) を観察した．そのメカニズムについて考察するとともに，PSB 強度がホールの線幅と関係するために，HB 材料選択のパラメータとして重要であることを指摘した．

# STUDIES ON LOCAL STRUCTURE AROUND RARE EARTH IONS IN GLASSES

SHIN-ICHI TODOROKI

1993

# Contents

# Introduction

Glass has been used as an optical material for lenses and prisms because of their high quality of optical isotropy and transmittance, and easy preparation. These glass products are classified as a passive optical device through which the input light is transmitted without absorption or changing its nature. On the contrary, an active optical device is the one in which the input light is absorbed and changed to emit light with different frequency. Recently, there is a growing need for an active device for ultra fast and enormously large data processing by light. Among various kinds of materials, intense interest is being given to rare-earth-doped glasses because they inherit advantages of both glass and rare earth (RE) ions. A discovery of stable fluorozirconate glasses has accelerated the research activities in this field[1–5]. Now, considerable works are being carried out on laser glasses[6–9] and upconversion fluorescent substance[10, 11].

Glass is isotropic on a scale of the wavelength of visible light (1–0.1 $\mu$m) because of its random structure on an atomic scale ($\sim$0.1 nm). This structural inhomogeneity makes the thermal conductivity lower than that of crystal as a consequence of large phonon scattering. This is one of the disadvantages for using glass as an active device in which the photon energy of light is absorbed. Moreover, when optically active ions are incorporated, the structural inhomogeneity of glass broadens their spectral lines. In actual cases, these disadvantages may be compensated by the advantage of glass, i.e., easy productivity of large shape glass rods or long fibers. Therefore, fiber lasers[8] and high-power pulsed glass lasers for nuclear fusion[6] have been successfully produced.

More recently, new types of glass devices are being proposed which utilize the inhomogeneous nature of glass rather than avoiding it. Photo-induced refractive index gratings[12–15] may be used for the purpose of holographic information storage and retrieval. This is realized by laser-induced redistribution of RE ions in the two level system of glass. Photo-chemical hole burning in glass hosts[16, 17] is expected to be advantageous because of large spectral inhomogeneous broadening.

In order to develop these new optical devices, it is important to know the local structure around optically active ions. Cations in oxide glass network are usually classified into three categories according to the single bond strength of M–O[18]. RE ions belong to the group of *network-modifiers* which breakup or depolymerize the glass-forming network[19, 20]. In the similar classification, Baldwin and Mackenzie classified RE ions in fluoride glasses as *intermediates*[5, 21] which are not able to form glasses by themselves but are able to participate in forming a continuous glass network with network-formers. In fact, RE ions are known to stabilize fluoride glasses and so to enlarge glass forming region[4].

From the view point of optical or laser spectroscopy, there exist a considerable number of investigations about the local environment of RE ions in glass[22–25]. Further, the coordination number of RE ions was directly determined on several oxide glasses by using X-ray absorption spectroscopy (XAS)[26–28]. These studies, however, are restricted to the the first coordination sphere around RE ions, i.e., within $LnO_n$ (or $LnF_n$, Ln=RE ion) polyhedra, and only few cases deal with the relation between RE ions and $MO_n$ polyhedra, i.e., mid-range order of glass structure. Furthermore, the relation between spectral inhomogeneous broadening and glass structure has not been mentioned, although inhomogeneity is a distinctive feature of glass and affects the coordination state of RE ions.

In the present study, the local structure around RE ions is investigated systematically on several glasses by some spectroscopic methods. On the basis of the experimental results, it is demonstrated that the structural modification of glass network around RE ions occur. Further, it is shown that the spectral inhomogeneous broadening is closely related to the local flexibility of glass network surrounding RE ions.

The first four chapters deal with $Eu^{3+}$-doped oxide glasses, where the relation between spectral inhomogeneous broadening and glass structure is discussed. The last two chapters deal with RE-doped fluoride glasses whose optical properties are affected by the local vibrational states or spectral inhomogeneous broadening.

In Chapter 1, the difference in vibrational mode between the glass matrix and the neighborhood of RE ions in several oxide glasses (silicate, germanate, and aluminosilicate glasses) is discussed based on the measurement of the phonon sideband of $Eu^{3+}$. It is shown that europium has an affinity for non-bridging oxygen.

In Chapter 2, the population of oxygen species in the first coordination sphere of $Eu^{3+}$ is estimated on the basis of the Mössbauer effect of $^{151}Eu$ in several oxide glasses (silicate, germanate, aluminosilicate, and borate glasses). From the compositional dependence of the value of isomer shift, it is shown that some structural modifications around $Eu^{3+}$ ions occur for silicate and aluminosilicate glasses.

In Chapter 3, the origin of the inhomogeneous broadening of $Eu^{3+}$ fluorescence for oxide glasses (silicate, germanate, aluminosilicate, and borate glasses) is discussed on the basis of the results in the foregoing chapters and of the site-selective fluorescence spectra within the inhomogeneously broadened site-distribution. It is explained in terms of the flexibility of the glass network around $Eu^{3+}$.

In Chapter 4, the local structure around $Eu^{3+}$ ions in phosphate glasses is investigated by measuring the phonon sideband and the origin of the inhomogeneous broadening of $Eu^{3+}$ fluorescence for this system is discussed. It is shown that the small inhomogeneous linewidth is due to the coordination of doubly bonded oxygens.

In Chapter 5, the upconversion fluorescence of $Er^{3+}$ in fluoride glasses is measured and the local vibrational state, which is related with the upconversion efficiency, is discussed based on phonon sideband measurement and molecular dynamic simulation.

In Chapter 6, spectral hole burning for $Sm^{2+}$-doped fluoride glasses is observed and the burning mechanism and the relation with the local vibration is discussed. It was pointed out that the hole width is related with the electron-phonon coupling strength.

Finally in Summary, the whole results and discussions in this thesis are summarized.

# Chapter 1

# Local vibrational state around $Eu^{3+}$ ions in several oxide glasses

## 1.1 Introduction

Vibronic spectroscopy (IR and Raman) is a standard technique to investigate glass structure and numerous studies have been published[29–39]. For oxide glasses, these methods are suitable for determining the coordination states of network forming cations such as Si, Ge, B, and Al, but it is hard to extract some information for modifier cations or minority components. Some workers overcome this problem by sophisticating the methods. Nelson *et al.*[35] measured Raman difference spectroscopy of $Sc^{3+}$-doped and undoped silicate glasses and investigated the solvation effect of the impurity ions. Durville *et al.*[40] measured resonant Raman spectroscopy of $Eu^{3+}$-doped oxide glasses and estimated the vibrational mode coupled to the $Eu^{3+}$ ions.

Phonon sideband (PSB, or vibronic sideband) measurement is another and simple method for probing the local vibrational state. Unlike the above two methods, the phonon energy obtained is used only by the multi-phonon relaxation of the excited states of RE ions. Therefore, this information is important for fluorescence properties in estimating nonradiative loss. Some works have been reported[41–45] but there are few works focusing the structural difference between glass matrix and RE-sites[45].

As pointed out in Introduction, RE ions in oxide glasses act as *network-modifiers*[18]. The interaction between RE ions and network forming cations ($MO_n$ polyhedra) can be made more clear by comparing various types of network forming cations. Therefore, four typical glass systems were chosen as the samples in the present study (and also in Chapter 2 and 3); silicate, germanate, aluminosilicate, and borate glasses. The structures of these glasses have been extensively investigated and some simple models have bees proposed[1, 18].

The silicate glass network is relatively simpler than those of other oxide glasses, consisting of five kinds of $SiO_{4/2}$ tetrahedra that differ only in the number of bridging oxygens (BO) and are denoted as $Q^n$ ($n = 4, 3, \cdots, 0$ : the number of BOs). As the alkali content increases, the relative quantities of them change and the amount of NBOs increases as follows,

$$-\overset{|}{\underset{|}{\mathrm{Si}}}-\mathrm{O}-\overset{|}{\underset{|}{\mathrm{Si}}}- \quad + \quad \mathrm{Na_2O} \quad \longrightarrow \quad 2\left(-\overset{|}{\underset{|}{\mathrm{Si}}}-\mathrm{O}^{\ominus}\mathrm{Na}^{+}\right), \tag{1.1}$$

and the coordination state of silicon remains tetrahedral. On the other hand, borate and germanate glasses are known to be more complicated, because the network forming cations change their coordination number with alkali content. In the low-alkali compositions, $Na_2O$ acts to form $BO_{4/2}$ tetrahedra or $GeO_{6/2}$ octahedra (Eqs. 1.2 and 1.4) rather than breaking the glass network and forming NBOs ($^{\ominus}O-BO_{2/2}$ rectangles or $^{\ominus}O-GeO_{3/2}$ tetrahedra, Eqs. 1.3 and 1.5).

$$\begin{array}{l} \diagdown \\ \quad \phi \\ \diagdown \\ \quad \mathrm{B}-\phi- \\ \diagup \\ \quad \phi \\ \diagup \end{array} \quad + \quad \frac{1}{2}\mathrm{Na_2O} \quad \longrightarrow \quad \begin{array}{c} \\ \quad \mathrm{O} \\ \quad | \\ -\phi-\mathrm{B}^{\ominus}-\phi- \\ \quad | \quad \mathrm{Na}^{+} \\ \quad \mathrm{O} \\ \quad | \end{array} \tag{1.2}$$

$$\begin{array}{l} \diagdown \\ \quad \phi \\ \diagdown \\ \quad \mathrm{B}-\phi- \\ \diagup \\ \quad \phi \\ \diagup \end{array} \quad + \quad \frac{1}{2}\mathrm{Na_2O} \quad \longrightarrow \quad \begin{array}{l} \diagdown \\ \quad \phi \\ \diagdown \\ \quad \mathrm{B}-\mathrm{O}^{\ominus}\mathrm{Na}^{+} \\ \diagup \\ \quad \phi \\ \diagup \end{array} \tag{1.3}$$

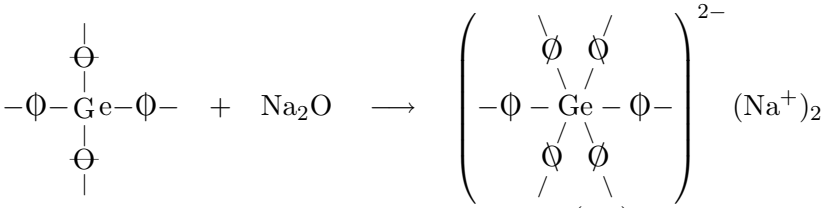

(1.4)

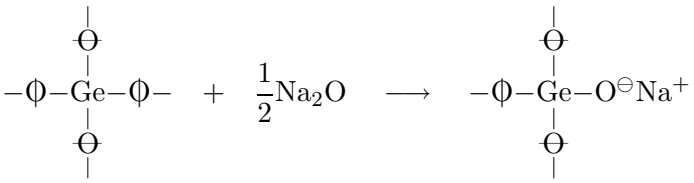

(1.5)

For aluminosilicate glasses, the NBO concentration decreases with increasing Al content to form $AlO_n$ polyhedra in such a way as Eqs. 1.6 and 1.7.

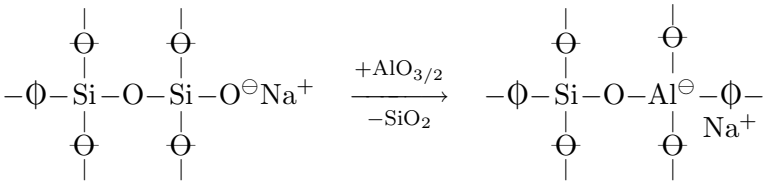

(1.6)

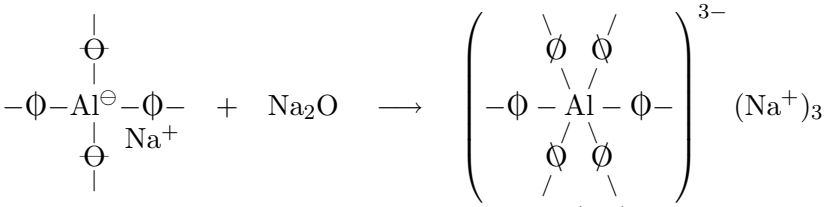

(1.7)

Tanabe and Todoroki have measured the PSB for $Eu^{3+}$-doped borate glasses[45] and concluded that $Eu^{3+}$ ions are coupled with some $B-O^{\ominus}$ bonds even in the alkali-poor compositions where the concentration of NBOs in the glass matrix is low. This suggests the local modification of glass network around $Eu^{3+}$ ions. In the present study, the local structure around $Eu^{3+}$ ions in other oxide glasses, namely, silicate, germanate, and aluminosilicate glasses were investigated to obtain further and general information about the local structure around $Eu^{3+}$ ions in oxide glass matrix.

## 1.2 Theory

PSB appears in the excitation and emission spectra as the result of a coupling of the $4f$ electrons to the lattice vibrations. Figure 1.1 shows the excitation spectra of $Eu^{3+}$ in several oxide glasses obtained by monitoring the $^5D_0 \rightarrow ^7F_2$ emission at 612 nm as a fixed wavelength. Smaller peaks in the higher energy side of the $^5D_2 \leftarrow ^7F_0$ transition were assigned to PSB. The appearance of these small peaks were due to the excitation by incident light coupled with an excess energy of the vibrational mode around RE ions as well as their electronic state (see Fig. 1.2). In general, the probability of multiphonon excitation is much smaller than that for one phonon excitation[46] (see Eqs. 5.1–5.3 [p.36]) and the electron-phonon coupling strength for RE ions is weak because $4f$-electrons are shielded by outer shells($5s$ and $5p$)[47]. Therefore, the energy gap between PSB and pure electric transition (PET) corresponds to one phonon energy, $\hbar\omega$, due to the lattice vibration around $Eu^{3+}$ ions.

PSB is observable for other RE ions such as $Gd^{3+}$[43] and $Tb^{3+}$[48]. $Eu^{3+}$ is, however, the most suitable element among RE ions for measuring PSB because of its simple electronic level structure. Therefore, PSB can be observed also for other transitions of $Eu^{3+}$ such as $^5D_1$,$^5D_0 \leftarrow ^7F_0$. Although these vibronic transitions are against the selection rule demonstrated by Stavola *et al.*[49], a weak PSB is observable because of a $J$-mixing effect, i.e., the mixture of the $^7F_2$ into the $^7F_0$ state[50].

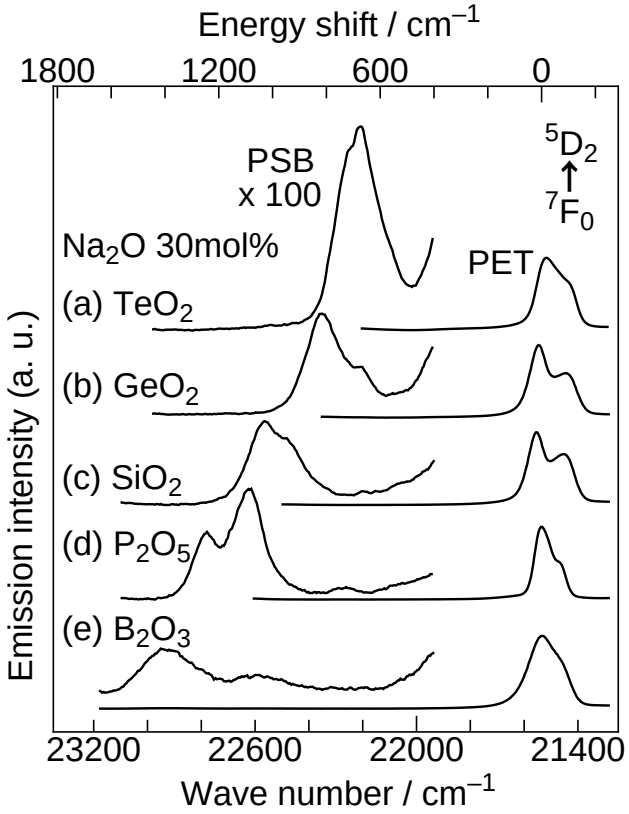


**Fig. 1.1.** *Excitation spectra of $^5D_0 \rightarrow ^7F_2$ emission of $Eu^{3+}$ doped in $70M_xO_y{\cdot}30Na_2O$ glasses at room temperature. Phonon sideband (PSB) associated with the $^5D_2 \leftarrow ^7F_0$ transition appears at higher energy side. The energy gap between PSB and pure electronic transition (PET) corresponds to phonon energy, $\hbar\omega$, due to the lattice vibration around $Eu^{3+}$ ions.*

## 1.3 Experimental

The glass samples employed in this study are listed in Table 1.1. In the present thesis, the denotation of the sample composition is unified to use $MO_n$ instead of $M_mO_n$, such as $60SiO_2{\cdot}40NaO_{1/2}$, $70BO_{3/2}{\cdot}30NaO_{1/2}$, etc... For convenience, simpler notations such as Si25Na, B30Na, etc... are used to represent the glass composition, as shown in Table 1.1. For the aluminosilicate system, $Si^{4+}$ ions are replaced by $Al^{3+}$ ions with constant [Na]/([Si]+[Al]) ratio.

All the glasses were prepared from reagent grade $SiO_2$, $GeO_2$, $Al_2O_3$, $B_2O_3$, $Na_2CO_3$, and $Eu_2O_3$ by mixing and melting the batches in platinum

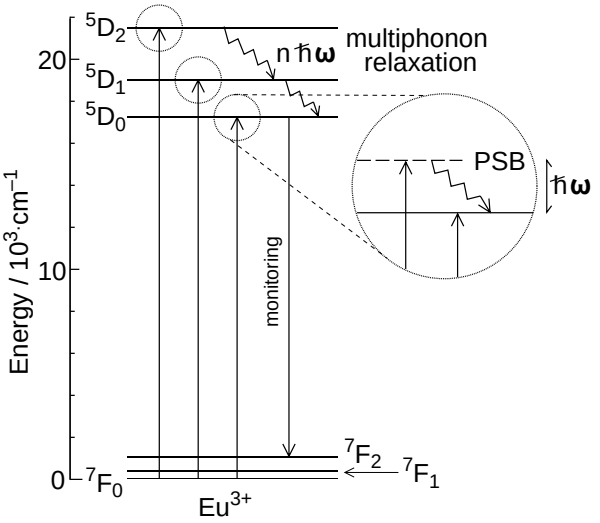


**Fig. 1.2.** *A schematic diagram of phonon sideband process.*

**Table 1.1.** *Composition of the glasses used in this study (mol%). Each sample contains 1 mol% (borate) or 2 mol% (others) of $EuO_{3/2}$.*

(a) silicate glasses

| $SiO_2$ | $NaO_{1/2}$ | $\frac{Na_2O}{Na_2O+SiO_2}$ | notation |
|---|---|---|---|
| 88.5 | 11.5 | 0.06 | Si6Na |
| 81.8 | 18.2 | 0.10 | Si10Na |
| 75.0 | 25.0 | 0.14 | Si14Na |
| 66.7 | 33.3 | 0.20 | Si20Na |
| 60.0 | 40.0 | 0.25 | Si25Na |
| 53.9 | 46.2 | 0.30 | Si30Na |
| 48.2 | 51.8 | 0.35 | Si35Na |
| 42.9 | 57.2 | 0.40 | Si40Na |
| 37.9 | 62.1 | 0.45 | Si45Na |
| 33.3 | 66.7 | 0.50 | Si50Na |

(b) germanate glasses

| $GeO_2$ | $NaO_{1/2}$ | $\frac{Na_2O}{Na_2O+GeO_2}$ | notation |
|---|---|---|---|
| 90.5 | 9.5 | 0.05 | Ge5Na |
| 81.8 | 18.2 | 0.10 | Ge10Na |
| 73.9 | 26.1 | 0.15 | Ge15Na |
| 66.7 | 33.3 | 0.20 | Ge20Na |
| 60.0 | 40.0 | 0.25 | Ge25Na |
| 53.9 | 46.2 | 0.30 | Ge30Na |
| 48.2 | 51.8 | 0.35 | Ge35Na |

**Table 1.1.** *continued*

(c) aluminosilicate glasses

| $SiO_2$ | $AlO_{3/2}$ | $NaO_{1/2}$ | Al:Na | notation |
|---|---|---|---|---|
| 75.0 | 0.0 | 25.0 | 0:10 | Si14Na |
| 65.0 | 10.0 | 25.0 | 2:8 | |
| 55.0 | 20.0 | 25.0 | 4:6 | |
| 50.0 | 25.0 | 25.0 | 5:5 | |
| 45.0 | 30.0 | 25.0 | 6:4 | |
| 40.0 | 35.0 | 25.0 | 7:3 | |

(d) borate glasses (for Chapters 2 and 3)

| $BO_{3/2}$ | $NaO_{1/2}$ | $\frac{Na_2O}{Na_2O+B_2O_3}$ | notation |
|---|---|---|---|
| 95.0 | 5.0 | 0.05 | B5Na |
| 90.0 | 10.0 | 0.10 | B10Na |
| 85.0 | 15.0 | 0.15 | B15Na |
| 80.0 | 20.0 | 0.20 | B20Na |
| 75.0 | 25.0 | 0.25 | B25Na |
| 70.0 | 30.0 | 0.30 | B30Na |
| 65.0 | 35.0 | 0.35 | B35Na |

crucibles in a SiC resistance furnace at temperatures between 1000 and 1600 °C for 30 to 90 min. The melt was poured on a stainless-steel plate and then quenched in air. Pale pink colored or pale yellow colored transparent glass samples were obtained. The yellow color is due to ultraviolet absorption by very small amount of $Eu^{2+}$, which is detectable by fluorescence but not by Mössbauer spectroscopy (p.14). This has no effect on the present study. Each sample was cut into a size of $8 \times 8 \times 3$ mm and its surfaces were polished to an optical finish.

The fluorescence spectra were measured with a Hitachi-850 Fluorescence Spectrophotometer and transferred in digital form to a personal computer where the sampling interval was 0.1 nm. For low temperature measurements, a closed-cycle He refrigerator (Iwatani CRT–006–2000) was used to keep the temperatures at 10 K.

## 1.4 Results

As shown in Fig. 1.1, PET peak of the $^5D_2 \leftarrow ^7F_0$ transition for silicate and germanate glasses was found to split in two as a result of Stark effect. This makes it difficult to extract the exact phonon distribution from the PSB spectra because PSB can be considered as the product of the phonon distribution and electronic level distribution as shown in Fig. 1.3[51]. Therefore, the $^5D_0 \leftarrow ^7F_0$ transition was selected as PET peak because both of the levels are singlet. In this case, however, the thermally excited state absorption peaks ($^5D_1 \leftarrow ^7F_1$, $^7F_2$) overlap with the PSB as shown in Fig. 1.4(a). In order to suppress these peaks, the sample was cooled to 10 K(see Fig. 1.4(b)).

Figures 1.5–1.7 show the excitation spectra of $Eu^{3+}$ at 10 K obtained by monitoring $^5D_0 \rightarrow ^7F_2$ emission at 612 nm as the fixed wavelength. An increase in intensity at the low wave number region is not due to the appearance of a large phonon density of state, but to the superposition of PSB and the tail of PET peak.

For the silicate glasses, a distinct PSB peak was observed in 1100–900 $cm^{-1}$ range and its energy shift decreased with increasing sodium content. Since the PSB peaks seem to consist of more than one peak, the spectra was deconvoluted by assuming a superposition of some Gaussian functions and the result is shown in Fig. 1.8. Four kinds of peaks were found and their positions are plot-

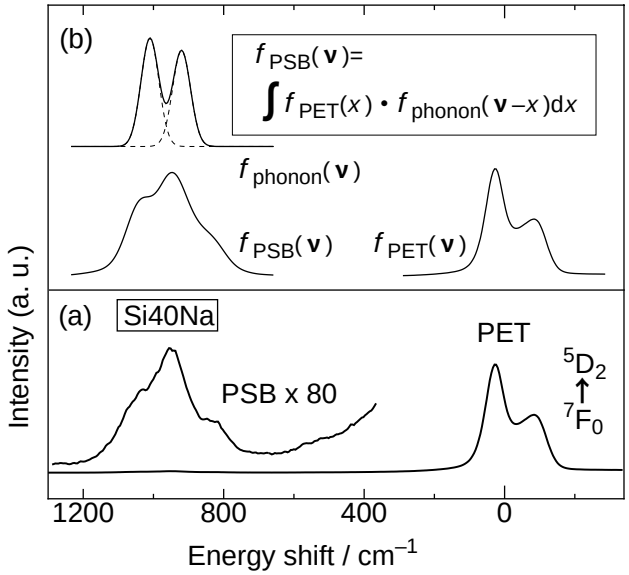


**Fig. 1.3.** *(a) Phonon sideband spectrum associated with* $^5D_2 \leftarrow {}^7F_0$ *transition of* $Eu^{3+}$ *in* Si40Na *glass at room temperature and (b) the diagram showing calculation of PSB curve,* $f_{\mathrm{PSB}}(\nu)$*, from the PET curve,* $f_{\mathrm{PET}}(\nu)$*, and the phonon distribution curve,* $f_{\mathrm{phonon}}(\nu)$*.*

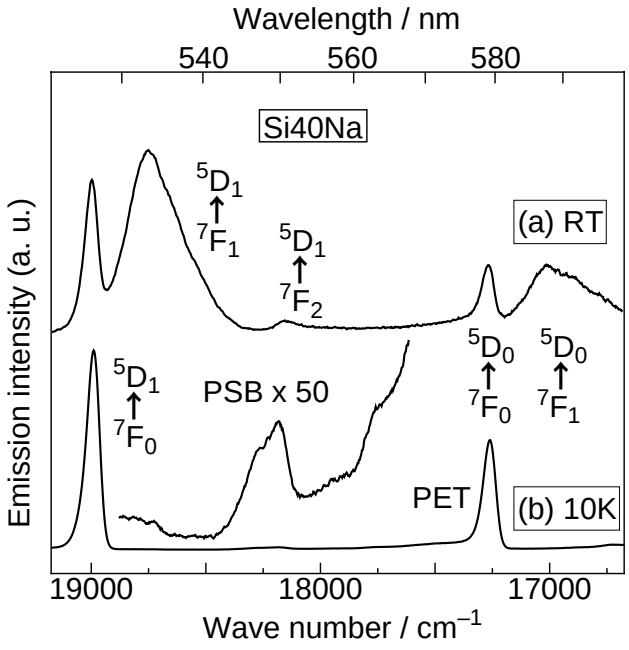


**Fig. 1.4.** *Phonon sideband spectrum associated with* $^5D_0 \leftarrow {}^7F_0$ *transition of* $Eu^{3+}$ *in* $60SiO_2 \cdot 40Na_2O \cdot 1Eu_2O_3$ *glass at (a) room temperature and (b) 10 K by monitoring* $^5D_0 \rightarrow {}^7F_2$ *emission at 612 nm.*

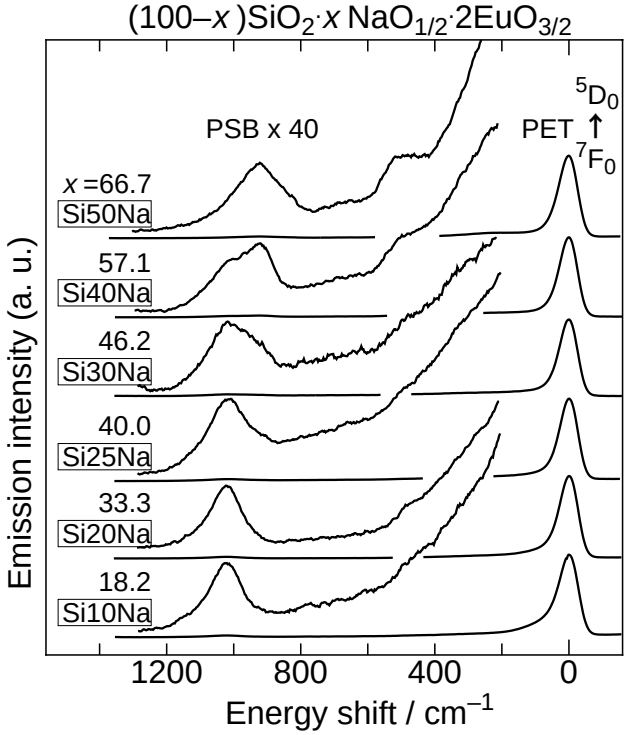


**Fig. 1.5.** *Phonon sideband spectra associated with* $^5D_0 \leftarrow {}^7F_0$ *transition of* $Eu^{3+}$ *in sodium silicate glasses at 10 K by monitoring* $^5D_0 \rightarrow {}^7F_2$ *emission at 612 nm.*

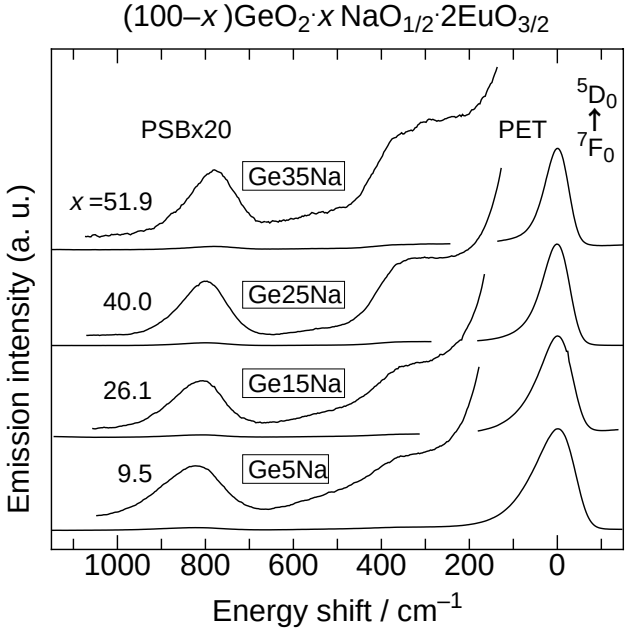


**Fig. 1.6.** *Phonon sideband spectra associated with* $^5D_0 \leftarrow {}^7F_0$ *transition of* $Eu^{3+}$ *in sodium germanate glasses at 10 K by monitoring* $^5D_0 \rightarrow {}^7F_2$ *emission at 612 nm.*

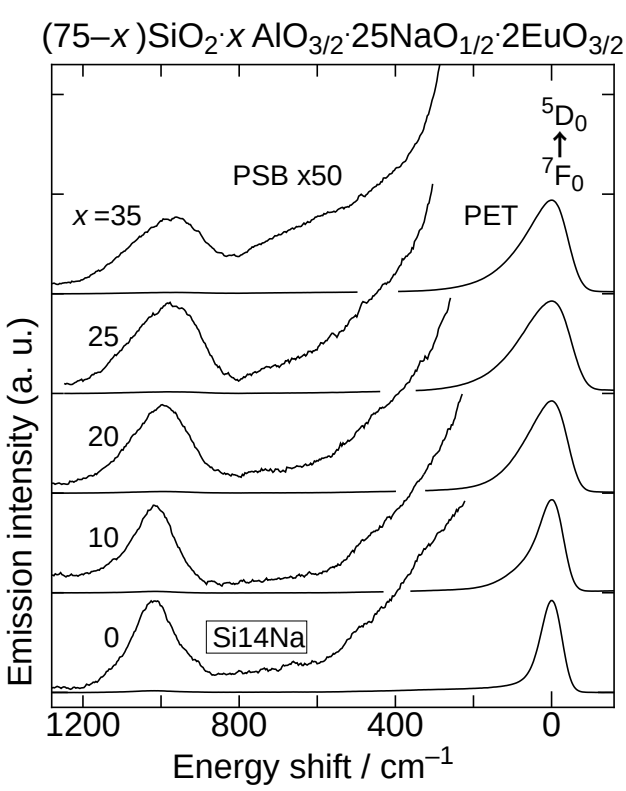


**Fig. 1.7.** *Phonon sideband spectra associated with* $^5D_0 \leftarrow {}^7F_0$ *transition of* $Eu^{3+}$ *in sodium aluminosilicate glasses at 10 K by monitoring* $^5D_0 \rightarrow {}^7F_2$ *emission at 612 nm.*

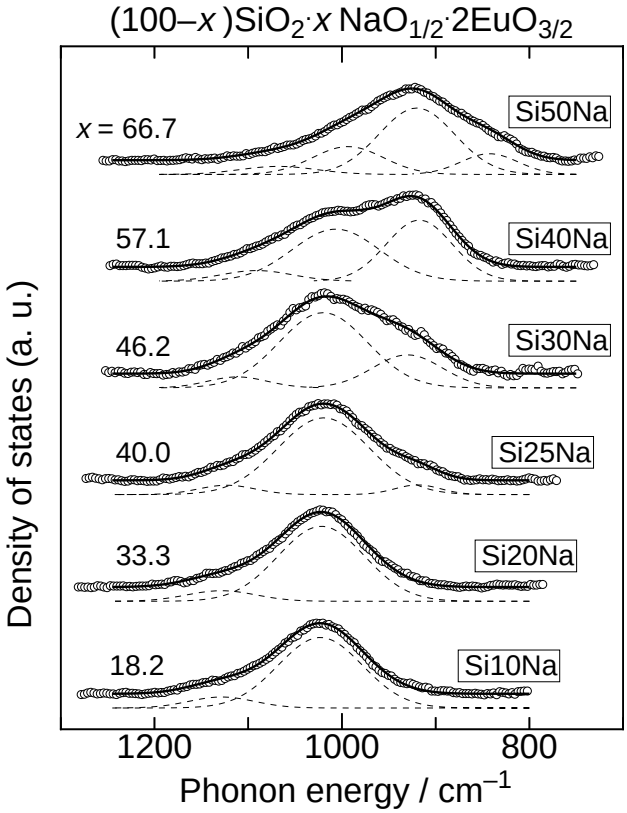


**Fig. 1.8.** *Deconvolution of the PSB spectra for sodium silicate glasses.* ○*: experimental data,* - - - - -*: Gaussian component, and* ——— *: sum of all the component.*

ted in Fig. 1.9. Another weak peak at 500 $cm^{-1}$ was found particularly for Si50Na. Its intensity decreases with a decrease of $Na_2O$ content.

For the germanate glasses, there were two PSB peaks in each spectra, whose energy shifts from PET were about 800 $cm^{-1}$ and 350 $cm^{-1}$. With increasing sodium content, the energy shift at around 800 $cm^{-1}$ decreased and the intensity at around 350 $cm^{-1}$ increased. A decrease in the width of PSB was also observed which was due to the decrease in full-width at half-maximum of PET.

For the aluminosilicate glasses, only one distinct PSB peak was observed at about 1000 $cm^{-1}$.

## 1.5 Discussion

### 1.5.1 Silicate glasses

#### Analysis of phonon sideband

For the glasses of $18.2 \leq x \leq 46.2$, the 1030 $cm^{-1}$ band is dominant. On the basis of the results of Raman and IR studies of RE-free silicate glasses summarized briefly in Table 1.2, this peak is assigned to the Si−O stretching vibration of $Q^3$ units. This assignment is supported by the result of $^{29}$Si MAS-NMR study[52, 53] that $Q^3$ units are dominant in the corresponding RE-free glasses. The frequency of 1030 $cm^{-1}$ is slightly lower than the corresponding one of RE-free silicate glasses. The reason of the shift is considered as follows. Since the vibration from PSB originates from local vibration around RE ions, the ions around them are located in a modified field which has a larger effective mass of the local vibration system than that in the RE-free glass matrix. Thus, it is expected that the frequency of the PSB peak shifts to the lower side as compared with that of IR or Raman spectra. In fact, Ellison and Hess reported[36, 37] that the 1030 $cm^{-1}$ peak in Raman spectra is attributed to the Si−NBO stretch of a $Q^3$ species whose NBO coordinates primarily with $RE^{3+}$.

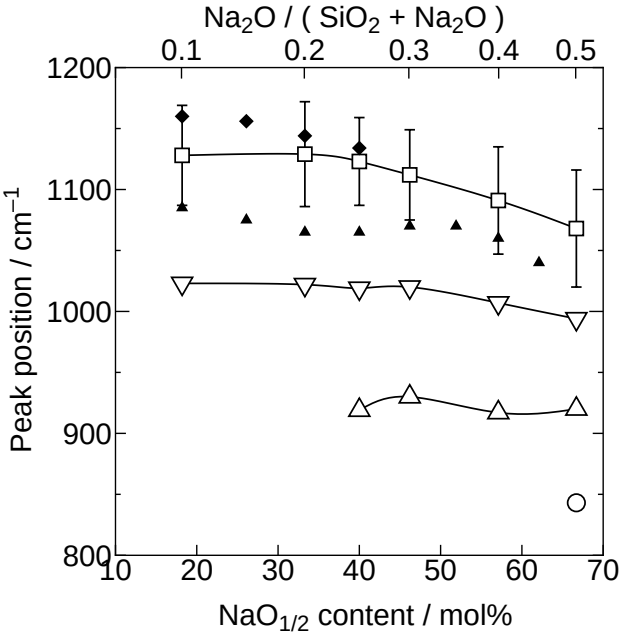


**Fig. 1.9.** *Compositional dependence of peak positions found in deconvoluted PSB spectra for silicate glasses shown in Fig. 1.8 (* □, ▽, △, *and* ○*) and in Raman or IR spectra of RE-free silicate glasses near 1100 $cm^{-1}$ band (closed triangle: IR peaks assigned as BO[32], closed diamond: Raman peaks ambiguously assigned[30]). The bars with* □ *represent the full-width at half-maximum of the peaks.*

It has been reported that the band due to Si−O−Si vibration appears at 1100–1050 $cm^{-1}$ in IR spectra of RE-free silicate glasses (see Table 1.2 and Fig. 1.9). This IR band, however, has no association with the present 1030 $cm^{-1}$ peak, because the compositional dependence of their intensities differ each other. The 1030 $cm^{-1}$ peak dramatically decreases with increasing sodium content, whereas the IR peak is not[31]. Furthermore, since BO(Si−O−Si) has no formal negative charge, it is expected that its interaction with the $f$-electron of $Eu^{3+}$ ion is weaker than NBO having a negative charge (in this case, $Si-O^{\ominus}$ of $Q^3$). In other words, $Q^4$ is likely to be PSB-inactive because their oxygen ions are all BOs having a limited negative charge. Therefore, the 1030 $cm^{-1}$ band is assigned as Si−O stretching vibration of $Q^3$ unit. In a similar way, the peak of 930 $cm^{-1}$, which appears in $40 \leq x \leq 66.7$ composition, is assigned to Si−O stretching vibration of $Q^2$ unit and 840 $cm^{-1}$ as that of $Q^1$.

In addition to the above three, a weak band is observable at 1120–1070 $cm^{-1}$. This band seems to shift to lower wave number but does not change its intensity as sodium content is increased. As described above, a distinct peak, which is assigned as the Si−O−Si vibration, appears in this frequency region in the vibronic spectra of RE-free silicate glasses. They are shown in Fig. 1.9 with closed points: Closed triangles represent the distinct peak in IR spectra and closed diamonds the

shoulder in Raman spectra. Its weak intensity is probably due to weak interaction with $f$-electron. An asymmetrical shape of PET peak may also contribute to it. Because of its weakness, this peak will not be considered further in this discussion.

The 500 $cm^{-1}$ peak observed for the glasses containing a large amount of $Na_2O$ is assigned as bending vibrations of the network on the basis of the results of Raman study. The compositional dependence of this peak is most likely to be related with the energy of 1000 $cm^{-1}$ band. In general, the phonon relaxation rate decreases with a decrease of the phonon energy[46] (see Eq. 5.1–5.3 [p.36]). Thus, as the energy of the main peak decreases, the fraction of phonon relaxation via 500 $cm^{-1}$-phonon relatively increases.

### Compositional dependence of $Q^n$ unit

The intensity ratio of each peak to PET peak, $g$, obtained from the deconvolution analysis is plotted in Fig. 1.10(a) as a function of $Na_2O$ content. For comparison, the NMR results of undoped silicate glass by Maekawa *et al.*[53] are shown in Fig. 1.10(b). It is noted that $g$ value is not directly proportional to the fraction. A marked difference between NMR and PSB results is that $g(Q^3)$ in PSB hardly varies in the region of composition below $x = 46.2$ unlike $Q^3$ fraction for $^{29}Si$ MAS-NMR results. This is most likely caused by the local modification of silicate glass network around $Eu^{3+}$ ions. It is obvious that $Eu^{3+}$ ions can not be substituted to $Si^{4+}$ sites because of their larger ionic radius and smaller negative charge, and act as network modifying cations. In fact, the silica glass network whose oxygen ions are all BOs is known to as a poor solvent for RE ions[54]. Therefore, it is expected that $Eu^{3+}$ ions in the $Na_2O$-poor compositions are surrounded by some NBOs of $Q^3$ in order to neutralize their positive charge.

Furthermore, as shown in Fig. 1.10, the tielines of $Q^3$ and $Q^2$ for PSB shift to lower-alkali composition as compared with those for NMR. This tendency gets stronger as the sodium content decreases. If $Eu^{3+}$ ions become most stable when just three NBOs join the first coordination shell, the $Q^2$ population need not increase in alkali-poor compositions. Thus, it is expected that $Eu^{3+}$ ions act not only to create three NBOs as *network-modifiers*, but also to modify the surrounding glass network just like alkali-rich matrix. In other words, $Eu^{3+}$ ions depolymerize the local

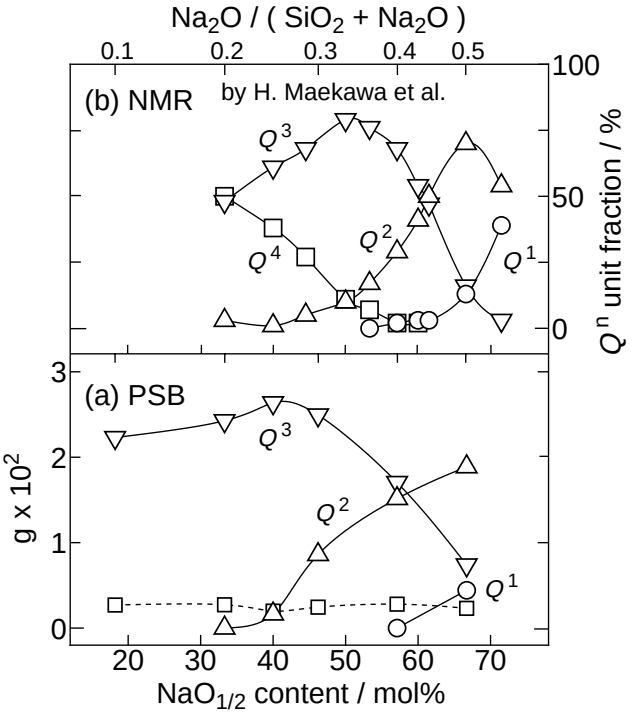


**Fig. 1.10.** *Compositional dependence of the amount of $Q^n$ units (a) in the local structure around $Eu^{3+}$ ions (this study) and (b) in rare earth-free sodium silicate glasses investigated by Maekawa et al. using $^{29}Si$ MAS-NMR[53]. The vertical axes are taken as (a) an intensity ratio of the peak to PET peak, g, and (b) the fraction of $Q^n$ unit. □ is the same as Fig. 1.9. (b) is reproduced using the Tables 1 and 2 in [53].*

glass network in order to dissolve themselves stably into silicate matrix. Further details will be described in Chapter 2. A certain type of phase separation may occur, but the transparency of the sample clearly shows that phase separation does not occur in the sub-micrometer range.

### 1.5.2 Germanate glasses

On the basis of the results of Raman and IR study of RE-free germanate glasses and crystals listed in Table 1.3, the PSB band at 800 $cm^{-1}$ band is considered to be due to $Ge-O^{\ominus}$ stretching vibration of $GeO_{4/2}$ tetrahedra, not to the vibration of $GeO_{6/2}$ octahedra. A large intensity of this peak even in sodium-poor compositions implies the preferential coordination of NBO for compensating the positive charge of $Eu^{3+}$ ions. A decrease of the peak frequency is due to the population change in $GeO_{4/2}$ units having one and two NBOs. Similar to the silicate system, the vibrational energies of those units are also smaller than those of the corresponding vibrations listed in Table. 1.3.

Consequently, it is assumed that $Eu^{3+}$ ions are mainly surrounded by $GeO_{4/2}$ tetrahedra. It is indeed conceivable that NBO of $GeO_{4/2}$ is more effective for charge compensation than BO of $GeO_{6/2}$ because of its compact nature. This does not mean that $GeO_{6/2}$ units are completely excluded from the second coordination shell of $Eu^{3+}$ ions, because they are likely to be PSB-inactive like $Q^4$ units of silicate glasses if the Coulomb interaction with $Eu^{3+}$ ions is small, that is, the excess negative charge of $GeO_{6/2}$ is not used for charge compensation of $Eu^{3+}$ ions. It is difficult to decide from these data whether or not $GeO_{6/2}$ octahedra coordinate $Eu^{3+}$ ions as a part of BO which does not compensate for positive charge of $Eu^{3+}$ ions. If they did exist, the absence of $GeO_{6/2}$ peak in PSB is probably due to longer distance and smaller negative charge of BO of $GeO_{6/2}$ than that of NBO of $GeO_{4/2}$, which brings only a weak electron-phonon coupling strength. Consequently, it is concluded that the positive charge of $Eu^{3+}$ ions is compensated mainly by NBOs of $GeO_{4/2}$ tetrahedra rather than the excess negative charge of $GeO_{6/2}$ octahedra. In other words, incorporated $Eu^{3+}$ ions in germanate glasses act, as *network-modifiers*, to create NBOs rather than macro anions.

The 350 $cm^{-1}$ band is considered to be a superposition of several kinds of vibrations, such as deformation, the Na−O mode and so forth (see Table 1.3). The increase in its intensity with increasing sodium content seen in Fig. 1.6 is partly due to an increase of Na−O(NBO) bonding around $Eu^{3+}$ ions.

### 1.5.3 Aluminosilicate glasses

Since the coordination number of $Al^{3+}$ ions incorporating in the glass structure is expected to be more than four, $Na^+$ ions act as the charge compensator of $AlO_{n/2}^{(n-3)-}$ macroanions rather than the network modifier to break Si−O−Si bond[1]. Therefore, the NBO concentration for aluminosilicate glasses decreases with increasing Al content. For PSB spectra, however, the 1000 $cm^{-1}$ band which is attributed to $Q^3$ is dominant throughout the composition. Any other Al-originated band listed in Table 1.4 was not found. Therefore, it is concluded that the preferential coordination of NBO to $Eu^{3+}$ ions also occurs and macroanions do not take part in charge-compensation of $Eu^{3+}$ ions in this system.

## 1.6 Conclusion

The local structure around $Eu^{3+}$ ions in sodium silicate, germanate and aluminosilicate glasses was explored employing the phonon sideband associated with the $^5D_0 \leftarrow {}^7F_0$ transition of $Eu^{3+}$. It was found that the vibrational energy around $Eu^{3+}$ ions is smaller than that of the corresponding structural unit in glass matrix because of the local mass effect of $Eu^{3+}$ ion. Further, the compositional dependence of $Q^n$ units around $Eu^{3+}$ in silicate glasses showed that the local depolymerization of glass network around RE ions occurs, which is due to the local charge compensation and the stabilization of $Eu^{3+}$. It was also found that the vibrations of Ge octahedra and Al polyhedra are not coupled with the relaxation of $Eu^{3+}$ ions. Therefore, the excess negative charge is not used for charge compensation of $Eu^{3+}$ ions. In other words, the incorporated $Eu^{3+}$ ions act, as *network-modifiers*, to create NBOs rather than macro anions.

**Table 1.2.** *Assignment of various bands in the vibrational spectra for silica and silicate glasses.*

| Raman† | | IR‡ | |
|---|---|---|---|
| $\hbar\omega/\mathrm{cm}^{-1}$ | assignment | $\hbar\omega/\mathrm{cm}^{-1}$ | assignment |
| 1200, 1060 | asym. Si−O vib. of $Q^4$ | 1100 | Si−O−Si vib. of $Q^4$ |
| 1100–1050 | sym. Si−O vib. of $Q^3$ | ∼1050 | Si−O−Si vib. |
| 1000–950 | sym. Si−O vib. of $Q^2$ | ∼950 | $Si-O^{\ominus}$ vib. |
| 900 | sym. Si−O vib. of $Q^1$ | | |
| 850 | sym. Si−O vib. of $Q^0$ | | |
| 590–650 | linkage between $Q^2$ | | |
| 520–600 | linkage between $Q^3$ | | |

† McMillan[29]. ‡ Sweet and White[31].

**Table 1.3.** *Assignment of various bands in the vibrational spectra for germanate glasses and $GeO_2$ crystals.*

| Raman† | | IR‡ | |
|---|---|---|---|
| $\hbar\omega/\mathrm{cm}^{-1}$ | assignment | $\hbar\omega/\mathrm{cm}^{-1}$ | assignment |
| 870 | $\nu Ge-O^{\ominus}$ of $GeO_{4/2}$ containing one NBO | 878 | $GeO_{4/2}$ in hexagonal and vitreous $GeO_2$ |
| 800 | $\nu_s Ge-O^{\ominus}$ of $GeO_{4/2}$ containing two NBO | | |
| 850, 770 | $\nu_{as}O-Ge-O$ | | |
| 653, 600 | $\nu_s O-Ge-O$ or $\nu_s GeO_{6/2}$ | 688 | $GeO_{6/2}$ in tetragonal $GeO_2$ |
| 530 | $\nu_s O-Ge-O$ | | |
| *below* 400 | deformation, $\nu$A−O and lattice modes (A: alkali ion) | | |

† Verweij and Buster[33]. ‡Murthy and Kirby[34].

**Table 1.4.** *Assignment of various bands in the vibrational spectra for aluminosilicate glasses and aluminate crystals. (T = tetrahedral Si or Al)*

| Raman† | | IR‡ | |
|---|---|---|---|
| $\hbar\omega/\mathrm{cm}^{-1}$ | assignment | $\hbar\omega/\mathrm{cm}^{-1}$ | assignment |
| 1110 | sym. stretching of $Q^3$ | | |
| 980 | T−O−T' vibration | | |
| | | 900–700 | "Condensed" $AlO_{4/2}$ |
| | | 680–500 | "Condensed" $AlO_{6/2}$ |

† McKeown *et al.*[38]. ‡ Tarte[39].

# Chapter 2

# Mössbauer spectroscopy of $^{151}$Eu in several oxide glasses

## 2.1 Introduction

The recoil-free gamma-ray resonant absorption by nuclei in solids, called the Mössbauer effect, is an effective method to obtain the information around specific ions. Various structural informations such as the site symmetry of the Mössbauer ion, the local electric and magnetic fields and the valence state are easily obtained. For the investigation of glasses, $^{57}$Fe is extensively studied and some reviews have been published[55–58]. As for $^{151}$Eu, only a few works have appeared[59–64]. This is partly because $^{151}$Eu is less informative than $^{57}$Fe. Because of its relatively small electric field gradient and moderately large natural linewidth of the resonance, the spectra usually consist of an unresolved single line spectrum[65, 66]. Nevertheless, from the value of isomer shift (IS), $^{151}$Eu Mössbauer spectroscopy can offer unique information which is not available by any other method, i.e., the $s$-electron density at the Eu nucleus.

An increase in $s$-electron density, as a consequence of increasing the electron donation ability of surrounding ligands, i.e., increasing the coordination number of Eu, decreasing Eu−O distance or increasing the covalency of Eu−O bondings, will result in an increase of the IS. Therefore, this method gives the information about the first coordination shell of $Eu^{3+}$.

On the other hand, there is a useful concept for evaluating the basicity of glasses, i.e., electron density carried by oxygens, called the theoretical optical basicity, $\Lambda_{\rm th}$, proposed by Duffy and Ingram[67–70]. This is originally determined by the frequency shift in the ultra-violet $(s-p)$ spectra of probe ions such as $Tl^{+}$, $Pb^{2+}$, and $Bi^{3+}$, and the calculated values of $\Lambda_{\rm th}$ represent the average basicity arising from all the oxide species, whether they are bridging or non-bridging.

In the present chapter, the IS of $^{151}$Eu and the optical basicity of host glass are compared and, by the aid of the result of Chapter 1, the local structure within the first coordination shell is discussed.

## 2.2 Experimental

The glass samples used are the same as described in Chapter 1. The absorbents were prepared by grinding the glass samples to powder, which was then placed between two thin polymer films. $^{151}$Eu−Mössbauer spectra were measured in transmission using a conventional constant acceleration spectrometer with a 1.85 GBq (=50 mCi) $^{151}$Sm in $Sm_2O_3$ as a 21.64 keV $\gamma$-ray source (see Fig. 2.1). All measurements were performed at room temperature. Isomer shifts, $\delta$, were calibrated against $EuF_3$ and the velocity was calibrated with a $^{57}$Co and an $\alpha$-iron foil. Each sample was measured by keeping it in the holder for one week.

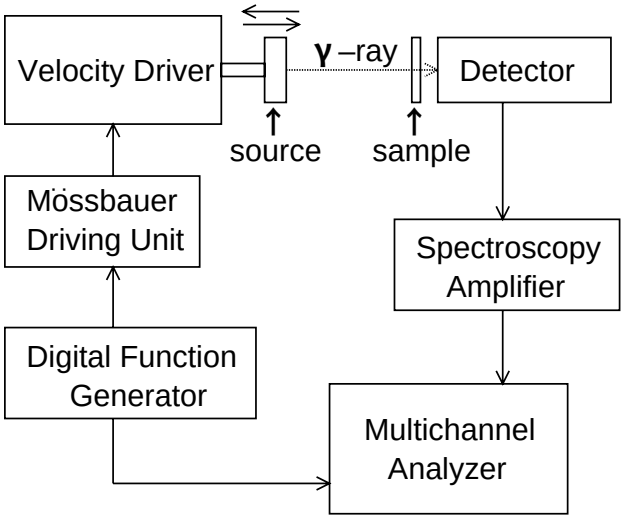


**Fig. 2.1.** *Schematic diagram of the experimental setup for Mössbauer spectroscopy.*

## 2.3 Results

Figures 2.2(a) and 2.2(b) show the samples of the Mössbauer spectra of $^{151}$Eu. For all the samples, there was no peak to be assigned as $Eu^{2+}$ whose IS is about $-13$ mm·s$^{-1}$. The peak position of each spectrum was determined by a single Lorentzian fit. Figures 2.3(a) and 2.3(b) show the compositional dependence of IS of $^{151}$Eu, $\delta$, for binary oxide glasses and sodium aluminosilicate glasses, respectively. Further, the IS is replotted as ordinate and the $\Lambda_{\rm th}$ as abscissa in Fig. 2.4. The calculation method of optical basicity is described in Appendix 2-A.

## 2.4 Discussion

As mentioned above, the theoretical optical basicity, $\Lambda_{\rm th}$, is used to estimate the average electron density carried by oxygens in oxide glasses. If the basicity of the ligands around $Eu^{3+}$ ions is equal to that of host glass, IS is to be in direct proportion to $\Lambda_{\rm th}$. Among the four glass systems, only the borate system showed a direct proportion. It is presumed that the local modification of glass matrix occurs and is related with the preferential coordination of non-bridging oxygen (NBO) to $Eu^{3+}$ described in Chapter 1.

In order to estimate the modification qualitatively, it is useful to introduce the theoretical microscopic optical basicity, $\lambda_{\rm th}$, of individual oxygen atoms[68, 70]. Namely, the degree of electron donation from each ligand to $Eu^{3+}$ ion is estimated by $\lambda_{\rm th}$. Figure 2.5 shows the value of microscopic optical basicity for the possible oxygen species in the present glass systems. First of all, let us consider the ligand characters for the silicate system. $Eu^{3+}$ ions have to be coordinated with the ligands whose local charge sum is $-3$, just enough for neutrality. Since NBO is the only species having a negative charge in silicate glasses and RE ions act as a network modifier in oxide glasses, it is certain that three NBOs are present in the first coordination sphere. The number of NBOs surrounding a $Eu^{3+}$ ion can be more than three if the negative charge of excess NBOs is compensated by $Na^+$ ions. In fact, Ellison and Hess[36] pointed out

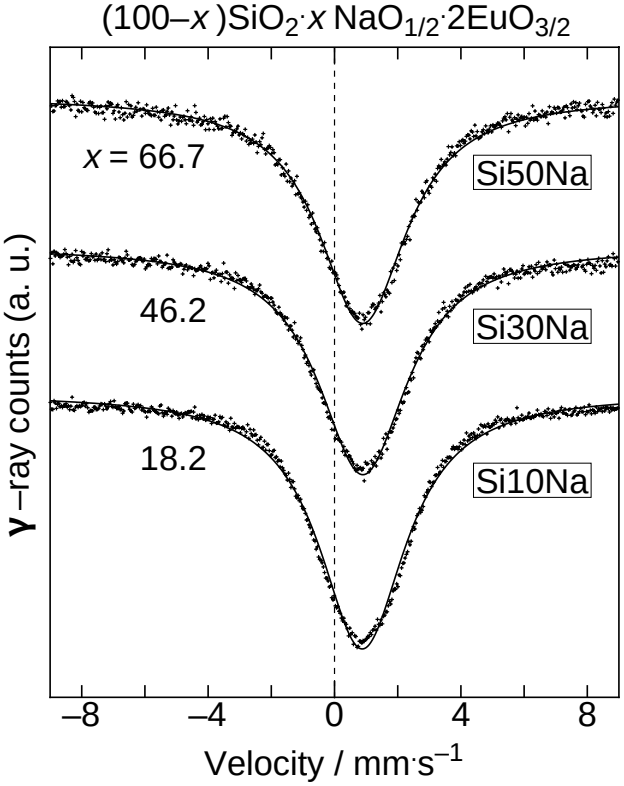


**Fig. 2.2.** *Mössbauer spectra of $^{151}$Eu in (a) sodium silicate and (b) sodium germanate glasses recorded at room temperature. Solid lines represent the fitted single Lorentzian curve.*

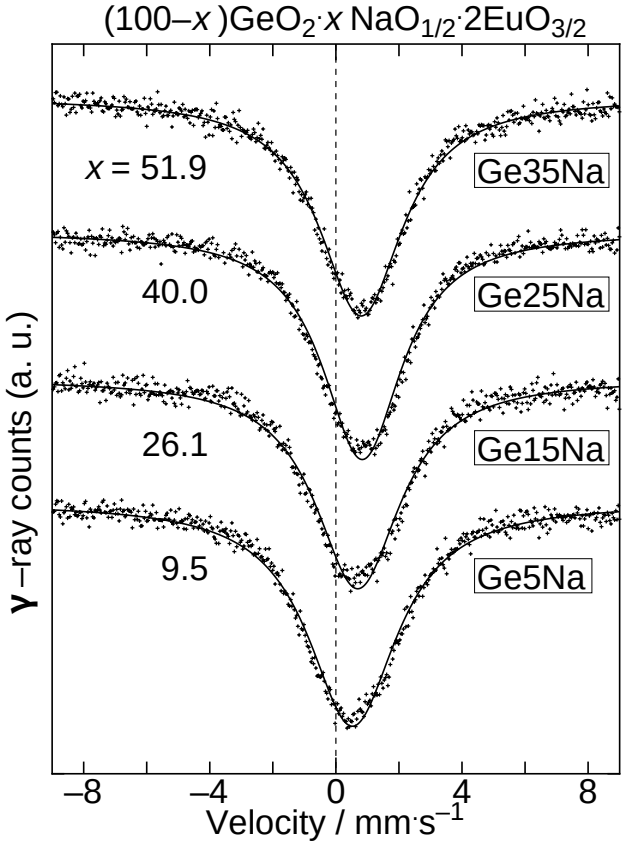


**Fig. 2.2.** *continued*

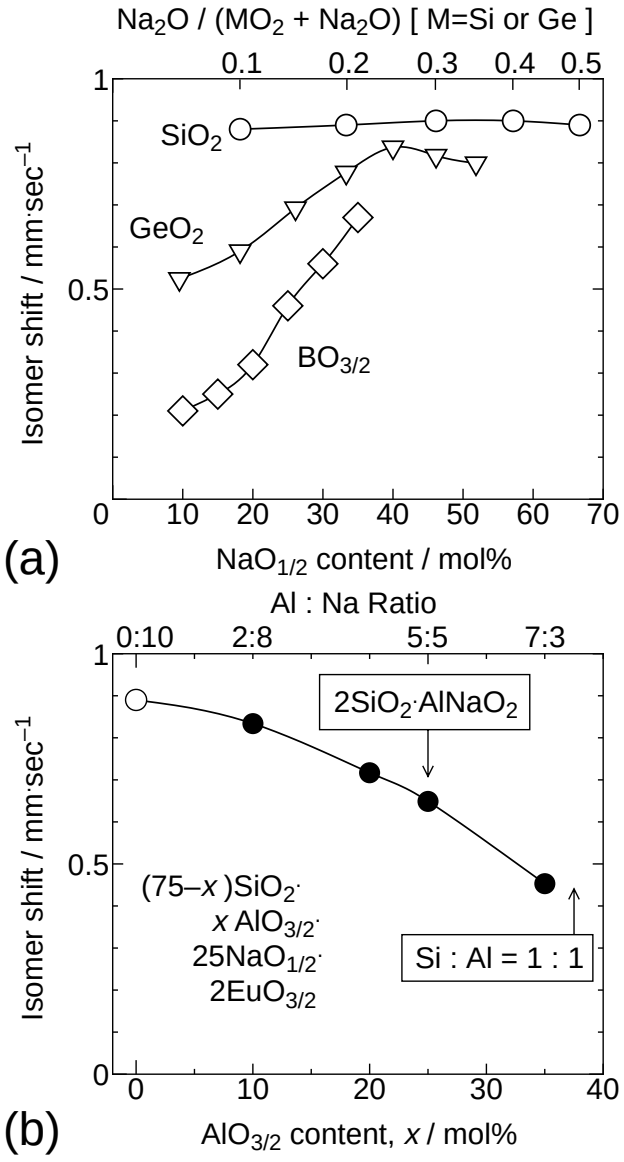


**Fig. 2.3.** *Compositional dependence of the isomer shift (IS) of* $^{151}Eu$*,* $\delta$*, (a) in sodium silicate, germanate, and borate glasses and (b) in sodium aluminosilicate glasses. IS was determined with respect to* $EuF_3$ *as a standard.*

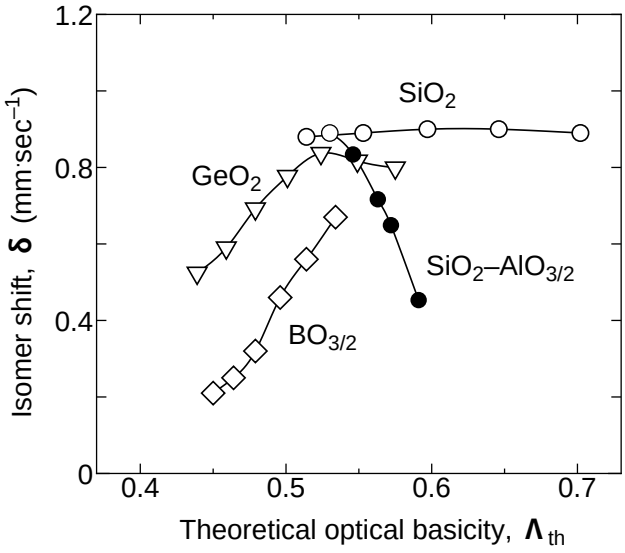


**Fig. 2.4.** *Relationship between the isomer shift of* $^{151}Eu^{3+}$ *and the theoretical optical basicity,* $\Lambda_{\rm th}$*, of the host glass.*

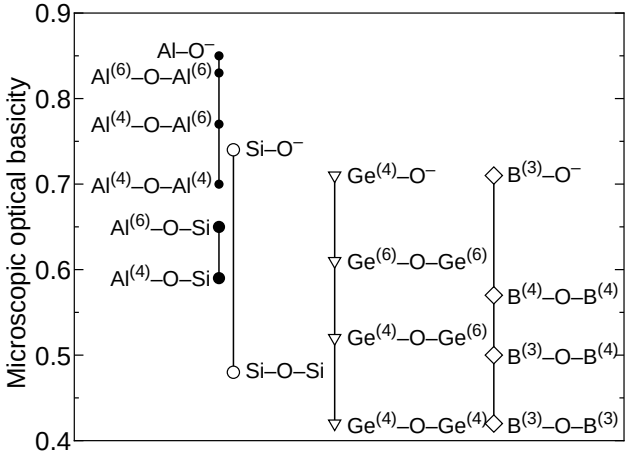


**Fig. 2.5.** *The value of microscopic optical basicity,* $\lambda_{\rm th}$*, for oxygen species that may be present in oxide glasses in this study. Numerals in parenthesis indicate the coordination number. See Appendix 2-A for detailed calculation.*

that there is a limited amount of NBOs shared with alkali and lanthanoid ions from an analysis of Raman spectra for $SiO_2-K_2O-La_2O_3$ glasses. Therefore, the ligands surrounding RE ions can be classified into three groups, NBO whose negative charge is compensated by a $Eu^{3+}$ ion, NBO paired with $Na^+$, and BO, as shown Fig. 2.6. In order to avoid confusion, these species are denoted by sans serif fonts, such as NBO, NBO−Na, and BO, respectively.

Although, NBO and NBO−Na may form a resonating structure, such as

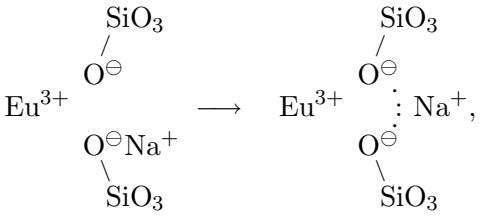


this classification is adequate for considering net charge neutrality. The electron donation toward $Eu^{3+}$ ion for NBO is, of course, expected to be larger than that for NBO−Na. The value of $\lambda_{th}(Si-O^-)$ shown in Fig. 2.5 should be regarded as the basicity of NBO−Na, because the values are calculated based on an assumption that only network forming cations can polarize oxygen ions[70]. If we consider $\lambda_{th}$ as the scale showing an electron donation to $Eu^{3+}$ ions, the apparent value of NBO is larger than $\lambda_{th}(Si-O^-)$. It is not necessary, however, to consider NBO for the system where the positive charge of $Eu^{3+}$ ions is compensated only by NBOs, such as silicate, germanate, and aluminosilicate, which is demonstrated in Chapter 1. For these systems, IS is considered to be affected by the amounts of NBO−Na and BO, and Eu-ligand distance.

According to Fig. 2.4, the $\delta$ of silicate glasses remain constant, even though the amount of NBOs increases with alkaline content. This is most likely due to a preferential coordination of NBO−Na because BO is known to be a poor solvent for RE ions in silica glass. Namely, Arai *et al.* assumed that $Nd^{3+}$ ions in the Al-doped silica glass prepared by plasma-torch chemical vapor deposition are surrounded preferentially by $AlO_n$ polyhedra[54]. Similarly, in the present case, $Eu^{3+}$ ions are considered to be more stabilized by NBO−Na coordination rather than by BO coordination. It is noted that the ratio of NBO/BO is not necessarily constant throughout the composition. A minor change of Eu-ligand distance, or the coordination number of $Eu^{3+}$ ions, may occur to make $\delta$ constant. This is clarified in Chapter 3.

The present result implies that $Eu^{3+}$ ions need some NBO−Na pairs to dissolve stably into silicate glass network. This is supported by the IS behavior of the aluminosilicate system, which is discussed later. Moreover, this is consistent with the increased fractions of $Q^3$ and $Q^2$ in low-alkali composition described in Chapter 1 (see Fig. 1.10 [p.10]). Namely, increased NBO−Na coordination are attained by local depolymerization. Consequently, it is assumed that $Eu^{3+}$ ions in the silicate system are surrounded by a certain amount of NBO−Na pairs for stabilization.

Such a local modification should also occur for the borate system. In fact, PSB results for sodium borate glasses[45] revealed that some NBOs coordinate $Eu^{3+}$ ions in alkali-poor composition where NBOs consumed to form $BO_{4/2}$ units (see Eq. 1.2 [p.3]). Therefore, the compositional dependence of $\delta$ in this system is most likely due to a change of the basicity of BOs. Since the fraction of tetrahedral B increases with alkaline content and reaches 0.45 at $65B_2O_3{\cdot}35Na_2O$[71], the local basicity of BO is expected to increase monotonously with Na content, such as

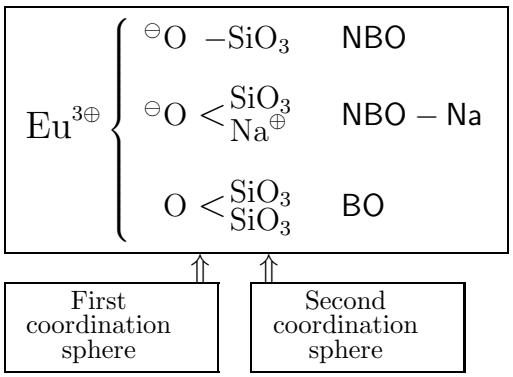


**Fig. 2.6.** *Three varieties of oxygen species that may coordinate $Eu^{3+}$ ions in silicate glasses.*

$$\underset{\lambda_{\rm th}=0.42}{\mathrm{B^{(3)}-O-B^{(3)}}} \longrightarrow \underset{\lambda_{\rm th}=0.50}{\mathrm{B^{(3)}-O-B^{(4)}}} \longrightarrow \underset{\lambda_{\rm th}=0.57}{\mathrm{B^{(4)}-O-B^{(4)}}}.$$

The behavior of $\delta$ of the germanate system is similarly explained. The PSB result described in Chapter 1 showed that the positive charge of $Eu^{3+}$ ions in germanate glasses are compensated with NBOs. On the other hand, the octahedral Ge fraction in this system is reported to reach a maximum of 0.25 at $80GeO_2{\cdot}20Na_2O$ ($NaO_{1/2}$ 33.3 mol%)[72]. Therefore, an increase of $\delta$ with increasing sodium content is most likely due to a change of the basicity of BOs. For the composition of more than 33.3 mol% of $NaO_{1/2}$ (20 mol% of $Na_2O$), a preferential NBO coordination like the silicate system is expected to occur. A small decrease of $\delta$ in the $Na_2O$-rich composition is probably due to a decreasing population of octahedral Ge. Consequently, an increase of $\delta$ with Na content for borate and germanate systems is reasonably explained by increasing of the basicity of BOs due to a change of cation coordination number.

For the aluminosilicate system, the IS showed an extraordinary behavior, i.e., $\delta$ decreases with increasing $\Lambda_{\rm th}$, which indicates strong local modification. It is consistent with the PSB result described in Chapter 1, that the positive charge of $Eu^{3+}$ is mainly compensated by NBOs rather than $AlO_{n/2}^{(n-3)-}$ macroanions although the NBO concentration decreases with increasing Al content. It is, however, unreasonable that the number of NBOs surrounding $Eu^{3+}$ remains constant when incorporating Al in the viewpoint of local basicity. If the number is constant, $\delta$ should increase with increasing Al content due to an increase of the basicity of BO, i.e., a replacement of Si−O−Si ($\lambda_{\rm th}=0.48$) by Al−O−Si ($\lambda_{\rm th}=0.59$ *or* 0.65; see Fig. 2.5). Therefore, it is most likely that some NBO−Na pairs are present around $Eu^{3+}$ in Al-free silicate glasses (see Fig. 2.6) and the pairs are replaced by some BOs shared with Si and Al with increasing Al content, such as

$$\underset{\lambda_{\rm th}=0.74}{\mathrm{Si-O^{\ominus}\cdots Na^{+}}} \longrightarrow \underset{\lambda_{\rm th}=\begin{cases}0.59(n=4)\\0.65(n=6)\end{cases}}{\mathrm{Al^{(n)}-O-Si}}.$$

Consequently, it was considered that $Eu^{3+}$ ions in silicate glasses are surrounded by a certain amount of NBO−Na pairs, which decreases with an incorporation of Al but remains almost constant with incorporating Na. This is because silicate network can localize NBOs by a disproportionation such as $Q^n \longrightarrow Q^{n+1} + Q^{n-1}$, whereas incorporated Al cannot release consumed NBO(s) in such a way as

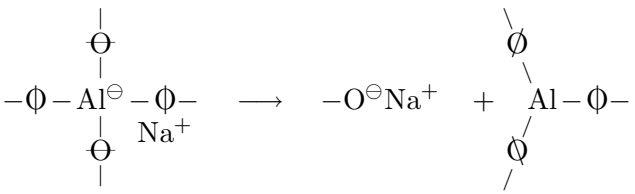

## 2.5 Conclusion

The local structure around $Eu^{3+}$ ions in several binary oxide glass systems ($SiO_2$–$Na_2O$, $GeO_2$–$Na_2O$, and $B_2O_3$–$Na_2O$) and aluminosilicate glasses was investigated from the isomer shift (IS) of $^{151}$Eu Mössbauer spectroscopy. In association with the results of Chapter 1, local modification around $Eu^{3+}$ was estimated. It was found that only for the silicate system the IS was independent on sodium content. It was assumed that this is due to a preferential NBO coordination around $Eu^{3+}$. For the borate and germanate systems, the compositional dependence of IS is well explained by the basicity change of BO due to the coordination change of the network forming cations. For the aluminosilicate glasses, a strong local modification was expected from an extraordinary behavior of the IS. This is also correlated with the preferential NBO coordination. It was reasonably explained by a replacement of NBO−$Na^+$ pair by BO(Al−O−Si) around $Eu^{3+}$ with an increase of Al content.

**Appendix 2-A:** Calculation of the theoretical optical basicity

The theoretical optical basicity, $\Lambda_{\rm th}$, for oxide system is determined so as to be unity for CaO, and expressed as,

$$\Lambda_{\rm th} = \sum_i \frac{X_i}{\gamma_i} \quad (2.1)$$

$$= 1 - \sum_i X_i \cdot \left(1 - \frac{1}{\gamma_i}\right) \quad (2.2)$$

$$X_i = \frac{z_i r_i}{|z_{\rm O}|} \quad (2.3)$$

where $\gamma$ is the basicity moderating parameter listed in Table 2.1, $z$ the oxidation number, and $r$ ratio of the cation with respect to the total number of $O^{2-}$ ions and, thus, $z_{\rm O} = -2$ and $\sum_i X_i = 1$. The basicity moderating parameter, $\gamma$, is derived from Pauling's electronegativity by the equation of $\gamma = 1.36(x - 0.26)$[67]. For example, $\Lambda_{\rm th}$ of $90SiO_2{\cdot}10Na_2O$ is calculated by following.

$$\Lambda_{\rm th} = \frac{z_{\rm Si} r_{\rm Si}}{2} \cdot \frac{1}{\gamma_{\rm Si}} + \frac{z_{\rm Na} r_{\rm Na}}{2} \cdot \frac{1}{\gamma_{\rm Na}}$$

$$= \frac{4 \cdot \frac{90}{190}}{2} \cdot \frac{1}{2.09} + \frac{1 \cdot \frac{20}{190}}{2} \cdot \frac{1}{0.87} = 0.51$$

The theoretical microscopic optical basicity, $\lambda_{\rm th}$, of a specific anion is also expressed by Eq. 2.2, but the summation is carried out only over the cation(s) linked to the anion and $r$ is taken as the reciprocal of the coordination number of the cation(s). Here, alkali and alkaline earth ions are out of consideration based on a assumption that these ions do not polarize oxygen ions.

For calculating fluoride optical basicity values, the basicity moderating parameters of all cations should be scaled as $\gamma_{\rm M}$(fluoride system)=$2.3\gamma_{\rm M}$(oxide system)[69](see Chapter 5, p.42). Only for $Zr^{4+}$, experimental value is available, $\Lambda_{\rm th}(ZrF_4)$=0.38.

**Table 2.1.** *Basicity moderating parameters, $\gamma$, for oxide systems[67, 68].*

| Cation | $\gamma$ | Cation | $\gamma$ |
|---|---|---|---|
| $Na^+$ | 0.87 | $Ba^{2+}$ | 0.87 |
| $Ca^{2+}$ | 1.00 | $La^{3+}$ | 1.14 |
| $Al^{3+}$ | 1.64 | $In^{3+}$ | 1.96 |
| $Si^{4+}$ | 2.09 | $Pb^{2+}$ | 2.09 |
| $B^{3+}$ | 2.36 | | |
| $Ge^{4+}$ | 2.38 | | |

# Chapter 3

# Origin of inhomogeneous linewidth of $Eu^{3+}$ fluorescence I.

— Silicate, germanate, aluminosilicate, and borate system

## 3.1 Introduction

Glasses are inevitably accompanied by the spectral characteristics of large inhomogeneous linewidth due to the disorder of glass structure. Therefore, in case of analyzing glass structure by spectroscopic method, the information obtained represents the averaged image of glass structure. As for practical application of glass to optical devices, this is one of the important factors that influence the efficiency. For stimulated emission, its cross section is inversely proportional to the emission linewidth[9]. For hole burning devices, a large linewidth is desirable for large data capacity. Consequently, it is important to elucidate the factors determining the inhomogeneous broadening, when designing new devices.

$Eu^{3+}$ is the most suitable element among various RE to be used for evaluating inhomogeneity of the sites of impurity ions in glass, because its electronic levels are quite simple (see Fig. 1.2 [p.5]). Since the $^5D_0$ and $^7F_0$ states are non-degenerate, the full width at half-maximum (FWHM) of the optical transition between them, $\Delta\nu_{\mathrm{IH}}$, can be a standard of the inhomogeneous nature of glass[73, 74].

This transition can be also used for the fluorescence line narrowing (FLN) technique by which a subset of the $Eu^{3+}$ population can be excited and site-selective spectra can be obtained[75–82]. Thus, this FLN method gives the information buried under the inhomogeneously broadened band, namely, the structure of electronic levels for each subset of the ions. Most of the works, however, mainly dealt with the determination of a set of crystal field parameters on the basis of a hypothesis that the site symmetry is $C_{2v}$ (although actual symmetry may be lower[75, 79]). There is no systematic study investigating the compositional dependence of site-selective spectra.

In the present chapter, the relation between the inhomogeneous broadening and the local structure around $Eu^{3+}$ ions is investigated by the aid of FLN method.

## 3.2 Theory

An example of the fluorescence spectrum of $Eu^{3+}$ ions in silicate glass is shown in Fig. 3.1. Since all of the ions are excited by broadband radi-

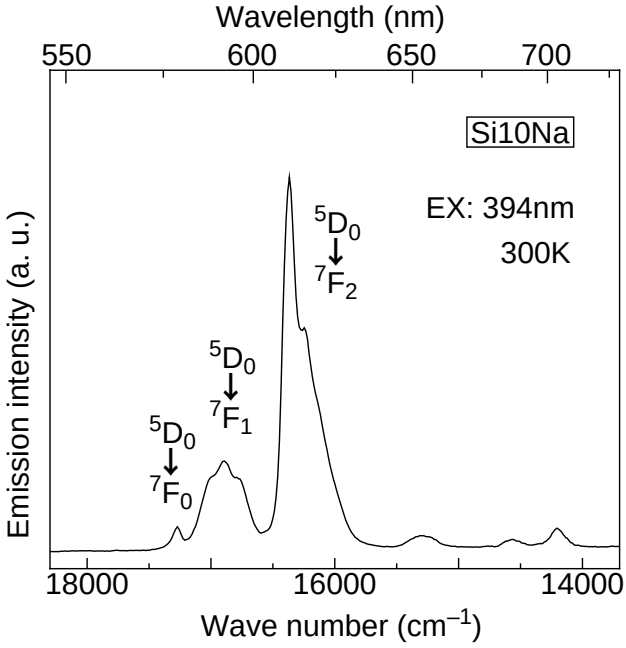


**Fig. 3.1.** *Fluorescence spectra of $Eu^{3+}$ in $90SiO_2{\cdot}10Na_2O{\cdot}1Eu_2O_3$ glass at room temperature excited by broadband excitation (Xe lamp) whose wavelength is 394 nm.*

ation (Xe lamp), the spectrum obtained is a superposition of the spectra of the whole ions. If a narrowband light source, such as a laser, is used for excitation, the laser light excites only these ions having $^5D_0 \leftarrow ^7F_0$ energy difference resonant with the laser energy, and fluorescence from this subset of ions is observed (see Fig. 3.2). However, careful considerations are needed about spectral diffusion, i.e., phonon-assisted energy transfer from an excited ion to an un-excited one[78, 82]. In order to suppress this energy transfer as much as possible, the specimen is usually cooled down and a time-resolved measurement is performed.

## 3.3 Experimental

The glass samples used are the same as described in Chapter 1. The fluorescence spectra were measured at room temperature with a Hitachi−850 Fluorescence Spectrophotometer. Measurements of the homogeneous linewidth were carried out by broad band excitation (bandpass: 1nm) using a Xe lamp.

The time-resolved FLN measurements were performed in the following way (see Fig. 3.3): Samples were mounted into a closed-cycle He refrigerator (Iwatani CRT−006−2000) and cooled down to 10 K. The emission was analyzed with a monochromator (Ristu MC−25NP, 25 cm, resolution limit of 2 $cm^{-1}$) equipped with a photomultiplier (Hamamatsu Photonics R955) and a box car integrator (Stanford Research Systems SR250). Pulse excitation was carried out with a dye laser (Spectra Physics PDL−3, operating with a mixture of Rhodamine−6G and Rhodamine−B in methanol) pumped by a pulsed YAG laser (Spectra physics GCR−11). The spectral width and pulse duration were 0.07 $cm^{-1}$ and 6 nsec, respectively.

## 3.4 Results

Figures 3.4(a)–3.4(d) show the positions of the $^5D_0 \rightarrow ^7F_0$ transition peak and their FWHM, $\Delta\nu_{IH}$, at room temperature (designated by symbols and bars, respectively) over a range of glass compositions. These are considered to be the energy-resolved distribution profile of $Eu^{3+}$ ions in these glasses. As a whole, the peak shifts towards a higher energy side as $\Delta\nu_{IH}$ increases.

Figure 3.5 shows the time-resolved FLN spectra of the $^5D_0 \rightarrow ^7F_1$ transition of $Eu^{3+}$ in silicate and borate glasses at 10 K excited at several

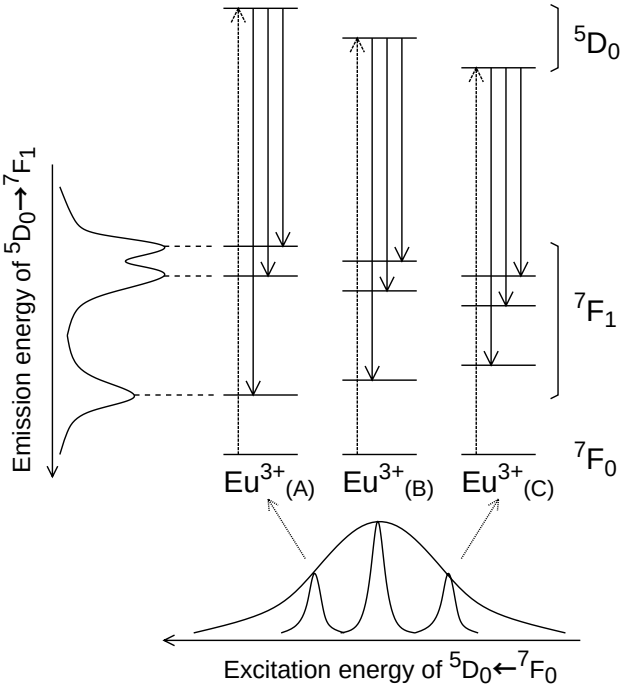


**Fig. 3.2.** *Schematic diagram showing the mechanism of fluorescence line-narrowing. The subscripts, (A)–(C), imply that these ions are located in different local environments.*

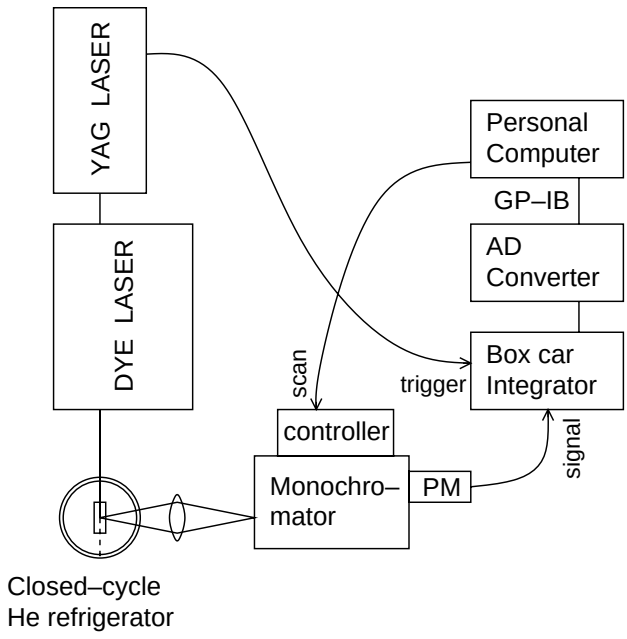


**Fig. 3.3.** *Schematic diagram of the experimental setup for the time-resolved FLN measurement. PM: photomultiplier.*

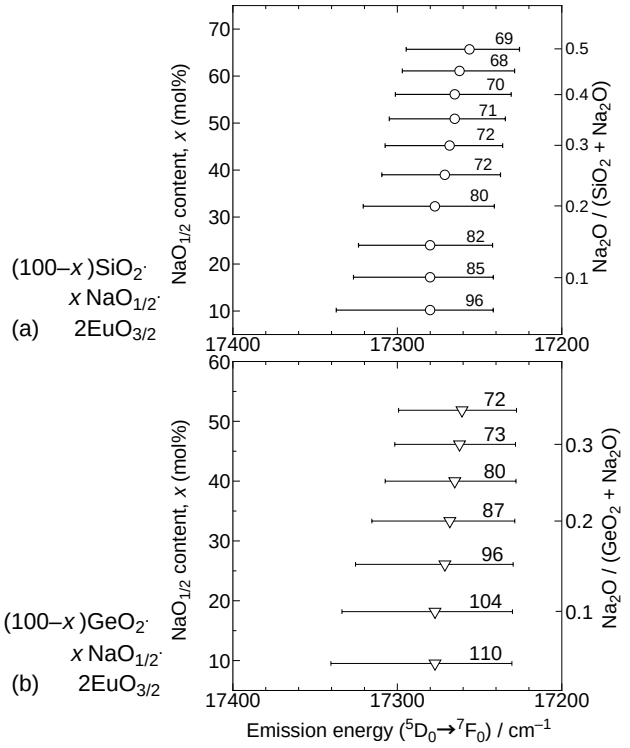


**Fig. 3.4.** *Peak position of the* $^5D_0 \rightarrow {}^7F_0$ *transition of* $Eu^{3+}$ *in sodium (a) silicate, (b) germanate, (c) aluminosilicate, and (d) borate glasses. The length of the bar represents the full width at half-maximum,* $\Delta\nu_{\mathrm{IH}}$*, numerals on the bar are the value of* $\Delta\nu_{\mathrm{IH}}$ *in* $cm^{-1}$ *and the symbols on the bar correspond to the top position of peak. Errors were estimated as* $\pm 5$ $cm^{-1}$*. See also Fig. 4.3 [p.29].*

wavelengths, indicated by triangles, within the inhomogeneously broadened $^5D_0 \rightarrow {}^7F_0$ absorption profile. Gang and Powell[78] reported that some energy transfer surely occurs within a few msec under similar conditions. In order to avoid energy transfer as much as possible, spectra were obtained at 0.2 msec after the exciting laser pulse. The excitation energy dependence of the fluorescence intensity was nearly corresponded to the inhomogeneous broadened peak profile.

Three distinct peaks appear because of the Stark splitting of the $^7F_1$ state, which shows that the $Eu^{3+}$ ions are located in sites with a symmetry of $C_{2v}$ or lower, and these peaks are tentatively denoted as $\epsilon_+$, $\epsilon_-$, and $\epsilon_0$ in order of increasing emission energy, respectively. For borate glasses, however, more than three peaks appeared as shown Fig. 3.5(b), although maximum splitting of the $^7F_1$ level is three. Such a phenomenon has also been reported for lithium borate glasses by Hegarty *et al.*[80], who explained this as due to superposition of fluorescence from two kinds of sites, or phase separation. It was found that as the sodium content decreased, the component with larger splitting width between $\epsilon_+$ and $\epsilon_-$ relatively increased (see Fig. 3.5(b)).

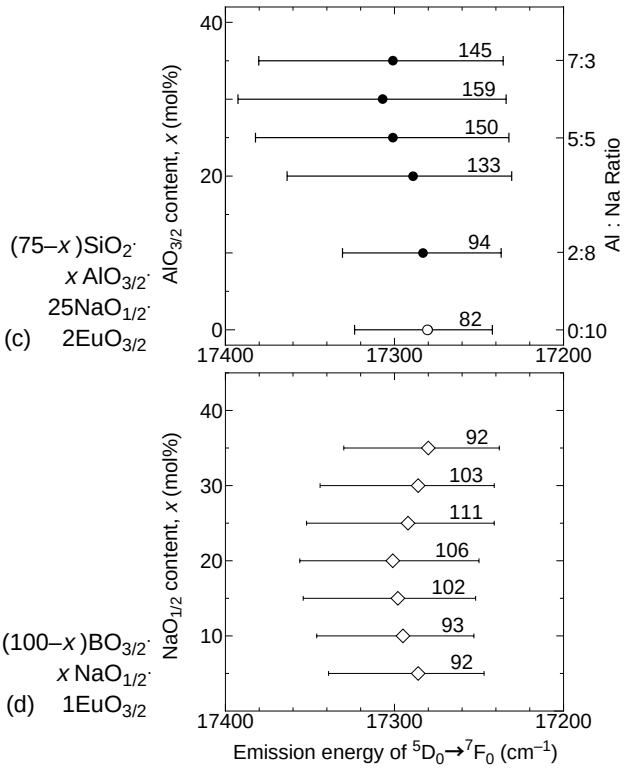


**Fig. 3.4.** *continued*

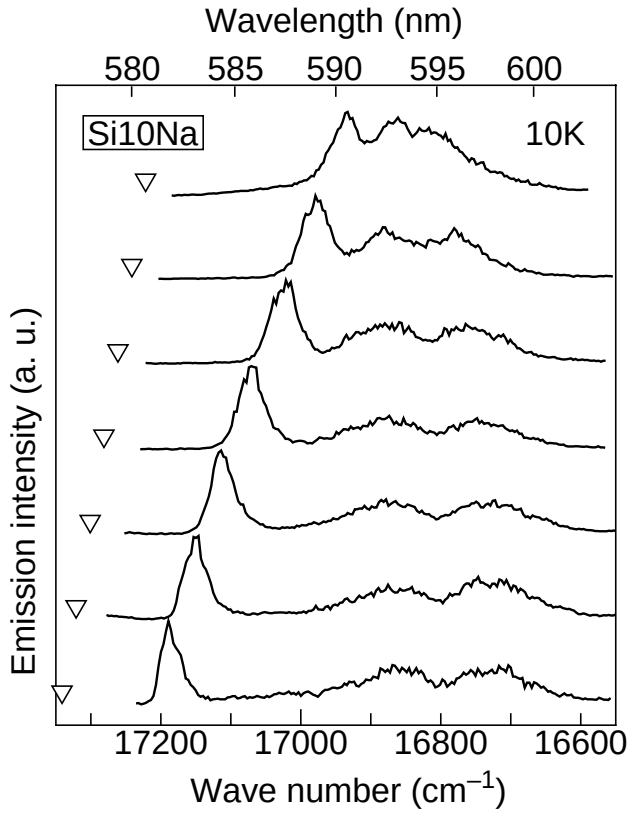


**Fig. 3.5.** *Time-resolved site-selective fluorescence spectra of the* $^5D_0 \rightarrow ^7F_1$ *transition of* $Eu^{3+}$ *in (a)* $81.8SiO_2{\cdot}18.2NaO_{1/2}$ *glass* (Si10Na) *excited by various energies (denoted by triangles) and (b) borate glasses excited at 17322* $cm^{-1}$*. The fluorescence was measured at 10 K and at a delay of 0.2 msec after the laser pulse. The spectra are normalized to the same height.*

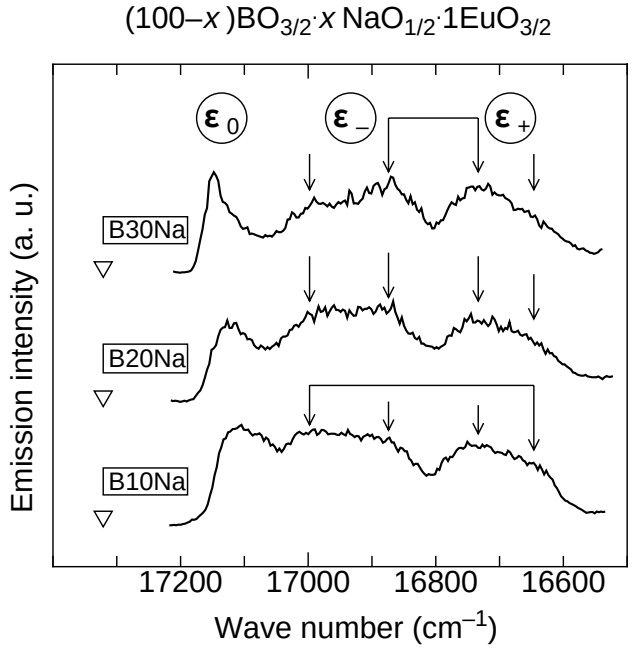


**Fig. 3.5.** *continued*

The peak positions of these three peaks ($\epsilon_+$, $\epsilon_-$, and $\epsilon_0$) were determined by fitting with three Gaussian bands, where an extra weak band due to energy transfer, if needed, was taken into consideration. They are plotted as a function of excitation energy in Figs. 3.6(a)–3.6(d), where the tie lines represent $\Delta\nu_{\rm IH}$, same as the ones shown in Figs. 3.4(a)–3.4(d). The splitting width increases with increasing excitation energy for all the systems. For only the silicate system, this behavior is found to be insensitive to the composition, i.e., all the data points lie on the same three curves. This is not true for other oxide glasses.

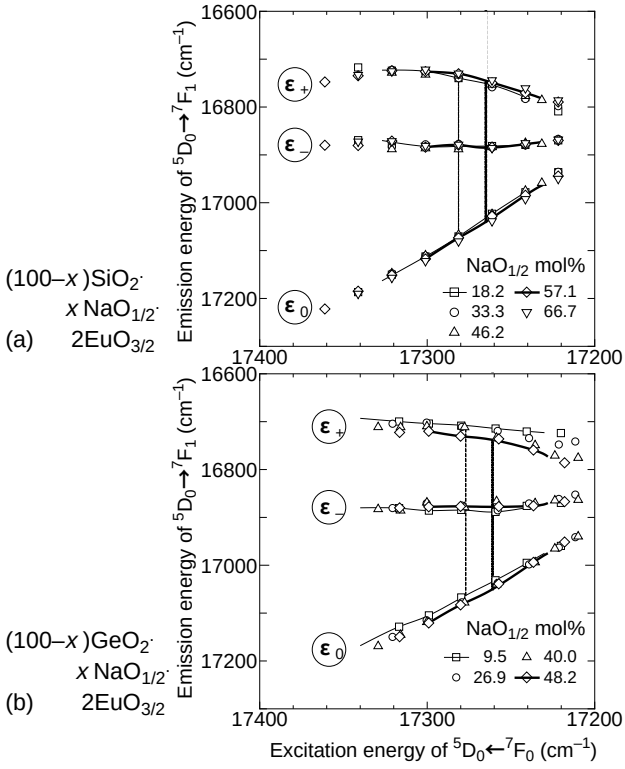


**Fig. 3.6.** *Variation of the splitting of* $^5D_0 \rightarrow ^7F_1$ *transition peak* ($\epsilon_+$, $\epsilon_-$, *and* $\epsilon_0$) *as a function of excitation energy for (a) silicate, (b) germanate, (c) aluminosilicate and (d) borate glasses. Errors are estimated to be equivalent to the size of each symbol. The tie lines represent the fluorescence peak profiles of the* $^5D_0 \rightarrow ^7F_0$ *transition and the vertical lines their peak position (See Figs. 3.4(a)–3.4(d)).*

## 3.5 Discussion

### 3.5.1 Silicate glasses

From the insensitivity of $^7F_1$ splittings on glass composition shown in Fig. 3.6(a), it is concluded that there is a one-to-one correspondence between $^7F_0$ and $^7F_1$ electronic levels in the sodium silicate glass system. In other words, $Eu^{3+}$ ions in silicate glasses with different alkali contents to be excited by a laser light with the same wavelength have the same $^7F_0$ and $^7F_1$ electronic levels. Therefore, $Eu^{3+}$-sites in this silicate glass system are labeled uniquely by one parameter, the $^5D_0 \rightarrow ^7F_0$ transition energy, $\nu_{0-0}$.

Then, it is necessary to identify the property of $Eu^{3+}$ site that determines the value of $\nu_{0-0}$. A number of workers have discussed the problem on the basis of FLN experiments and/or the measurements of homogeneous linewidth, $\Delta\nu_H$. Most of the workers assumed that the symmetry of $Eu^{3+}$ sites in glass is $C_{2v}$ because the number of the crystal field parameters for this symmetry is small enough for practical calculation and the $^7F_1$ level still splits in three in this symmetry. Although, there is no evidence to prove that this symmetry is realistic, the information obtained from this $C_{2v}$ crystal field analysis helps us to carry out further discussion.

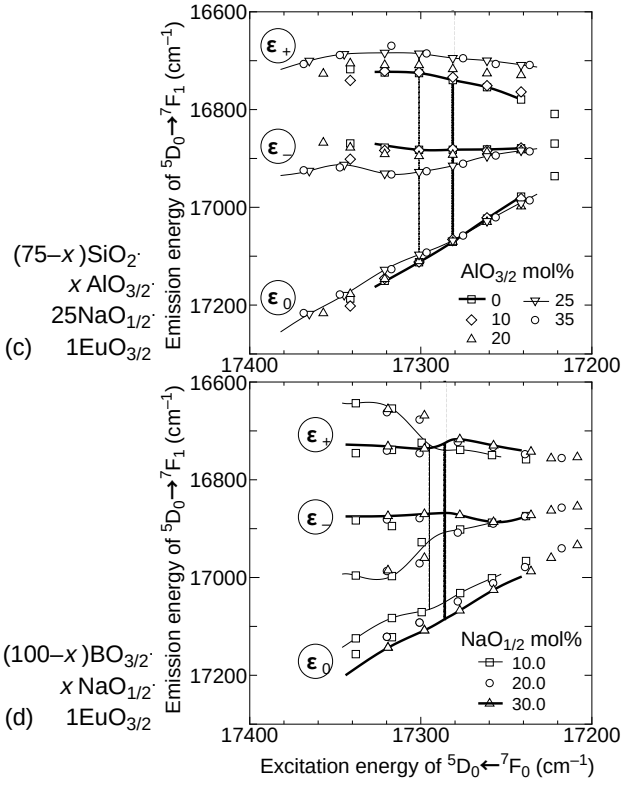


**Fig. 3.6.** *continued; (d) For simplification, the tie lines connect the stronger component of the $\epsilon_\pm$ peaks (See Fig. 3.5(b)).*

Belliveau and Simkin pointed out that there is a rough correlation between the splitting width of the $^7F_1$ level and the Eu–ligand distance on the basis of the estimation of the crystal field parameter for a $C_{2v}$ field[77], namely, the splitting width increases with decreasing the Eu–ligand distance. In other words, the Eu–ligand distance decreases with an increase of $\nu_{0-0}$.

Moreover, there are some experimental data supporting this result. Avouris *et al.* and some workers succeedingly showed that there was a general increase in homogeneous linewidth, $\Delta\nu_H$, with increasing the transition frequency, $\nu_{0-0}$, within the inhomogeneous profile[40, 74, 81]. This was assumed to be due to a site-dependent electron-phonon coupling strength, i.e., the coupling strength between ligands and $f$-electrons, which is expected to increase as the ligand approaches to $Eu^{3+}$ ion. It should be noted, however, that the anisotropy of $f$-orbitals may cause some directional dependence of the coupling strength. Consequently, it is concluded that Eu−ligand distance generally decreases with increasing $\nu_{0-0}$. Since a reduction in Eu−ligand distance necessarily reduces the volume available for coordination, it is reasonable to conclude that the coordination number (CN) of $Eu^{3+}$ ions decreases with increasing $\nu_{0-0}$.

Now it is possible to consider the relation between inhomogeneous linewidth and local structure in terms of $\nu_{0-0}$. Inhomogeneous broadening of fluorescence spectra is caused by overlapping $4f$ electronic levels of the RE ions that are located in various sites in glass matrix. Electronic levels are mainly determined by the configuration of coordinating ions, that is, ions within the first coordination shell. Therefore, the behavior of $\Delta\nu_{IH}$ for the silicate system shown in Fig. 3.4 tells that the inhomogeneity in configuration of ligands increases with decreasing $Na_2O$ content. Further, it was found that the peak energy increases with decreasing alkali content. Therefore, it is concluded that the population of low-CN sites increases with increasing alkali content.

As discussed in Chapter 2, it is expected that $Eu^{3+}$ ions should attract more than three NBOs regardless of the $Na^+$ concentration in the glass matrix. However, in low-alkali compositions, it is

difficult for $Eu^{3+}$ ions to attract NBOs not only because of the low NBO concentration but also the low flexibility of the glass network. As the alkali content decreases, the number of NBOs in $SiO_{4/2}$ tetrahedra decreases and the intertetrahedra linkage increases (see Fig. 3.7), which brings about lower network flexibility. This decrease of local network flexibility should lead to an increase in the population of $Eu^{3+}$ sites with a lower number of surrounding NBOs. At the same time, the CN of $Eu^{3+}$ ions should decrease because further BO coordinating in compensation for lacking NBO is less probable because of the bulky nature of the linked tetrahedra. Consequently, the increase of the population of low-CN sites leads to an increase of the linewidth. Although the IS is sensitive to CN and Eu−ligand distance as described in Chapter 2, $\delta$ did not show a compositional dependence because both Eu−ligand distance and CN decrease with increasing $\nu_{0-0}$, namely, the electron donation ability of ligands increases with decreasing Eu−ligand distance but decreases with decreasing the number of NBOs around $Eu^{3+}$.

Thus, it is concluded that the inhomogeneous linewidth increases with decreasing the amount of NBOs. This is most likely due to a decrease of the flexibility of local glass network, which is related to a decrease of both NBO concentration and the number of the intertetrahedra linkage around RE ions.

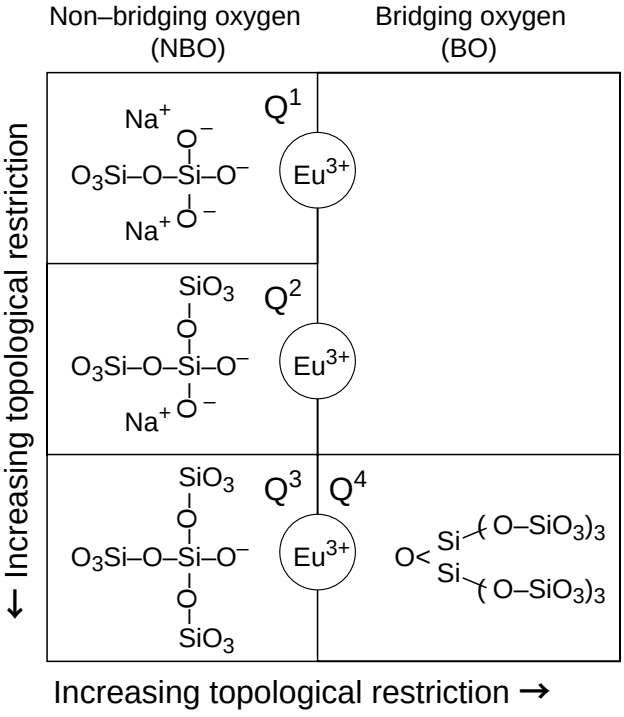


**Fig. 3.7.** *A schematic diagram showing the flexibility of silicate glass network around $Eu^{3+}$. The flexibility decreases with increasing the amount of oxygen linked with another $SiO_{4/2}$ tetrahedra, i.e., in the order of $Q^1 < Q^2 < Q^3 < Q^4$.*

### 3.5.2 Other oxide glasses

The $^7F_1$ splittings for the glasses other than silicate glasses give the compositional dependence as shown in Figs. 3.6(b)–3.6(d). This is because of occurrence of the succeeding change in ligand character as described in Chapter 2. Therefore, unlike the silicate system, $\nu_{0-0}$ can not be used as a universal parameter to identify each site. The compositional dependence of $\Delta\nu_{\mathrm{IH}}$ can be, however, also explained for these systems by using the idea of the flexibility of local glass network.

#### Germanate glasses

The inhomogeneous linewidth for this system varies similarly to the silicate system but the value is larger. This is most likely due to the effect of $GeO_{6/2}$ units on network flexibility. The appearance of $GeO_{6/2}$ units with increasing $Na_2O$ up to a certain amount brings about not only reducing the NBO concentration around $Eu^{3+}$ ions but also increasing the interpolyhedra linkage of local glass network. Namely, the number of the linkage points of $GeO_{6/2}$ units is larger than those of $GeO_{4/2}$ units, as shown in Figs. 3.8[(b), (c), and (d)]. Thus, the value of $\Delta\nu_{\mathrm{IH}}$ of the germanate system becomes larger than that of the silicate system.

Let us examine Fig. 3.4(b). The increase of population with larger $^7F_1$ splitting width with decreasing $Na_2O$ content is probably due to an increase of low-CN cites similar to the silicate system. The reduced NBO donating ability should make low-CN sites increase because the replacement of a NBO with a BO is not easy.

#### Aluminosilicate glasses

The increase of $\Delta\nu_{\mathrm{IH}}$ for the aluminosilicate system is also explained in terms of the network flexibility, which decreases with increasing $AlO_{n/2}^{(n-3)-}$ macroanion content. The value of $\Delta\nu_{\mathrm{IH}}$ increases significantly and becomes the largest of all the systems in this study because of the following reasons. (1) The content

of macroanions in the aluminosilicate system is large; the maximum fraction of macroanions, such as $GeO_{6/2}^{2-}$, $AlO_{n/2}^{(n-3)-}$ and $BO_{4/2}^{-}$, are 45% in $65B_2O_3{\cdot}35Na_2O$[71], 25% in $80GeO_2{\cdot}20Na_2O$[72], and 43% in $40SiO_2{\cdot}30AlO_{3/2}{\cdot}25NaO_{1/2}$ ($0.43 = 30/(30+40)$; all of the aluminum ions become macroanions). (2) All of the polyhedra in aluminosilicate glasses, $AlO_{n/2}^{(n-3)-}$ and $SiO_{4/2}$, are more than three-hold unlike the borate system ($BO_{3/2}$ and $BO_{4/2}$). A small decrease in the most Al-rich region is probably due to another decrease in flexibility caused by Al−O−Al bonding since the $Al_2O_3$ content is as much as that of $SiO_2$ in the composition.

Similar to the germanate system, the low-CN cites population probably increases with increasing Al content increases as shown in Figs. 3.4(c). This is consistent with the Mössbauer result described in Chapter 2, where it was mentioned that the substitution of Al for Si leads to a decrease of NBO−$Na^+$ pairs and an increase of BOs(Al−O−Si) within the first coordination shell of $Eu^{3+}$ ions.

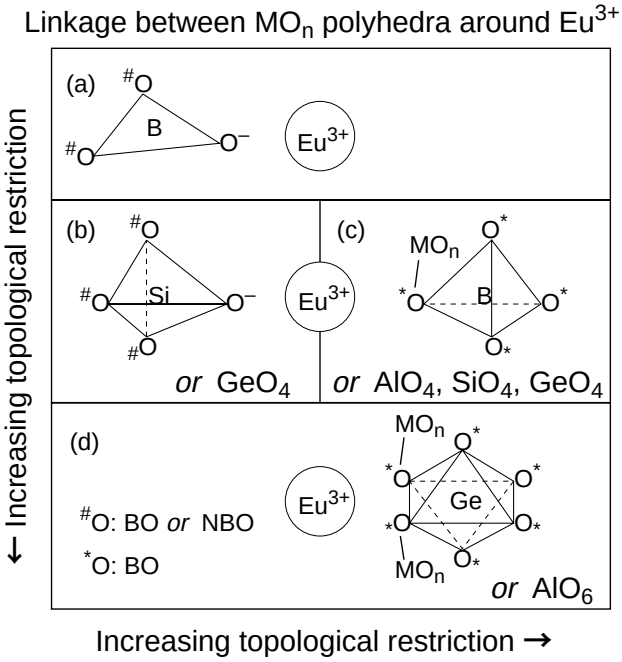


**Fig. 3.8.** *A schematic diagram showing the flexibility of glass network around $Eu^{3+}$. The flexibility decreases with increasing the amount of oxygen linked with another $MO_n$ polyhedra, i.e., increasing CN or decreasing the amount of NBO in a polyhedron.*

**Borate glasses**

In contrast to other systems, $\Delta\nu_{\rm IH}$ of the borate system reaches a maximum value in the middle of the range. Morgan *et al.*[74] reported that there are two maximum points in this system. However, they defined $\Delta\nu_{\rm inh}$ as the half-width at half-maximum measured on the high-energy side, which does not reflect the whole inhomogeneous broadening. As the alkali content increases, the population of $BO_{4/2}$ tetrahedra increases, which reduces the flexibility of the glass network because they possess more linkage points with other polyhedra than do the $BO_{3/2}$ triangles (see Figs. 3.8(a) and 3.8(b)). Thus, in $Na_2O$-poor compositions the value of $\Delta\nu_{\rm IH}$ increases with $Na_2O$ content as the lattice stiffens, while in $Na_2O$-rich compositions, it decreases because the NBO content starts to increase.

## 3.6 Conclusion

The relation between the inhomogeneous linewidth of $Eu^{3+}$ fluorescence and the local structure around $Eu^{3+}$ ions in several oxide glasses was investigated. For silicate glasses, the inhomogeneous linewidth of the $^5D_0 \rightarrow {}^7F_0$ transition, $\Delta\nu_{\rm IH}$, showed a compositional dependence, increasing with decreasing alkali content. On the basis of the change of the $^7F_1$ splitting width within the inhomogeneous profile, this was attributed to a decrease in the flexibility of the local glass network, which is related with the structure outside of the first coordination shell, i.e., the degree of the interpolyhedra linkage. As the NBO content decreases, the population of $Eu^{3+}$ ions having low coordination number increases, which brings about the increase in $\Delta\nu_{\rm IH}$. This was found to be also the case for other oxide glasses, such as borate, germanate and aluminosilicate glasses, but the effect of macroanions should be also considered. A formation of macroanions leads to a decrease in network flexibility by consuming NBOs and increasing the interpolyhedra linkages. Consequently, it is concluded that the inhomogeneous broadening of $Eu^{3+}$ fluorescence for oxide glasses increases with decreasing the flexibility of the local glass network.

# Chapter 4

# Origin of inhomogeneous linewidth of $Eu^{3+}$ fluorescence II.

— Phosphate and borophosphate system

## 4.1 Introduction

Through the discussion in Chapter 3 for some typical oxide glasses, it was revealed that the inhomogeneous linewidth of fluorescence is strongly dependent on the flexibility of local glass network. The glasses dealt with were, however, restricted to ones where each ion is linked with others by a single bond. There left another typical oxide glasses where each network forming cation has a doubly bonded oxygen (DBO), i.e., phosphate glasses.

In general, phosphorus ions in phosphate glasses retain four-fold coordination[83]. Classically, a Q-site model has been proposed to describe the structure of phosphate glasses in a similar manner for silicate systems as follows,

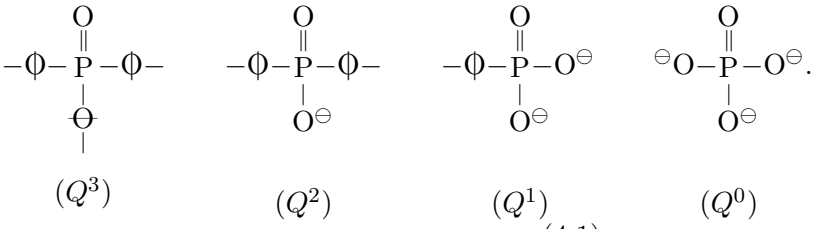

$(Q^3)$ $(Q^2)$ $(Q^1)$ $(Q^0)$ (4.1)

Since the DBO could be resonant with other NBOs, the following structures have been also proposed.

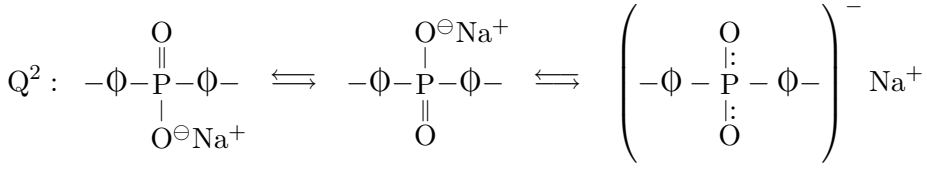

(4.2)

$$\mathrm{Q}^1: \quad -\phi - \underset{\underset{\mathrm{O^{\ominus}Na^{+}}}{|}}{\overset{\overset{\mathrm{O}}{\|}}{\mathrm{P}}} - \mathrm{O^{\ominus}Na^{+}} \quad \rightleftharpoons \quad -\phi - \underset{\underset{\mathrm{O^{\ominus}Na^{+}}}{|}}{\overset{\overset{\mathrm{O^{\ominus}Na^{+}}}{|}}{\mathrm{P}}} = \mathrm{O} \quad \rightleftharpoons \quad -\phi - \underset{\underset{\mathrm{O}}{\|}}{\overset{\overset{\mathrm{O^{\ominus}Na^{+}}}{|}}{\mathrm{P}}} - \mathrm{O^{\ominus}Na^{+}}$$

$$\uparrow\downarrow \qquad (4.3)$$

$$\left( -\phi - \underset{\underset{\mathrm{O}}{|:}}{\overset{\overset{\mathrm{O}}{|:}}{\mathrm{P}}} = \mathrm{O} \right)^{2-} \quad 2\mathrm{Na^{+}}$$

$$\mathrm{Q}^0: \quad \left( \mathrm{O} = \underset{\underset{\mathrm{O}}{|:}}{\overset{\overset{\mathrm{O}}{|:}}{\mathrm{P}}} = \mathrm{O} \right)^{3-} \quad 3\mathrm{Na^{+}} \qquad (4.4)$$

At any rate, since the double bonds terminate the network linkage, the flexibility of these glass networks is expected to be relatively higher. Compositional dependence of the $\mathrm{Q}^n$ fraction for an alkali phosphate system has been determined by $^{31}$P MAS-NMR[84] and Raman spectroscopy[85] as shown in Fig. 4.1.

An borophosphate system is also interesting because crystalline $BPO_4$ consists of the following $BPO_4$ units,

$$-\phi - \underset{\underset{\mathrm{O}}{|}}{\overset{\overset{\mathrm{O}}{|}}{\mathrm{B^{\ominus}}}} - \mathrm{O} - \underset{\underset{\mathrm{O}}{|}}{\overset{\overset{\mathrm{O}}{|}}{\mathrm{P^{+}}}} - \phi -, \qquad (4.5)$$

which construct a silica-like structure. At the early stage of the investigation, it was believed that the borophosphate glass network also consisted of $BPO_4$ units[86]. Recently, however, it was found some evidence showing that the $BPO_4$ model is partly insufficient to explain various properties. Scagliotti and Villa *et al.* concluded from the results of Raman and $^{31}$P MAS-NMR spectroscopy that the oxygens introduced with alkali oxide are preferentially taken by phosphate units to form $\mathrm{Q}^2$ and/or $\mathrm{Q}^1$ units[87, 88]. A Raman study by Osaka *et al.*[89] revealed that $BO_{3/2}$ and $PO_{5/2}(\mathrm{Q}^3)$ units coexist instead of crystalline

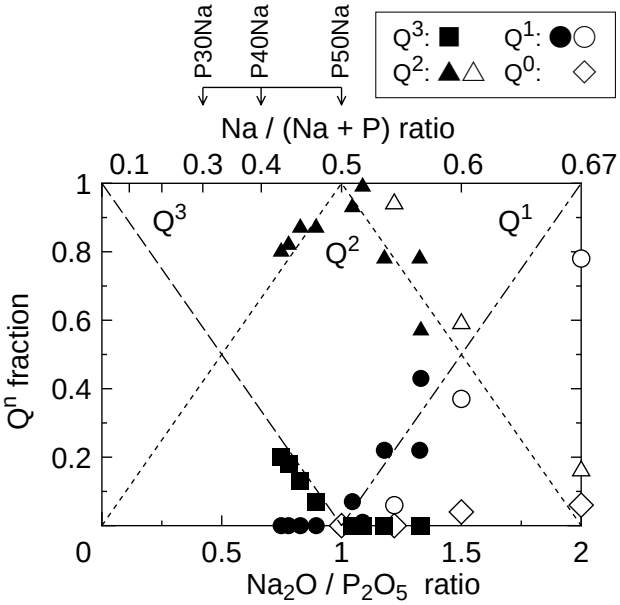


**Fig. 4.1.** *Compositional dependence of the fraction of $Q^n$ sites in $M_2O$+$H_2O$+$P_2O_5$(M: alkali metal) glasses as determined by $^{31}$P MAS-NMR (solid symbols, Brow et al.[84]) and Raman spectroscopy (open symbols, Tatsumisago et al.[85]). The lines represent the calculated fractions based on the assumption that the equilibrium constants of the following equations are zero, i.e., the reactions go on the right side.*

$$2\mathrm{Q}^3 + \mathrm{M_2O} \overset{K_1}{\rightleftharpoons} 2\mathrm{Q}^2$$

$$2\mathrm{Q}^2 + \mathrm{M_2O} \overset{K_2}{\rightleftharpoons} 2\mathrm{Q}^1$$

$BPO_4$ type network as follows,

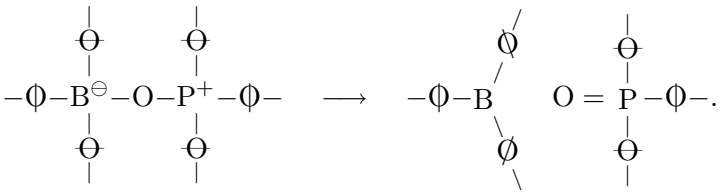

$(Q^3)$

(4.6)

In the present chapter, the local structure around $Eu^{3+}$ ions in such glass networks containing DBOs is investigated by using the techniques described in the previous chapters.

## 4.2 Experimental

The glass samples employed in the present chapter are listed in Table 4.1. 1 mol% of $EuO_{3/2}$ was added to each batch composition. Hereafter, series (b) and (c) are denoted as B–P system and Na system, respectively. The glasses were prepared from reagent grade $P_2O_5$, $B_2O_3$, $Na_2CO_3$, and $Eu_2O_3$ by mixing and melting in platinum or alumina crucibles in a SiC resistance furnace at temperatures between 700 and 1300 °C for 20 to 30 min. Alumina crucibles were used for the batches including more than 27% of $PO_{5/2}$. The melt was poured on a stainless-steel plate and then quenched in air.

The fluorescence of the $^5D_0 \rightarrow ^7F_0$ and the phonon sideband associated with $^5D_2 \leftarrow ^7F_0$ were measured. For Na system, site-selective fluorescence spectra and Mössbauer spectra were measured in order to compare with the silicate system in Chapter 3. Their experimental procedures were described in the previous chapters.

## 4.3 Results

The fluorescence peak profiles of the $^5D_0 \rightarrow ^7F_0$ transition of $Eu^{3+}$ are shown in Figs. 4.2(a)–4.2(c). For comparison with other glass systems, the compositional dependence of $\Delta\nu_{\mathrm{IH}}$ for the borophosphate (Na system) and phosphate systems is shown in Fig. 4.3. The linewidth for the phosphate system is smaller than that for any other oxide system. The phonon sideband spectra of $Eu^{3+}$ in these glasses are shown in Figs. 4.4–4.6. Unlike the systems treated in Chapter 1, PSB associated with the $^5D_2 \leftarrow ^7F_0$ transition is measured because this line can be regarded as a singlet (compare with Fig. 1.1 [p.5]).

**Table 4.1.** *Composition of the glasses used in this study (mol%). Each sample contains 1 mol% of $EuO_{3/2}$.*

(a) phosphate glasses

| $PO_{5/2}$ | $NaO_{1/2}$ | $\frac{Na_2O}{Na_2O+P_2O_5}$ | notation |
|---|---|---|---|
| 70.0 | 30.0 | 0.30 | P30Na |
| 60.0 | 40.0 | 0.40 | P40Na |
| 50.0 | 50.0 | 0.50 | P50Na |

(b) borophosphate glasses (B–P system; $\frac{Na}{P+B}$=const.)

| $BO_{3/2}$ | $PO_{5/2}$ | $NaO_{1/2}$ | $\frac{B_2O_3}{B_2O_3+P_2O_5}$ | notation |
|---|---|---|---|---|
| 70.0 | 0.0 | 30.0 | 1.00 | B30Na |
| 65.0 | 5.0 | 30.0 | 0.93 | |
| 55.0 | 15.0 | 30.0 | 0.79 | |
| 45.5 | 25.0 | 30.0 | 0.64 | |
| 35.0 | 35.0 | 30.0 | 0.50 | BP30Na |
| 25.0 | 45.0 | 30.0 | 0.36 | |
| 15.0 | 55.0 | 30.0 | 0.21 | |
| 5.0 | 65.0 | 30.0 | 0.07 | |
| 0.0 | 70.0 | 30.0 | 0.00 | P30Na |

(c) borophosphate glasses (Na system; P/B=const.)

| $BO_{3/2}$ | $PO_{5/2}$ | $NaO_{1/2}$ | $\frac{Na_2O}{Na_2O+BPO_4}$ † | notation |
|---|---|---|---|---|
| 40.0 | 40.0 | 20.0 | 0.20 | BP20Na |
| 37.5 | 37.5 | 25.0 | 0.25 | BP25Na |
| 35.0 | 35.0 | 30.0 | 0.30 | BP30Na |
| 32.5 | 32.5 | 35.0 | 0.35 | BP35Na |
| 30.0 | 30.0 | 40.0 | 0.40 | BP40Na |
| 27.5 | 27.5 | 45.0 | 0.45 | BP45Na |

† This is equivalent with $\frac{NaO_{1/2}}{NaO_{1/2}+(BPO_4)_{1/2}}$

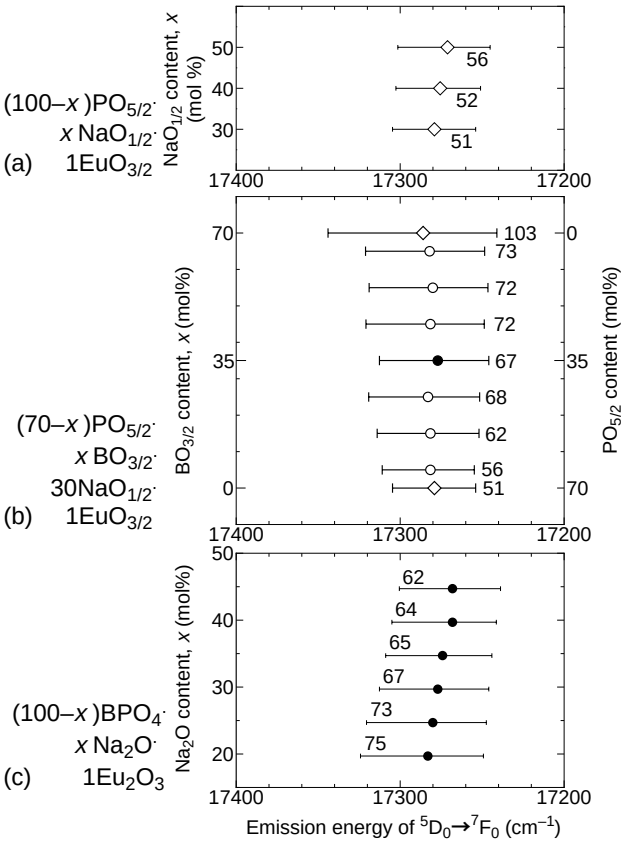


**Fig. 4.2.** *Peak position of the* $^5D_0 \rightarrow ^7F_0$ *transition of* $Eu^{3+}$ *for (a) phosphate glasses, (b)* B–P system, *and (c)* Na system. *The length of the bar represents the full width at half-maximum,* $\Delta\nu_{\mathrm{IH}}$*, numerals on the bar are the value of* $\Delta\nu_{\mathrm{IH}}$ *in* $cm^{-1}$ *and the symbols on the bar correspond to the top position of peak. Errors were estimated as* $\pm 5$ $cm^{-1}$.

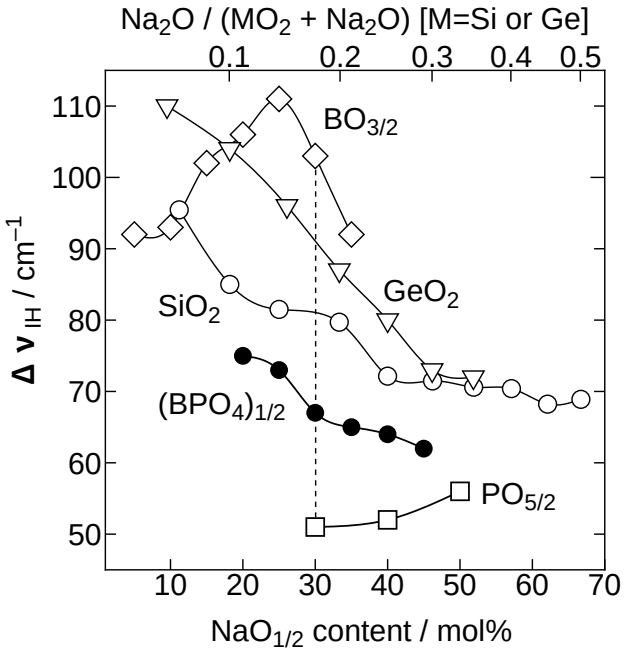


**Fig. 4.3.** *Compositional dependence of the linewidth of the* $^5D_0 \rightarrow ^7F_0$ *transition of* $Eu^{3+}$*,* $\Delta\nu_{\mathrm{IH}}$*, in several oxide glasses. The dashed line represents* B–P system.

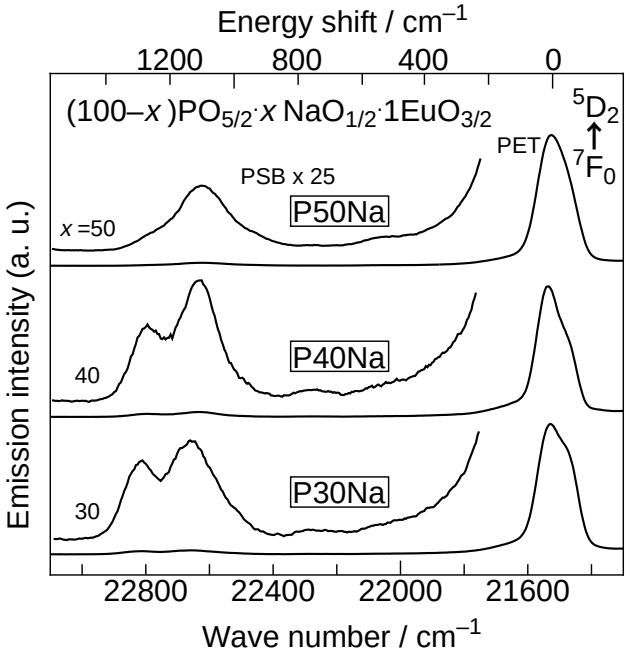


**Fig. 4.4.** *Phonon sideband spectra associated with* $^5D_2 \leftarrow ^7F_0$ *transition of* $Eu^{3+}$ *in sodium phosphate glasses at room temperature by monitoring* $^5D_0 \rightarrow ^7F_2$ *emission at 612 nm.*

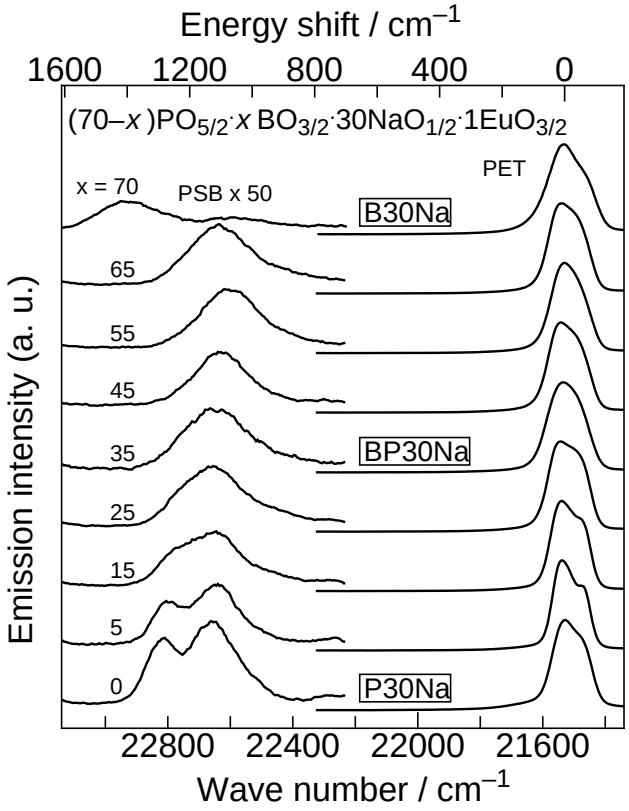


**Fig. 4.5.** *Phonon sideband spectra associated with* $^5D_2 \leftarrow ^7F_0$ *transition of* $Eu^{3+}$ *in sodium borophosphate glasses* (B–P system) *at room temperature by monitoring* $^5D_0 \rightarrow ^7F_2$ *emission at 612 nm.*

## 4.4 Discussion

### 4.4.1 Phosphate glasses

In the phonon sideband spectra shown in Fig. 4.4, two kinds of peaks were found, i.e., 1300 $cm^{-1}$ and 1100 $cm^{-1}$, and the relative intensity of the former peak decreased with increasing alkaline content. For the RE-free phosphate glasses in this compositional region (see Fig. 4.1), the amount of $Q^3$ units decreases and that of $Q^2$ units increases with an increase of $Na_2O$ content. Considering the peak assignments of Raman and infrared spectroscopy for RE-free phosphate glasses listed in Table 4.2, these two peaks are reasonably assigned as $Q^3$ and $Q^2$, respectively. The phonon energy estimated by PSB is lower than that of the corresponding vibration listed in Table 4.2 again, which is, as described in Chapter 1, due to the large effective mass of the local vibration system.

The compositional dependence of DBO amount around $Eu^{3+}$ ions seems to be related with a small increase of $\Delta\nu_{IH}$ in the sodium-rich composition. As a ligand, Coulombic interaction between DBO and $Eu^{3+}$ and/or other ligands is expected to be small because DBO has no formal charge. Thus,

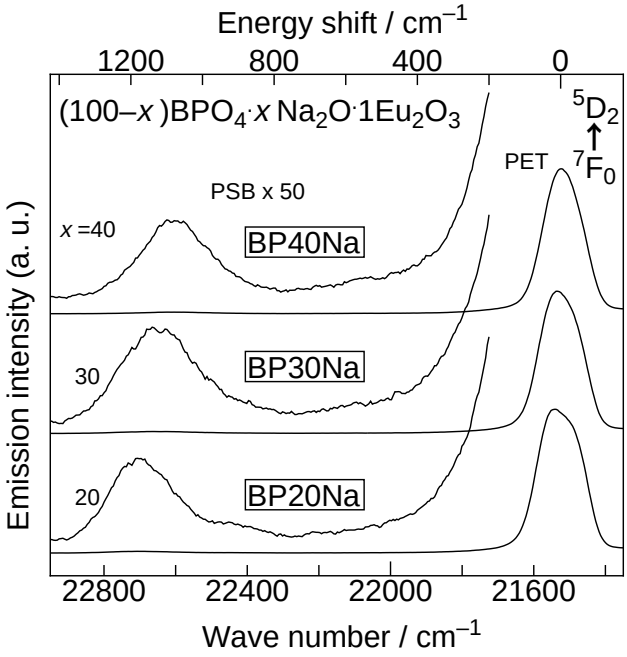


**Fig. 4.6.** *Phonon sideband spectra associated with* $^5D_2 \leftarrow ^7F_0$ *transition of* $Eu^{3+}$ *in sodium borophosphate glasses* (Na system) *at room temperature by monitoring* $^5D_0 \rightarrow ^7F_2$ *emission at 612 nm.*

if some DBOs join the first coordination shell of $Eu^{3+}$, the local flexibility of glass matrix should be large. Therefore, $\Delta\nu_{IH}$ increases with decreasing DBO amount, i.e., decreasing the relative intensity of 1300 $cm^{-1}$ peak in the PSB spectrum. Similar situation is also observed for B–P system in the $P_2O_5$-rich composition range.

Consequently, it is concluded that the small linewidth for phosphate system is due to the presence of DBOs. DBOs out of the coordination shell terminates the interpolyhedra linkage of surrounding glass network and DBOs within the shell interacts weakly with other ions, both of which increases the local flexibility of glass network.

### 4.4.2 Borophosphate glasses

#### B–P system

It is surprising that a small addition of $P_2O_5$ (5 mol%) to borate glass (B–P system) leads to a significant decrease of $\Delta\nu_{IH}$ as shown in Fig. 4.2. A corresponding change is also observed for PSB as shown in Fig. 4.5. The 1400 $cm^{-1}$ peak for borate glass ($x = 70$), assigned as NBO and BO in $BO_{3/2}$ units[45, 91] (see Table 4.3) disappeared with incorporating 5 mol% of $P_2O_5$ and instead, a new peak of 1100 $cm^{-1}$ appeared. This peak exists in all the spectra except $x = 70$ and corresponds to the vibration energy of $Q^2$ unit for phosphate glasses (see Table 4.2). This frequency also matches the vibration of tetraborate groups (1050 $cm^{-1}$; IR) and diborate groups (1120 $cm^{-1}$; Raman) for RE-free borate glasses[91](see Table 4.3), but it is not probable because there is no distinct corresponding peak for the PSB of $x = 70$. Further, as mentioned above, it is reported that $Q^2$ units are present[87, 88] but $B-O^{\ominus}$ is absent[86, 89] in this composition. Thus, this is most likely due to a preferential coordination of NBOs, i.e., $P-O^{\ominus}$ in $Q^2$. Considering the local charge compensation of the positive charge of $Eu^{3+}$, it is reasonable that $Eu^{3+}$ ions attract phosphate units with NBOs. Therefore, the significant decrease of $\Delta\nu_{IH}$ with a small addition of $P_2O_5$ (5 mol%) to borate glass is most likely caused by the change of the surrounding glass network, a rigid borate network to a flexible phosphate network.

#### Na system

The compositional dependence of $\Delta\nu_{IH}$ for Na system is similar to that for the silicate system described in Chapter 3, i.e., $\Delta\nu_{IH}$ increases with a decrease in sodium content (see Fig. 3.4 [p.21] and Fig. 4.3). Throughout the composition range, $\Delta\nu_{IH}$ for Na system is smaller than that of the silicate system. This is probably because borophosphate network contains DBOs which increases the flexibility of glass matrix.

Besides the behavior of $\Delta\nu_{IH}$, both the isomer shift of $^{151}Eu^{3+}$, $\delta$, and the splitting of the $^7F_1$ level determined by site-selective fluorescence spectra show compositional independences similar to those of the silicate system (see Figs. 4.7, 4.8, and 3.6 [p.22]). These results might be reasonably explained if the structure of borophosphate glasses were similar to that of silicate glasses due to the presence of $BPO_4$ units, but this explanation contradicts the Raman and NMR results mentioned above. The PSB spectra for this system show that the $Q^2$ vibration is also dominant similar to B–P system (see Fig. 4.6). The shift from 1200 $cm^{-1}$ to 1100 $cm^{-1}$ of this peak is probably due to the minor contribution of $Q^3$ units, which is, according to Osaka *et al.*[89], present in this system and decreases with an increase of $Na_2O$ content. Thus, in analogy with silicate system, it is assumed that this compositional independence is due to the preferential coordination of NBO of $PO_{4/2}$ tetrahedra. That is, regardless of the NBO concentration of glass matrix, $Eu^{3+}$ ions attract a certain amount of NBO for compensation of their positive charge.

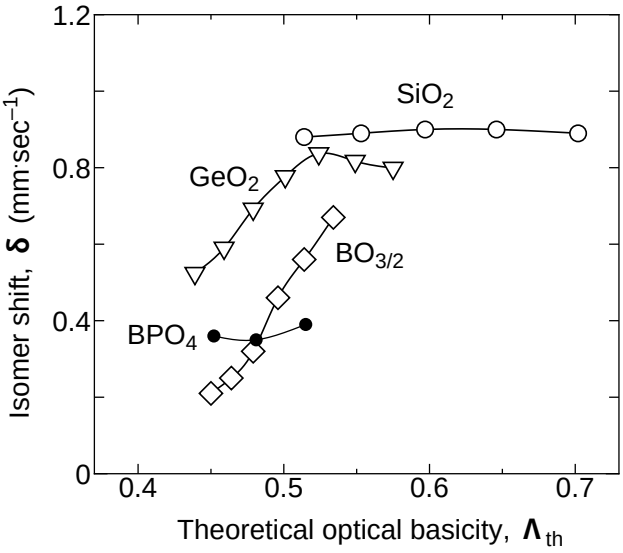


**Fig. 4.7.** *Relationship between the isomer shift of $^{151}Eu^{3+}$ and the theoretical optical basicity, $\Lambda_{th}$, of the host glass.*

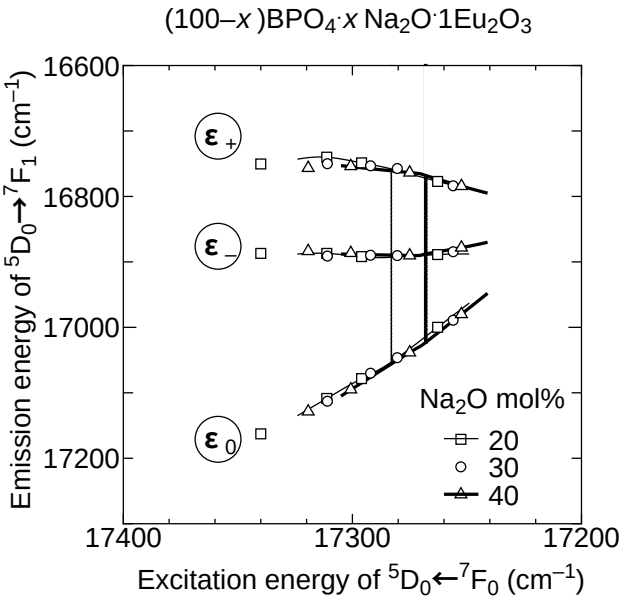


**Fig. 4.8.** *Variation of the splitting of* ${}^5D_0 \rightarrow {}^7F_1$ *transition peak* ($\epsilon_+$, $\epsilon_-$, *and* $\epsilon_0$) *as a function of excitation energy for borophosphate glasses. Errors are estimated to be equivalent to the size of each symbol.*

**Table 4.2.** *Assignment of various bands in the vibrational spectra for phosphate crystals and glasses.*

| Raman[†] | | IR[‡] | |
|---|---|---|---|
| $\hbar\omega/\mathrm{cm}^{-1}$ | assignment | $\hbar\omega/\mathrm{cm}^{-1}$ | assignment |
| 1390 | sym. stretch of $Q^3$ | | |
| 1165 | sym. stretch of $Q^2$ | 1300–1250 | asym. stretch of $Q^2$ |
| 1025 | sym. stretch of $Q^1$ | 1120–1080 | asym. stretch of $Q^1$ |
| 945 | sym. stretch of $Q^0$ | 940–860 | P–O–P asym. stretch |

[†] Martin[83]. [‡] Rulmont *et al.*[90].

**Table 4.3.** *Assignment of various bands in the vibrational spectra for borate glasses (Kamitsos et al.[91]).*

| Raman | | IR | |
|---|---|---|---|
| $\hbar\omega/\mathrm{cm}^{-1}$ | assignment | $\hbar\omega/\mathrm{cm}^{-1}$ | assignment |
| | | —$BO_3$ stretching— | |
| 1430–1500 | $B-O^{\ominus}$ bonds | 1420–1550 | $B-O^{\ominus}$ bonds |
| | attached to large | 1350–1400 | B−O vibration of various borate rings |
| | borate groups | 1250 | boroxol rings and tetraborate groups |
| | | —$BO_4$ stretching— | |
| 1120 | diborate groups | 1050 | tetraborate groups |
| | | 900–1000 | diborate groups |
| 805 | boroxol rings | 880 | tetraborate groups |

## 4.5 Conclusion

The compositional dependence of inhomogeneous linewidth of $Eu^{3+}$ fluorescence for a borophosphate system was investigated and the relation with the local structure was discussed. The glasses containing $Q^3$ units ($PO_{4/2}$ with one DBO) showed the narrowest linewidth among the oxide glasses dealt with in the present thesis. This was assumed to be due to the increased flexibility of glass network by DBOs. It was also concluded that $Eu^{3+}$ ions are preferentially surrounded by NBOs of $PO_{4/2}$ tetrahedra even in the glass with 5 mol% of $P_2O_5$ due to the local charge compensation by NBOs.

Through the discussions of the previous and present chapters, it was revealed that the inhomogeneous linewidth of $Eu^{3+}$ fluorescence is significantly related with the flexibility of local glass network (summarized in Fig. 4.9). Both NBO concentration in matrix and the degree of interpolyhedra linkages around $Eu^{3+}$ ions are associated with the flexibility of local glass network. The former increases with an increase of alkali content and a decrease of macroanion content such as $BO^-_{4/2}$, $AlO^{(n-3)-}_{n/2}$, and $GeO^{2-}_{6/2}$ polyhedra.

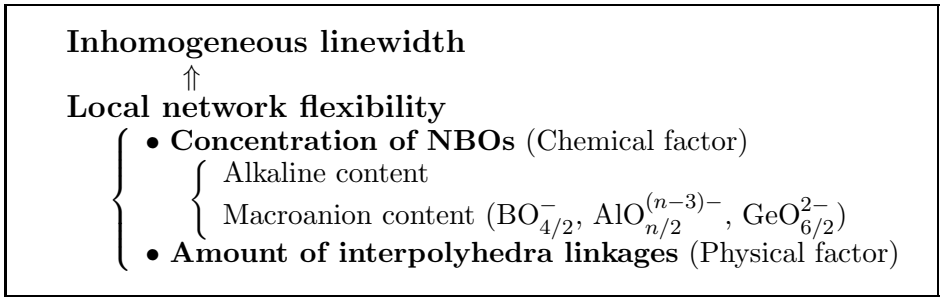


**Fig. 4.9.** *Origin of inhomogeneous linewidth.*

# Chapter 5

# Local vibrational state of $Er^{3+}$ ions in up-conversion fluoride glasses

## 5.1 Introduction

Upconversion fluorescence of rare earth (RE) ions in glass matrix attracts much interest because it has potential to be utilized as a laser light source in the green to blue region pumped by a diode laser[10, 11]. For this purpose, various glass hosts have been examined such as heavy metal fluorides[92], oxyfluorides[93], and oxides[94]. Recently, the room temperature continuous-wave oscillations of some RE-doped fibers have been successively reported[95–98]

In order to design a glass material with higher efficiency in upconversion, it is better to select the glass matrix in which the maximum phonon energy is small, because the nonradiative loss due to multiphonon relaxation is expected to be small. As described in Chapter 1, however, the vibration energy around RE ions in an oxide glass is different from that of the oxide glass matrix. The same is expected to hold for fluoride glasses.

Therefore, in this study, upconversion fluorescence of $Er^{3+}$ in fluoride glasses was measured and the effect of the local vibrational state of RE ions on its efficiency was discussed. Since RE elements resemble each other in atomic weight and ionic radius, the chemical environment is expected to be also similar. Thus, phonon sideband of $Eu^{3+}$ was measured to obtain the energy of local vibration. Further, using molecular dynamic simulation, the vibrational energies of fluoride glass matrix and the local structure around RE ions were calculated. The ionic nature of fluoride glasses is favorable for applying simple two-body ionic potentials. $^{151}$Eu–Mössbauer spectra were also measured in order to estimate the local modification.

## 5.2 Experimental

Three kinds of glasses chosen in the present study were, fluoroaluminate, fluorozirconate, and In- and Pb-based fluoride glasses. Their glass compositions are listed in Table 5.1 with their notations and Er concentrations. Glass batches were prepared by using reagent grade $ZrF_4$, $AlF_3$, $InF_3$, $LaF_3$, $BaF_2$, $CaF_2$, $PbF_2$, and $ErF_3$ or $EuF_3$ as the starting materials. The batch, about 6 g, with a small amount of $NH_4F{\cdot}HF$ was melted in a platinum crucible for 15 min at a suitable temperature. The melt was poured on a stainless-steel plate and pressed with another stainless-steel plate quickly. The glass obtained was about 0.5 mm in thickness.

The fluorescence spectra were measured with a Hitachi–850 fluorescence spectrophotometer. As the ultraviolet and infrared excitation sources, a Xe lamp and a GaAlAs diode laser ($\lambda$=802 nm, SONY SLD302XT) were used, respectively. In order to compare the efficiency of upconversion fluorescence, each sample was cut and polished into the same size, 4 × 6 × 0.36 mm. The laser beam was irradiated perpendicular to the plate. In order to detect fluorescence of 550 nm band clearly, a photomultiplier was mounted in such a way that the laser beam did not enter directly into it, but with a 40° angle from laser line. All the specimens were measured under the same condition.

IR spectra were measured with a Shimadzu FTIR–4100 Fourier-transform infrared spectrophotometer. $^{151}$Eu–Mössbauer spectra were measured at room temperature, using $^{151}Sm_2O_3$ (50 mCi) as a 21.63 keV $\gamma$-ray source. Experimental details were described in Chapter 2. In order to compensate the poor sensitivity due to $\gamma$-ray absorption of heavy metal ions, Eu-rich samples were used in ZBL and IPBL where Eu was

substituted for La in their compositions.

## 5.3 Results

Fig. 5.1 shows the upconversion spectra of $Er^{3+}$-doped samples. Green emission was observed on all three samples. The energy diagram of $Er^{3+}$ is shown in Fig. 5.2, together with an example of electric transitions related to upconversion mechanism with 802 nm excitation. The intensity of the upconversion fluorescence ($^4S_{3/2} \rightarrow {}^4I_{15/2}$ transition) decreased in the order of IPBL, ZBL, and ABC. This decrease was also confirmed by visual observation. The relative intensities of the fluorescence are listed in Table 5.2, where the values are normalized to be ones per one $Er^{3+}$ ion.

The phonon energy, $\hbar\omega$, which is associated with multiphonon relaxation within the electronic levels of RE ion, can be estimated from the measurement of PSB spectra of $Eu^{3+}$[42]. Figure 5.3 shows the excitation spectra of $Eu^{3+}$ obtained on the present glasses by monitoring the emission with wavelength of 612 nm corresponding to the$^5D_0 \rightarrow {}^7F_2$ relaxation, and Fig. 5.4 shows the energy diagram of $Eu^{3+}$ where both pumping and emission paths are shown. The small

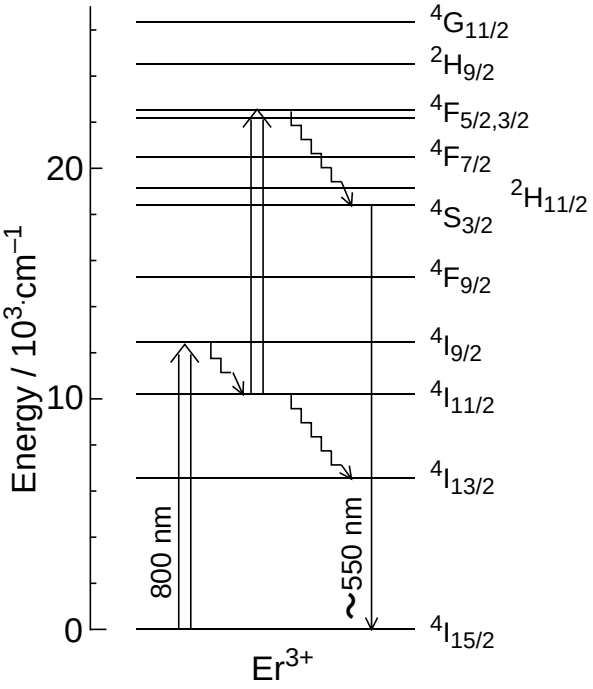


**Fig. 5.2.** *Energy level diagram of $Er^{3+}$ ion where one of the possible mechanisms of two-photon excitation is shown. $\Longrightarrow$: excitation by 802 nm light, $\wwvy$: nonradiative transition, and $\longrightarrow$: emission.*

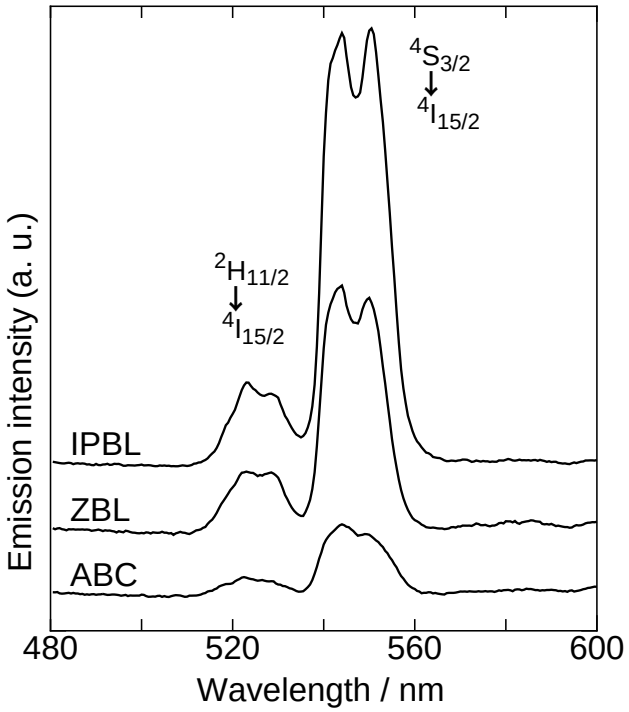


**Fig. 5.1.** *Upconversion fluorescence spectra of $Er^{3+}$ in fluoride glasses. The wavelength of excitation is 802 nm.*

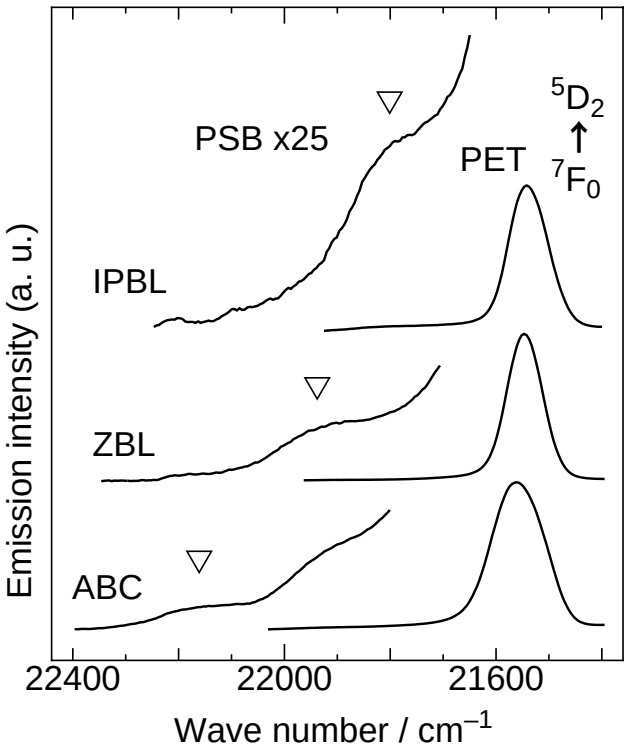


**Fig. 5.3.** *Phonon sideband spectra of $Eu^{3+}$ in fluoride glasses. The monitoring wavelength of emission is 612 nm.*

peak present in the higher energy side of $^5D_2 \leftarrow ^7F_0$ transition is PSB, and the difference in peak position between PSB and $^5D_2 \leftarrow ^7F_0$ transition peak corresponds to the phonon energy, $\hbar\omega$. The values estimated are listed in Table 5.2 together with the IR-active maximum phonon energy, $h\nu_{\max}$.

Figure 5.5 show the fluorescence spectra of $Eu^{3+}$-doped glasses. The wavelength of excitation light is 394 nm, which corresponds to $^5L_6 \leftarrow ^7F_0$ transition shown in Fig. 5.4. Isomer shift (IS) of $^{151}$Eu was determined with respect to $EuF_3$ as a standard. The value of IS, $\delta$, is proportional to the density of $6s$ electron at the nucleus, and in the case of $^{151}$Eu, $\delta$ increases with increasing the covalency of Eu−F[63]. These values are listed in Table 5.2.

## 5.4 Discussion

### 5.4.1 Upconversion efficiency

According to Miyakawa and Dexter's theory[46], the multiphonon decay rate, $W_p(0)$, at 0 K decreases with a decrease of phonon energy, $\hbar\omega$, associated with nonradiative relaxation of RE ions, as follows

$$W_p(0) = W_0(0) \cdot \exp\left[-\frac{\alpha \Delta E}{\hbar\omega}\right] \tag{5.1}$$

$$\alpha = \ln(p/g) - 1 \tag{5.2}$$

$$p = \frac{\Delta E}{\hbar\omega} \tag{5.3}$$

where $\Delta E$ is the energy gap to the next lower level, $g$ is the electron-phonon coupling strength, $p$ is the phonon number consumed during multiphonon relaxation and $W_0(0)$ is the decay rate at $\Delta E = 0$, i.e., $p = 0$. Since a small value of $W_p$ brings about a long lifetime of an excited level (see Fig. 5.2), the probability of the excited state absorption is enhanced when $W_p$ is small. Thus, it is expected that the intensity of upconversion fluorescence increases as $\hbar\omega$ decreases. This is in accordance with the present result as shown in Table 5.2, columns (i) and (ii).

The dependence of the upconversion efficiency on $W_p$ is also confirmed by the fluorescence spectra of $Eu^{3+}$ (see Fig. 5.5). Since the energy gap of $^5D_0 \rightarrow ^7F_6$ is much larger than the phonon energy of fluoride glasses as shown in Fig. 5.4, the $f$-electrons in $^5D_0$ state relax mainly by radiative process. On the other hand, the $f$-electrons in $^5D_J$ $(J = 3, 2, 1)$ state relax partly by nonradiative process because energy gaps between the levels are small. Since the fluorescence intensities

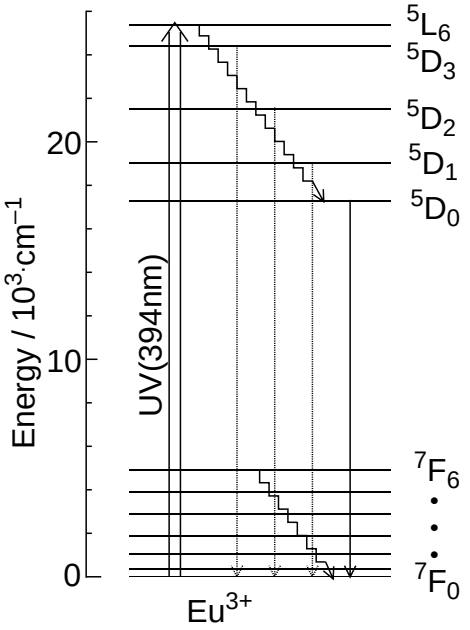


**Fig. 5.4.** *Energy level diagram of $Eu^{3+}$ ion. $\Longrightarrow$: excitation, $\vee\vee\vee$: multi-phonon relaxation, and $\longrightarrow$: emission. The inset is a magnified diagram showing the appearance of PSB.*

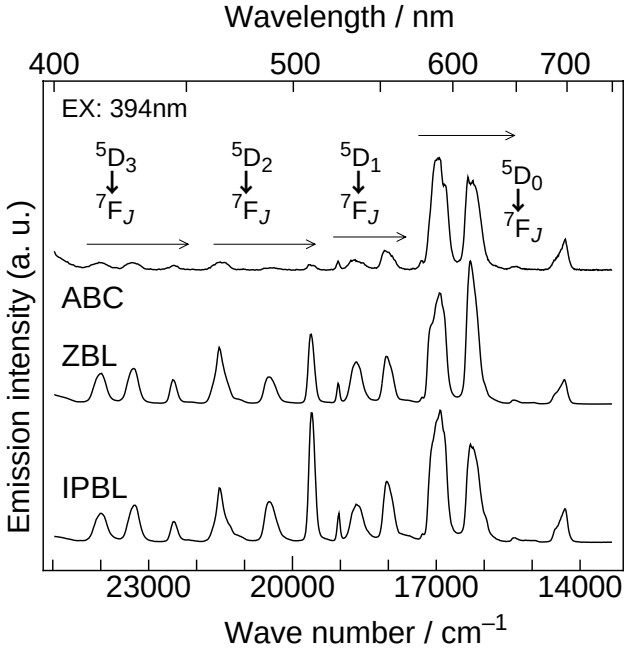


**Fig. 5.5.** *Fluorescence spectra of $Eu^{3+}$ in fluoride glasses. The wavelength of excitation is 394 nm.*

from these levels are affected by the nonradiative decay rate, $W_p$, the intensity of the fluorescence from ${}^5\mathrm{D}_J$ ($J = 3, 2, 1$) level to ${}^7\mathrm{F}_{J'}$ increases as $\mathrm{W}_p$ from ${}^5\mathrm{D}_J$ to the next level decreases. As shown in Fig. 5.5, the fluorescence intensity of ${}^5\mathrm{D}_J \rightarrow {}^7\mathrm{F}_{J'}$ ($J = 3, 2, 1$) relatively increases with the order of increasing upconversion intensity. Therefore, $Eu^{3+}$ is a good probe to estimate the degree of nonradiative loss, and this is helpful to select the composition of host matrix for upconversion glass.

### 5.4.2 Difference in $\hbar\omega$ and $h\nu_{\mathrm{max}}$

As shown in Table 5.2, all the values of $\hbar\omega$ obtained by PSB were smaller than those of IR-active maximum phonon energy, $h\nu_{\mathrm{max}}$. As stated in the previous chapters, the vibrational state of the local structure around RE ions is different from that of glass matrix. Generally, $h\nu_{\mathrm{max}}$ corresponds to the stretching vibrational energy of the strongest bonding in the glass matrix, i.e., the vibration of the framework of glass. On the other hand, $\hbar\omega$ is considered to be due to the local vibration around RE ions. Precisely speaking, it corresponds to the strongest one among several local vibrations around RE, because the contribution to $W_p$ increases as $\hbar\omega$[99].

In this section, this difference is discussed more quantitatively by considering the local vibrations with or without $Eu^{3+}$ ions by means of two different models. They are: a point mass model and molecular dynamic (MD) simulation.

#### A point mass model

The simplest model to explain this difference is the one which consists of two springs and three point masses as shown in Fig. 5.6. In this model, the strongest bonding in the glass matrix and the strongest bonding around RE ions are regarded as M−F−M and M−F−Eu, respectively. For simplicity, each bonding is regarded to provide a simple harmonic oscillation, that is, M−F−M and M−F−Eu can not bend and all atoms move only along the molecular axis. The frequencies of M−F−M and M−F−Eu vibration are calculated from those of M−F and Eu−F, $\omega_{\mathrm{M-F}}$, which are estimated by the following equation[100]

$$\omega_{\mathrm{M-F}} = A\sqrt{\frac{Z_{\mathrm{M}}Z_{\mathrm{F}}}{m_{\mathrm{MF}}r_0^3}} \qquad (5.4)$$

where $Z$ is the effective ionic charge, $m_{\mathrm{MF}}$ the reduced mass of the ions, $r_0$ the separation between the ions and $A$ a constant. Equation 5.4 can be derived by assuming that the bonds are completely ionic and harmonic[100] (see Appendix 5-A for detailed derivation) and is useful to the estimate single-bond strength of ions. With the values from Eq. 5.4, the frequency of the coupled oscillation (M − F − M′; M′ = M or Eu), $\omega_{\mathrm{M-F-M'}}$, is shown as

**Table 5.1.** *Composition of the glasses used in this study. (mol%; Ln = Eu or Er)*

| notation | Sample composition | Er concentration ($10^{20}$ atom/cm$^3$) |
|---|---|---|
| IPBL | $48InF_3 \cdot 24PbF_2 \cdot 24BaF_2 \cdot 3LaF_3 \cdot 1LnF_3$ | 1.82 |
| ZBL | $60ZrF_4 \cdot 33BaF_2 \cdot 6LaF_3 \cdot 1LnF_3$ | 1.60 |
| ABC | $49AlF_3 \cdot 20BaF_2 \cdot 30CaF_2 \cdot 1LnF_3$ | 2.23 |

**Table 5.2.** *Summary of results. (i) Relative intensity of upconversion fluorescence per one $Er^{3+}$ ion. (Er concentrations listed in Table 5.1 were used as conversion factors.) (ii) Phonon energy, $\hbar\omega$, which is associated with nonradiative relaxation and was estimated by measuring PSB of $Eu^{3+}$. (iii) Maximum energy peak in IR spectra, $h\nu_{\max}$. (iv) Isomer shift of $^{151}Eu$, $\delta$. The IS of* IPBL *and* ZBL *are of the samples where $EuF_3$ was used instead of $LaF_3$ in their composition (see text). Errors were determined by averaging successive measurement (i) and estimating a resolution of the apparatus (ii)–(iv), respectively.*

| Sample | (i) Intensity of upconversion fluorescence (ZBL=1.0) | (ii) $\hbar\omega$ (cm$^{-1}$) | (iii) $h\nu_{\max}$ (cm$^{-1}$) | (iv) $\delta$ (mm/sec) |
|---|---|---|---|---|
| IPBL | 1.7 | 260 | 470 | −0.02 |
| ZBL | 1.0 | 390 | 490 | −0.13 |
| ABC | 0.19 | 600 | 650 | −0.04 |
| $EuF_3$ crystal | — | 280 | — | 0.00 |
| error | ±13% | ±10 | ±5 | ±0.02 |

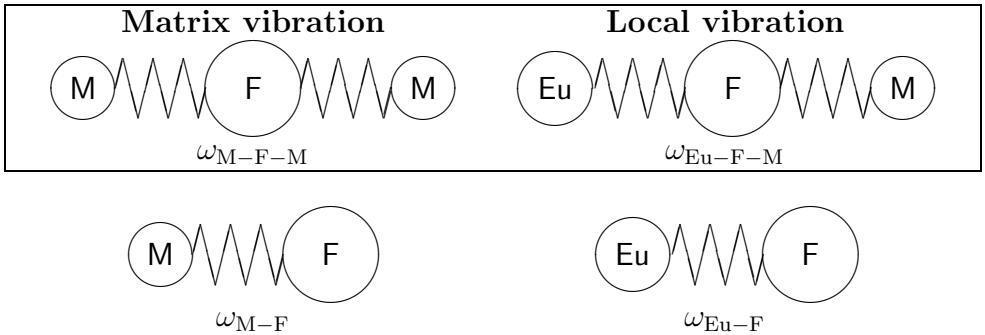


**Fig. 5.6.** *A model of coupled oscillation used for the explanation of the differences observed between $\hbar\omega$ and $h\nu_{\max}$. The estimated coupled oscillation frequencies are shown in Table 5.3.*

$$\omega^2_{\mathrm{M-F-M'}} = \frac{\omega^2_{\mathrm{M-F}} + \omega^2_{\mathrm{M'-F}}}{2} \pm \frac{1}{2}\sqrt{(\omega^2_{\mathrm{M-F}} - \omega^2_{\mathrm{M'-F}}) + 4\kappa\omega^2_{\mathrm{M-F}}\omega^2_{\mathrm{M'-F}}}, \tag{5.5}$$

$$\kappa = \left[\left(1 + \frac{m_{\mathrm{F}}}{m_{\mathrm{M}}}\right)\left(1 + \frac{m_{\mathrm{F}}}{m_{\mathrm{M'}}}\right)\right]^{-1}, \tag{5.6}$$

where $m$ is the mass. By using Eqs. 5.4–5.6, the frequencies of various combined systems such as M−F, M−F−M, and M−F−Eu were calculated and the results are listed in Table 5.3.

It is clear that $\omega_{\mathrm{M-F-M}}$ (M = Al, Zr, In) is larger than $\omega_{\mathrm{Eu-F-M}}$. Although this model is far from the actual vibration systems, it gives a reasonable explanation.

### Molecular dynamic simulation

A more realistic approach is to use the molecular dynamic (MD) simulations to obtain the local structure around RE ion and its vibration. A Zr−Ba−La−F glass was simulated and calculated the frequency spectra of the matrix glass and the local structure around $La^{3+}$ ions are calculated separately.

The MD program, `MDORTO`, developed by Kawamura[101] was used here. The Verlet algorithm for ion motion and the Ewald method for the summation of electrostatic interactions were employed in the program. The interatomic potential used is the following Busing approximation of Born-Mayer-Huggins' form,

$$U_{ij} = \frac{Z_i Z_j e^2}{r_{ij}} + f_0(b_i + b_j)\,\exp\left[\frac{a_i + a_j - r_{ij}}{b_i + b_j}\right] \tag{5.7}$$

**Table 5.3.** *Calculation of the frequencies of various combined oscillation systems such as M−F, M−F−M, and M−F−Eu using a simple model which consists of some springs and point masses (Fig. 5.6). A is the constant in Eq. 5.4.*

| M | $\frac{\omega_{\mathrm{M-F}}}{A} \times 10^{11}$ | $\frac{\omega_{\mathrm{M-F-M}}}{A} \times 10^{11}$ | $\frac{\omega_{\mathrm{Eu-F-M}}}{A} \times 10^{11}$ |
|---|---|---|---|
| Al | 1.574 | 1.983 | 1.700 |
| Zr | 1.224 | 1.729 | 1.483 |
| In | 1.106 | 1.508 | 1.346 |
| Eu | 0.837 | 1.150 | 1.150 |
| La | 0.796 | — | 1.121 |
| Ca | 0.840 | — | 1.118 |
| Pb | 0.640 | — | 1.029 |
| Ba | 0.611 | — | 1.008 |

where $f_0$ is a constant ($6.9742\times10^{-11}$N), $Z$ the electron charge, $e$ the unit charge, $a$ and $b$ are the values related with the radius and the compressibility of each ion, respectively, and $r_{ij}$ is the distance between $i$ and $j$ ions. The parameters employed here are listed in Table 5.4. These parameters were empirically determined so as to reproduce the structure of some fluoride crystals (see Appendix 5-B for detailed derivation).

The number of ions contained in the basic cell was selected so as to satisfy the Zr:73, Ba:40, La:7, and F:393, which corresponds to the composition of ZBL glass used in the present chapter. The pressure was maintained at about 1 atmosphere by scaling the length of MD unit cell, and the temperature was controlled by means of scaling of ion velocities. The shape of the basic cell was maintained in a form of rectangular parallelpiped to achieve the fast computation.

In order to obtain the quenched state, the equilibration run for 5000 step (1 step corresponds to 2 $\times$ $10^{-15}$ sec) was carried out after increasing temperature up to 3000 K during the first 5000 step and then the temperature was reduced to room temperature in 5000 step. The glass structure obtained in the simulation is shown in Fig. 5.7. The density and the Zr−F distance of Zr for the glass obtained were found to be close to the value experimentally determined as shown Table 5.5.

To estimate the vibrations for the glass matrix and the vicinity of RE ions separately, the distance autocorrelation functions of Zr−F bonds connected with or without RE ions, as shown in Fig. 5.8, were calculated from

$$\gamma(t) = \frac{\left\langle \sum_i \dot{\boldsymbol{r}}_i(t_0)\cdot\dot{\boldsymbol{r}}_i(t_0+t)\right\rangle}{\left\langle \sum_i \dot{\boldsymbol{r}}_i(t_0)\cdot\dot{\boldsymbol{r}}_i(t_0)\right\rangle}, \tag{5.8}$$

where $\boldsymbol{r}_i(t)$ is the distance of ion pairs $i$ at some time $t$. In this calculation, every time step acted as the $t_0$ for all the subsequent time steps in the statistical average of $\gamma(t)$. The frequency spectrum $D(\omega)$ was calculated from the Fourier transform of the velocity autocorrelation function, given as

$$D(\omega) = \int_0^\infty \gamma(t)\cos\omega t\,\mathrm{d}t \tag{5.9}$$

The frequency spectra obtained is shown in Fig. 5.9. The fluctuation of spectra in Fig. 5.9 is due to the limited number of bonds in the unit cell when Fourier transform was carried out.

Although the value of vibrational frequency calculated is higher than that for the actual glass systems ($\sim$ 500 cm$^{-1}$), it is apparently shown that the frequency of Zr−F vibration decreases as Zr is replaced by La.

The above two models clearly show that the vibration energy around RE ions is lower than that of matrix due to the participation of RE ions to the local vibration. So it is concluded that the behavior observed on oxide glasses is also appear on fluoride glasses.

**Table 5.4.** *Potential parameters used in this study. The determining procedure is described in Appendix 5-B.*

| Atom | $Z$ | $a$ (Å) | $b$ (Å) | Atom | $Z$ | $a$ (Å) | $b$ (Å) |
|---|---|---|---|---|---|---|---|
| F | −1 | 1.400 | 0.060 | La | +3 | 1.560 | 0.060 |
| Zr | +4 | 1.262 | 0.060 | Eu | +3 | 1.465 | 0.060 |
| Ba | +2 | 1.750 | 0.080 | Y | +3 | 1.400 | 0.060 |

**Table 5.5.** *Comparison of the calculated results with the experimental results.*

| | Zr−F distance | density |
|---|---|---|
| $ZF_4$−$BaF_2$ glasses[102] | 2.09–2.11 | |
| 62Zr–30Ba–8La–F[103] | | 4.58 |
| Experimental | 2.08 | 4.47 |

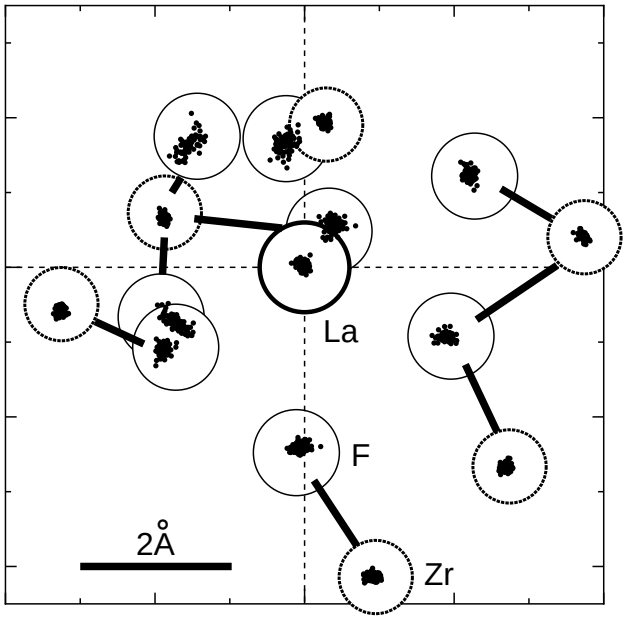


**Fig. 5.7.** *Snapshot of the local structure within the second coordination sphere of $La^{3+}$ ion (within 5 Å) at 300 K. The trajectories of the atoms for 1000step (2 psec) are also shown.*

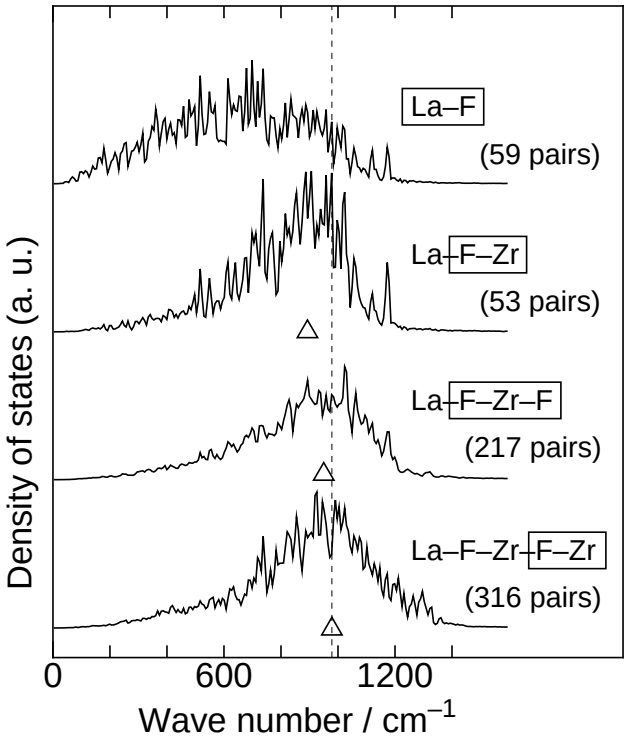


**Fig. 5.9.** *Phonon energy for each bond in simulated fluorozirconate glass.*

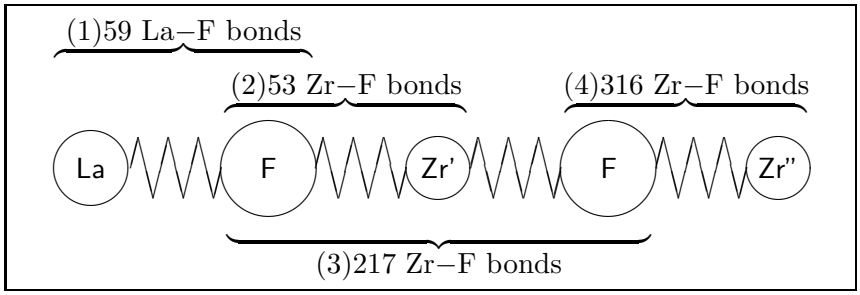


**Fig. 5.8.** *The four groups of bonds in the MD-simulated glass.* Zr': *within the second coordination shell of La ions,* Zr'': *out of the second coordination shell of La ions. (1) La−F, (2) Zr−F surrounding La ions, (3) Zr−F within the third coordination shell, and (4) Zr−F out of the second coordination shell.*

### 5.4.3 Local structure around rare earth ions

As already noted, IS of $^{151}$Eu increases as the 6*s* electron density at Eu nucleus increases. This increase is caused by increasing electron donation from the surrounding anions. Figure 5.10 shows the relation of $\delta$ and theoretical optical basicity, $\Lambda_{\rm th}$, which indicates the averaged basicity of anions and is originally proposed by Duffy[69] (see Appendix 2-A [p.18] for detailed calculation). Against expectation, $\delta$ decreases with increasing $\Lambda_{\rm th}$. This means that a local modification of glass structure around RE ions occurs for some or all of the glasses, but we cannot specify in further detail at this stage.

From the view point of phonon energy, at least, the fact that $\hbar\omega$ for IPBL is as much as that for $EuF_3$ indicates that RE ions in IPBL are surrounded by weak bonds such as Ba−F and La−F, rather than In−F. If $Eu^{3+}$ ions are surrounded by In−F, $\hbar\omega$ of IPBL should be larger than $\hbar\omega$ of $EuF_3$ according to Table 5.3. Further investigation of fluoride glass structure, both the vicinity of RE and glass matrix, is needed to clarify this local structure modification.

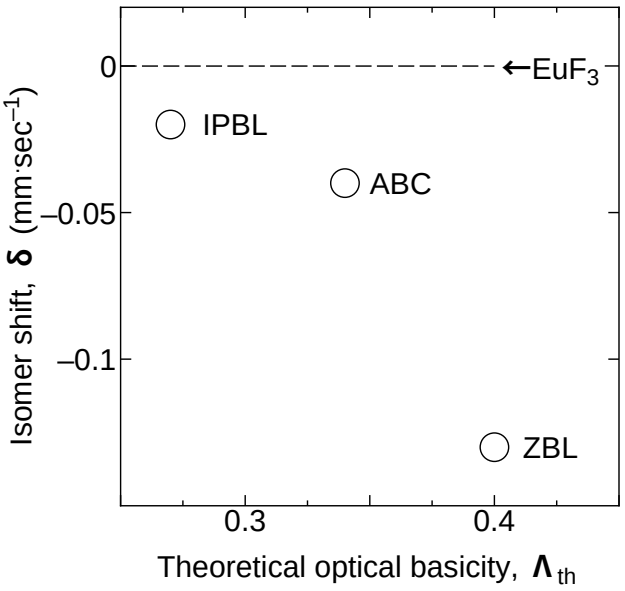


**Fig. 5.10.** *Relationship between the isomer shift of $^{151}Eu^{3+}$ and the theoretical optical basicity of the host glass (see Appendix 2-A [p.18] for detailed calculation).*

## 5.5 Conclusion

Local vibrational state of rare earth (RE) ions in fluoride glasses, as host materials for upconversion phosphor, was investigated on the basis of phonon sideband (PSB) of $Eu^{3+}$ and molecular dynamic (MD) simulation. Upconversion fluorescence of $Er^{3+}$ in In- and Pb-based fluoride glasses was compared with that of fluorozirconate and fluoroaluminate glasses. Its efficiency was increased in the order of decreasing the phonon energy, $\hbar\omega$, which is associated with multiphonon relaxation of RE ions estimated by PSB. It was found that $\hbar\omega$ was not in agreement with the IR-active maximum phonon energy of glass matrix. By demonstrating MD simulation, it was concluded that this lack of agreement is due to the participation of RE ions in the local vibration mode. Local modification of glass structure around RE ions can also be contribute to the mismatch, which is mentioned by the result of Mössbauer spectroscopy of $^{151}$Eu.

**Appendix 5-A:** Derivation of Eq. 5.4

Here, the following simple Born potential was employed

$$U = -\frac{Z_1 Z_2}{r} + \frac{b}{r^n} \quad (9 \le n \le 12) \tag{5.10}$$

where $r$ is the separation of ions in crystal, $Z_1$ and $Z_2$ are the effective ionic charges of anion and cation, respectively. We assume the vibration of ion pair is completely harmonic at the minimum of the potential well. Since the force constant $f$ for a simple harmonic oscillator corresponds the second derivative of $U$ with respect to $r$ at the equilibrium separation, $r_0$,

$$f = \left(\frac{{\rm d}^2 U}{{\rm d}r^2}\right)_{r=r_0} \propto -\frac{Z_1 Z_2}{r_0^3} \tag{5.11}$$

is obtained on the condition of $({\rm d}U/{\rm d}r)_{r=r_0} = 0$ and $n^{-1} \simeq 0$. The simple harmonic oscillator relation ship between the force constant and frequency $\omega_0$ is

$$\omega_0 = 2\pi\sqrt{\frac{f}{m}} \tag{5.12}$$

where $m$ is the reduced mass of the ion pair. Thus, the frequency of the ion pair is described as

$$\omega_0 \propto \sqrt{\frac{Z_1 Z_2}{m r_0^3}}. \tag{5.13}$$

**Appendix 5-B:** Determination of the potential parameters

The set of potential parameters used in the present chapter (see Table 5.4) is determined in such a way that the MD calculations of several crystals listed in Table 5.6 could reproduce well the experimentally derived crystal structures[104–107]. The parameters of $Eu^{3+}$ and $Y^{3+}$ are also determined to improve the validity of the set of parameters so as to reproduce the two polymorphs of rare earth trifluoride, tysonite, and $\beta$-$YF_3$ types[108]. Temperature was kept at 300 K. Figure 5.11 shows the trajectories of ions in $\beta$-$BaZrF_6$ crystal. The simulation based on the set of parameters determined gave the values of mean squared displacement less than 0.04 $Å^2$ for $F^-$ and 0.02 $Å^2$ for cations, respectively.

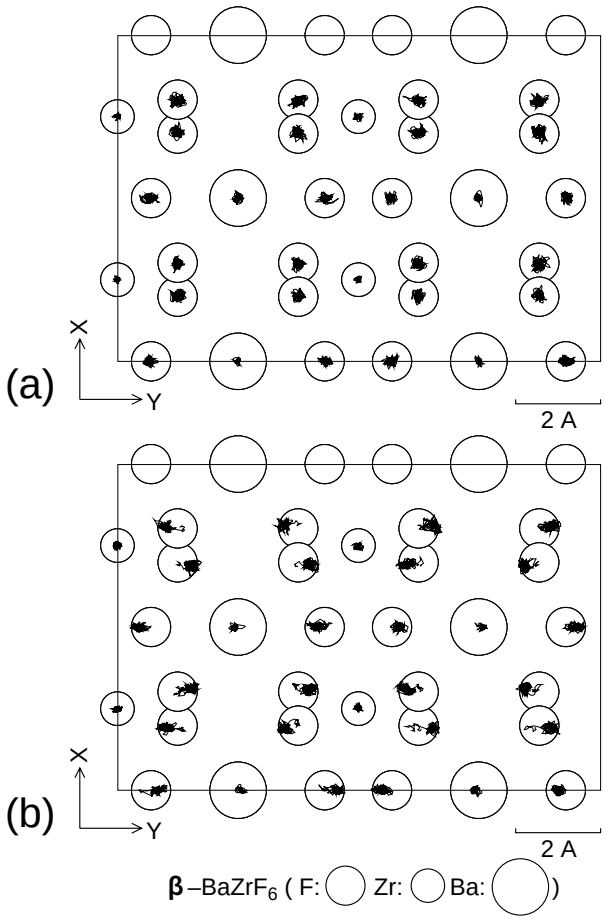


**Fig. 5.11.** *The trajectories of ions in MD-simulated $BaZrF_6$ crystal during 1000 steps at intervals of 5 steps using (a) proper and (b) wrong potential parameters.*

**Table 5.6.** *The crystals used for the determination of potential parameters.*

| Compound | Crystal system | Cation coordination | N | MD cell size(Å) |
|---|---|---|---|---|
| $\alpha$-$ZrF_4$ | tetragonal[109] | 8 | 320 | $15.79 \times 15.79 \times 15.45$ |
| $\beta$-$BaZrF_6$ | orthorhombic[110] | 8(Zr) 10(Ba) | 192 | $15.36 \times 11.35 \times 16.53$ |
| $BaF_2$ | cubic[A][111] | 8 | 216 | $18.60 \times 18.60 \times 12.40$ |
| $LaF_3$ | trigonal[B][112]†‡ | 9 | 192 | $14.37 \times 12.44 \times 14.70$ |
| $\alpha$-$EuF_3$ | trigonal[B][113]† | 9 | 192 | $13.84 \times 11.98 \times 14.18$ |
| $\beta$-$EuF_3$ | orthorhombic[C][113]† | 9 | 192 | $13.24 \times 14.04 \times 13.19$ |
| $\beta$-$YF_3$ | orthorhombic[C][114]† | 9 | 192 | $12.71 \times 13.71 \times 13.19$ |

[A]fluorite type. [B]tysonite type. [C]$\beta$-$YF_3$ type. †see also [108]. ‡see also [115].

# Chapter 6

# Spectral hole burning in $Sm^{2+}$-doped fluoride glasses

## 6.1 Introduction

Recently, there has been considerable activity on persistent spectral hole burning(HB), because of its importance for the application to frequency domain optical storage as a ultra-high density memory device[116]. HB is substantially an equivalent phenomenon to FLN described in Chapter 3 except that it includes a photo-induced reaction. That is, the state of a subset of ions (or molecules) excited by laser light is changed chemically or physically to be observed as a hole in their absorption spectrum (See Fig. 6.1 and compare it with Fig. 3.2 [p.20]).

Many attempts have been made to prepare HB materials using organic compounds doped with dye molecules[117–119] and inorganic crystals[120] containing transition metal[121–123] or rare-earth ions[16, 124–129], although its operating temperature is restricted to low temperature. Generally, this restriction comes from a small activation energy of photo-induced reaction, where a thermally activated reverse reaction easily occurs. Among them, $Sm^{2+}$-doped system has attracted special interest recently because room temperature HB is observed for the first time in an alkaline earth halide single crystal with $Sm^{2+}$[130, 131]. Moreover, since the electronic configuration of $Sm^{2+}$ is the same as that of $Eu^{3+}$, [Xe]$4f^6$, the electronic level structure of $Sm^{2+}$ is similarly expressed as that of $Eu^{3+}$ (shown in Fig. 1.2[p.5] and Fig. 5.4[p.36]). This implies that most of the experimental techniques for and the discussions on $Eu^{3+}$ systems can be applied to $Sm^{2+}$ systems.

There is, however, no report of HB in inorganic glass above liquid helium temperature, although glass is considered to be advantageous in much wider inhomogeneous linewidth due to the multisite occupancy unlike a crystalline state and in easier preparation of large sample. Since $Sm^{2+}$ is much more unstable than $Sm^{3+}$, strong reducing atmosphere is needed in preparation[132]. Thus, other reducible components have to be avoided from the batch. Furthermore, an oxide matrix is considered inappropriate, because $4f^6\,{}^7\mathrm{F}_0 \rightarrow 4f^5 5d$ absorption band overlaps to $4f^6\,{}^7\mathrm{F}_J \rightarrow 4f^6\,{}^5\mathrm{D}_0$ line[132], which is due to the strong crystal field strength of $Sm^{2+}$ site. Therefore, heavy metal fluoride glass can be a candidate for glass matrix.

In the present study, the HB in $Sm^{2+}$-doped fluorohafnate glasses at room temperature was observed and the burning mechanism and the relation between the hole width and the local vibrational state are discussed.

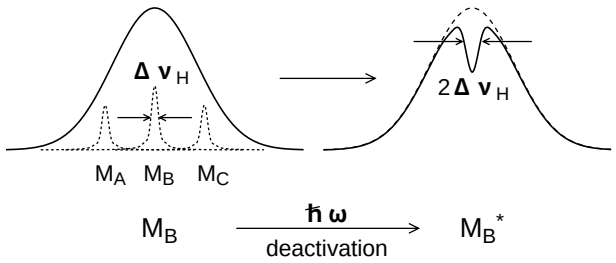


**Fig. 6.1.** *Schematic diagram showing the mechanism of hole burning. The subscripts, A–C, indicates that these ions (or molecules) located in different local environments.*

## 6.2 Experimental

The glass compositions are listed in Table 6.1 with their notations. The glasses were prepared by using $HfF_4$, $AlF_3$, $YF_3$, $LaF_3$, $MgF_2$, $CaF_2$, $SrF_2$, $BaF_2$, NaF, and $SmF_3$ as the starting materials, which were, then, mixed thoroughly and melted in a glassy carbon crucible and in strong reducing atmosphere in order to reduce $Sm^{3+}$ to $Sm^{2+}$. Transparent brown colored glasses were obtained. This coloring is due to the strong absorption of $f \rightarrow d$ ($4f^6\,{}^7\mathrm{F}_0 \rightarrow 4f^5 5d$) transition

of $Sm^{2+}$. The samples employed for the optical measurement were cut and polished into 5 × 25 × 25 mm.

The experimental setup for the measurement of the HB effect at room temperature is shown in Fig. 6.2. For low temperature measurement, the sample was kept to a fixed temperature between 4.5 K to 180 K by using a gas-flow type cryostat (Oxford CF1204), and a double monochromator (Spex model 14018). Further, a photomultiplier (Hamamatsu R-928) and a single photon counting electornics (Stanford SR400) were used for the detection system in order to obtain high resolution. The sample was irradiated with a DCM dye laser pumped by an $Ar^+$ laser. The dye laser wavelength was tuned so as to resonate with the $^5D_0 \leftarrow ^7F_0$ line. As soon as the irradiation was discontinued, the excitation spectrum for the $^5D_0 \rightarrow ^7F_2$ fluorescence around 723 nm was measured by varying the wavelength of the exciting DCM laser.

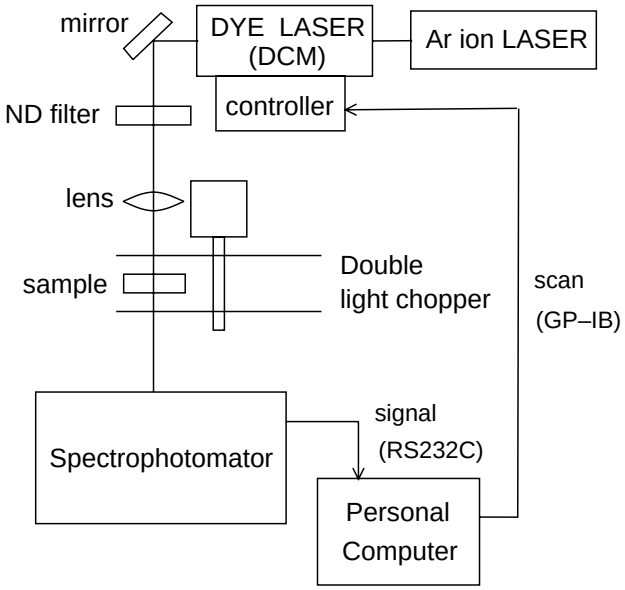


**Fig. 6.2.** *Schematic diagram of the experimental setup for the measurement of hole burning effect at room temperature.*

## 6.3 Results and Discussion

### 6.3.1 Mechanism of hole burning

The fluorescence spectrum of the sample under excitation by $Ar^+$ ion laser is shown in Fig. 6.3, where both emission of $Sm^{3+}$ and $Sm^{2+}$ were also observed. The linewidth of $^5D_0 \rightarrow ^7F_0$ line for $Sm^{2+}$ ion was 71 $cm^{-1}$ and it was about three times larger than that of $BaFCl_xBr_{1-x}$:$Sm^{2+}$ systems[126, 127] because of its amorphous random structure.

Figure 6.4 shows the excitation spectra of AH4 obtained at 4.5K. The hole width is about 1.5 $cm^{-1}$ at 4.5 K and becomes 10 $cm^{-1}$ at 140 K. It should be noted that the hole is clearly observed even at room temperature as shown in Fig. 6.5. The hole widths for both glasses are about 25 $cm^{-1}$. The saturation effect is considered to make a considerable contribution to the

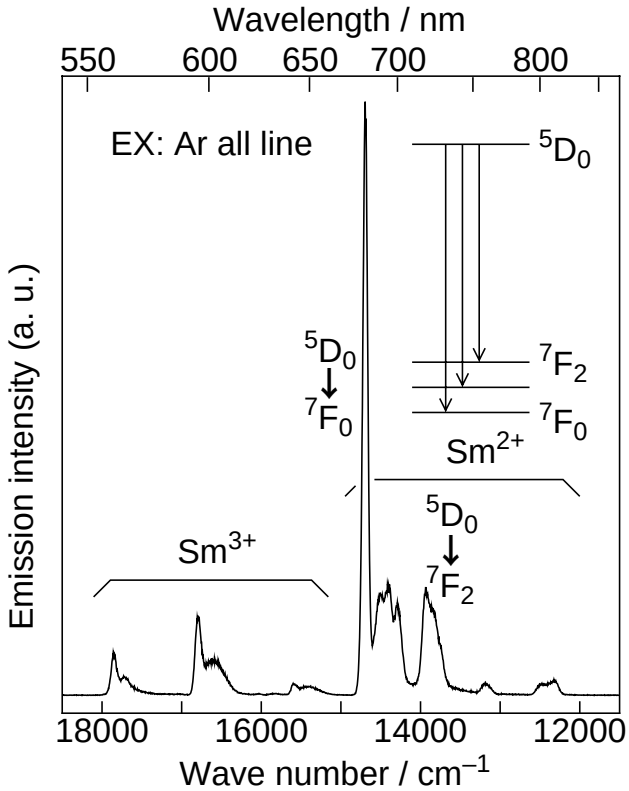


**Fig. 6.3.** *Fluorescence spectrum at 4.5 K of* AH4 *under excitation by $Ar^+$ ion laser (all line) and energy diagram of $Sm^{2+}$.*

**Table 6.1.** *Batch composition of the glasses used in this study. (mol%)*

| notation | Batch composition |
|---|---|
| AH4 | $28.2AlF_3 \cdot 12.2HfF_4 \cdot 8.3YF_3 \cdot 3.5MgF_2 \cdot 18.3CaF_2 \cdot 13.1SrF_2 \cdot 12.6BaF_2 \cdot 3.8NaF \cdot 1SmF_3$ |
| HBLAN | $53HfF_4 \cdot 20BaF_2 \cdot 4LaF_3 \cdot 3AlF_3 \cdot 20NaF \cdot 1SmF_3$ |

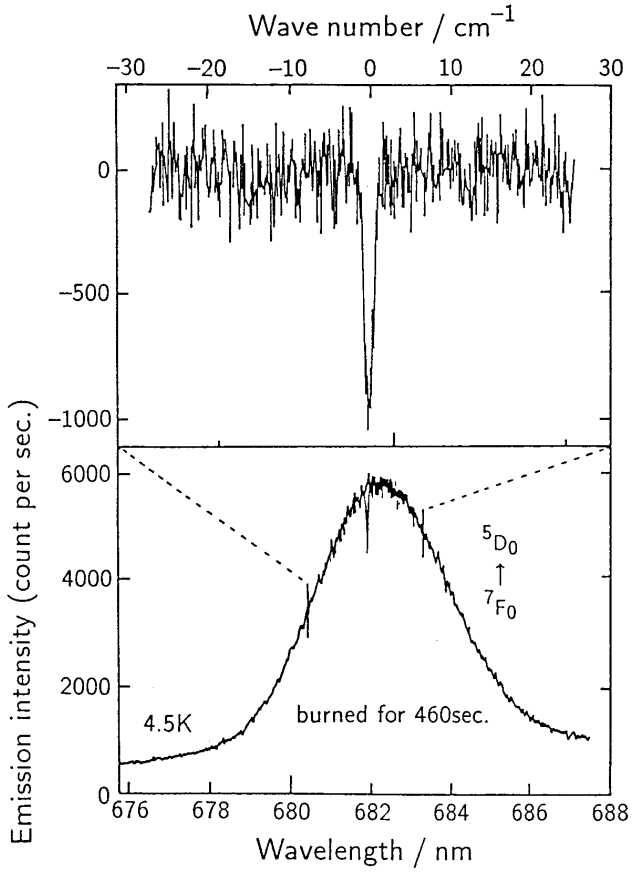


**Fig. 6.4.** *Bottom: Excitation spectrum at 4.5 K of* AH4 *obtained by monitoring the* $^5D_0 \rightarrow {}^7F_2$ *emission before and after irradiation with a DCM dye laser of 681.8 nm. Burning time is 460 sec. Top: The difference signal at 4.5 K, magnified by a factor of 2.*

hole spectrum in these cases. For the spectrum at 4.5 K, the linewidth of the laser light is also non-negligible. Therefore, it is probable that the homogeneous width of the $^7F_0 \leftarrow {}^5D_0$ line in this material is much narrower than the hole width shown in Fig. 6.4. The hole width is plotted with temperature in Fig. 6.6, where an about $T^2$ dependence is shown which is characteristic of amorphous materials[133].

No "anti-hole", or increased emission peak, was observed around the burnt hole as shown in Figs. 6.4 and 6.5. Anti-hole is caused, if any, by photo-induced redistribution of $Sm^{2+}$ ions within the inhomogeneous linewidth. Therefore, it is clearly suggested that the dominant burning mechanism in this system is not photo-physical such as

$$Sm_A^{2+} \xrightarrow{\hbar\omega} Sm_B^{2+}, \tag{6.1}$$

where the light energy of $\hbar\omega$ is resonant with $Sm_A^{2+}$ but not with $Sm_B^{2+}$. In other words, the photochemical HB is likely to be dominant, where this photo-ionization reaction is described as

$$Sm^{2+} + (\text{trap}) \xrightarrow{\hbar\omega} Sm^{3+} + (\text{trap})^-. \tag{6.2}$$

Figure 6.7 shows the burning time dependence

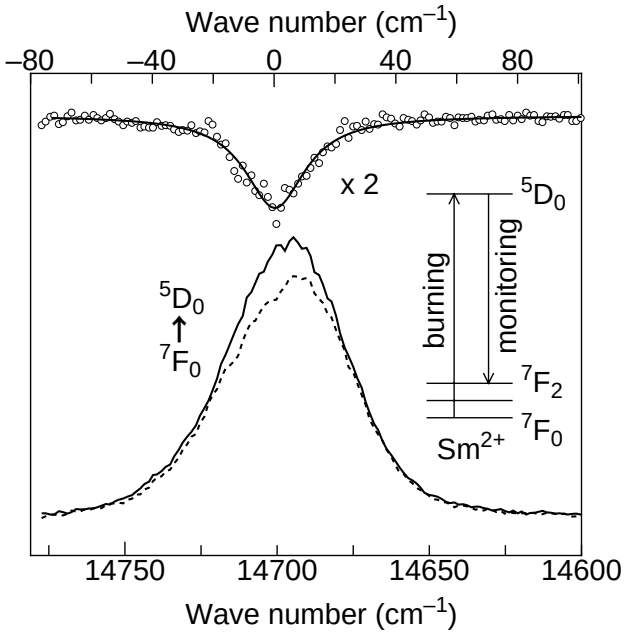


**Fig. 6.5.** *Bottom: Excitation spectrum at room temperature of* HBLAN *obtained by monitoring the* $^5D_0 \rightarrow {}^7F_2$ *emission before and after irradiation with a DCM dye laser of 681 nm. Burning time is 900 sec. Top: The difference signal, magnified by a factor of 2.*

of the hole depth. A decrease of hole depth with increasing temperature is due to both an increase of hole width (homogeneous linewidth of $Sm^{2+}$) and a thermal assisted reverse reaction of Eq. 6.2 (releasing electrons from traps).

The dominant electron trap in the present material can be $Hf^{4+}$ or $Sm^{3+}$. Or, if $F_2^-$ molecular ions and $F^0$ defects are present in the present strongly reduced glass, these are likely to be the dominant traps. These defects are reported to be stable at 180 K in X-irradiated fluoride glasses[134]. Further studies are necessary to clarify the actual HB mechanism.

### 6.3.2 Hole width and local vibrational state

Generally, the hole width is twice the homogeneous width of the optical transition, $\Delta\nu_{\rm H}$, (because both excitation and emission processes are involved), if any instrumentation width, such as the laser linewidth or the resolution of the detection system, can be neglected. The homogeneous broadening is caused by (1) the excited state lifetime of the optical centers and (2) dynamical perturbations such as phonons or fluctuating local magnetic fields due to nuclear or electron spins. It can be expressed by the following,

$$\frac{\Delta\nu_{\rm hole}}{2} = \Delta\nu_{\rm H} = \frac{1}{2\pi\tau_1} + \frac{1}{\pi\tau_2'} \qquad (6.3)$$

where $\tau_1$ is the excited state population decay (*or* energy relaxation) time and $\tau_2'$ the pure dephasing (*or* phase relaxation) time. The energy relaxation time is governed by the combination of probabilities for radiative and nonradiative processes, and is given by,

$$\frac{1}{\tau_1} = A + W_p \qquad (6.4)$$

where $A$ and $W_p$ are the radiative and nonradiative decay rate, respectively. Usually the temperature dependence of $A$ may be neglected, while $W_p$ and $1/\tau_2$ depend strongly on temperature. Therefore, since the hole width shows a strong temperature dependence, a contribution of the radiative decay to the hole width is considered to be small. Further, the fluorescence lifetime ($\tau_1$) of the $^5D_0$ state is known to be few msec, its contribution to $\Delta\nu_{\rm H}$ is about $10^{-8}$ $cm^{-1}$ (1 kHz). Thus, it is concluded that $1/\tau_2$ is directly related with the hole width.

As temperature increases, the electron-phonon interaction increases and, thus, $1/\tau_2$ increases. The electron-phonon coupling strength is estimated by Debye-Waller factor, $\alpha$, given by,

$$\alpha = \frac{S_0}{S_0 + S_{\rm p}} \qquad (6.5)$$

where $S_0$ and $S_{\rm p}$ are the integrated intensities of the hole and the accompanying phonon sideband (PSB). Since $\alpha$ for RE ions is small, PSB is not detectable by this HB measurement (see Figs. 6.4 and 6.5). The PSB in excitation spectra described in Chapter 1 can give an alternative information, although the information of low-energy phonons is masked by the inhomogeneous broadening. Figure 6.8 shows PSB spectra of $Eu^{3+}$ in several

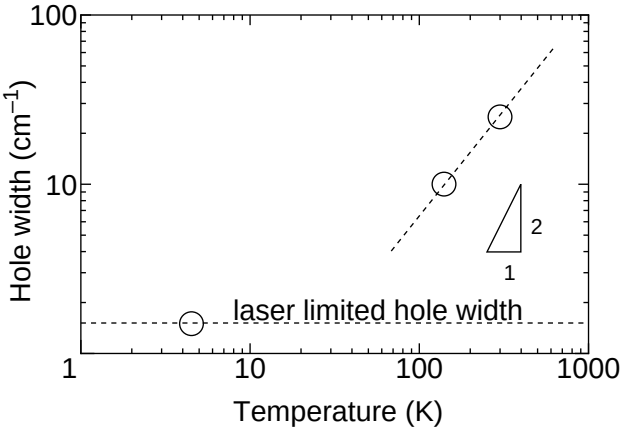


**Fig. 6.6.** *Temperature dependence of the hole width.*

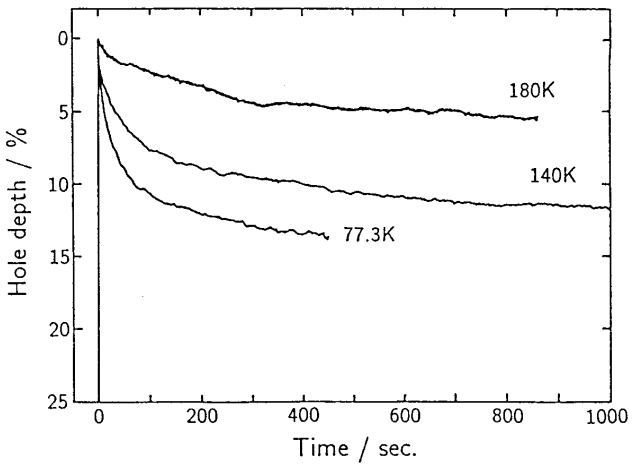


**Fig. 6.7.** *The burning time dependence of the persistent hole depth for* AH4 *obtained by monitoring the* $^5D_0 \rightarrow {}^7F_2$ *emission in the presence of burning irradiation of a DCM dye laser of 681.8 nm.*

glasses. The PSB intensity of fluoride glasses is much smaller than that of oxide glasses, which shows that fluoride glasses are suitable host materials for HB. It is concluded that the PSB intensity is one of important parameters for further investigations.

## 6.4 Conclusion

$Sm^{2+}$-doped heavy metal fluoride glasses were synthesized under a strongly reduced atmosphere, and persistent spectral hole burning was observed even at room temperature. In this system, photochemical process is likely to be dominant because of the absence of anti-hole adjacent to the hole. It was shown that since the hole width is directly related with the electron-phonon coupling strength, a suitable host for HB is the one whose PSB strength is small, shch as fluoride glasses.

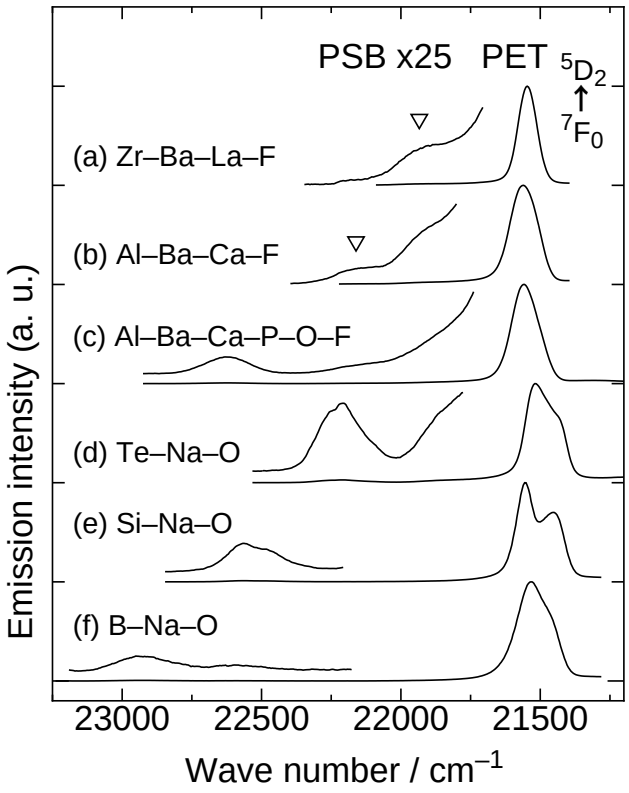


**Fig. 6.8.** *Excitation spectra of* $^5D_0 \rightarrow ^7F_2$ *emission of* $Eu^{3+}$ *doped in oxide and fluoride glasses at room temperature.*

# Summary

In the present thesis, local structure around rare earth (RE) ions in inorganic glass systems, particularly in oxide glasses, was investigated systematically based on fluorescence and Mössbauer spectroscopies. On the basis of the experimental results, the structural modification of glass network around RE ions was demonstrated and it was shown that the spectral inhomogeneous broadening is closely related to the local flexibility of glass network surrounding RE ions. Furthermore, as the phenomena which depends on the local structure around RE ions, upconversion fluorescence and spectral hole burning of RE-doped fluoride glasses were investigated. The contents of the respective chapters are summarized as follows:

In Introduction, the general background and the purpose of the present study were outlined. The previous studies on RE ions in inorganic glasses were reviewed. The necessity of the studies on the spectral inhomogeneous broadening and the mid-range structure was pointed out.

In Chapter 1, the local structure out of the first coordination sphere of $Eu^{3+}$ ions in silicate, germanate, and aluminosilicate glasses was investigated by measuring the phonon sideband (PSB) associated with the $^5D_0 \leftarrow ^7F_0$ transition of $Eu^{3+}$. It was found that the vibrational energy of the structural units surrounding $Eu^{3+}$ ions is lower than that in the glass matrix because of the participation of a heavy $Eu^{3+}$ ion in the local vibration. Further, the compositional dependence of $Q^n$ units around $Eu^{3+}$ ions in silicate glasses showed the local depolymerization of glass network around $Eu^{3+}$ ions in the sodium-poor compositions. This is most likely due to the charge compensation around $Eu^{3+}$ ions and to the larger affinity of $Eu^{3+}$ ions to non-bridging oxygens (NBOs) rather than to bridging oxygens (BOs). It was also found that the interaction between $Eu^{3+}$ ions and the excess negative charge on macroanions ($GeO_{6/2}^{2-}$ and $AlO_{n/2}^{(n-3)-}$) is weak. Therefore, it was concluded that the excess negative charge of macroanions is not used for charge compensation of $Eu^{3+}$ ions, or, in other words, the incorporated $Eu^{3+}$ ions act, as *network-modifiers*, to create NBOs rather than macro anions.

In Chapter 2, $^{151}$Eu Mössbauer effect was measured for several oxide glasses. From the value of isomer shift (IS), the basicity of ligands are estimated and compared with theoretical optical basicity, $\Lambda_{\mathrm{th}}$, in order to evaluate the modification of local structure as shown in the previous chapter. For germanate and borate systems, the local basicity changed according to the population ratio of network-forming cation polyhedra with different coordination numbers. For sodium silicate and aluminosilicate systems, compositional dependence of the local basicity was not in agreement with that of theoretical optical basicity. This is most likely due to the preferential coordination of NBOs rather than BOs. It was assumed that $Eu^{3+}$ ions in silicate glasses are surrounded by a certain amount of NBO−Na pairs, which remains almost constant with incorporating Na but decreases with an incorporation of Al.

In Chapter 3, the origin of the inhomogeneous linewidth of $Eu^{3+}$ fluorescence, $\Delta\nu_{\mathrm{IH}}$, for several oxide glasses was discussed on the basis of the local structure described in the previous chapters. The value of $\Delta\nu_{\mathrm{IH}}$ for silicate glasses increased with decreasing $Na_2O$ content. On the basis of the transition frequency dependence of the splitting width of the $^7F_1$ level obtained by the site-selective fluorescence spectra, it was assumed that the population of the sites with lower coordination number increases with decreasing alkali content. Thus, it was concluded that inhomogeneous linewidth is affected by the local flexibility of glass network, which is related with the structure outside of the first coordination shell, i.e., the degree of the interpolyhedra linkage and NBO concentration. As the network flexibility decreases, the population of $Eu^{3+}$ ions in unstable sites having low coordination number increases, which brings about an increase in $\Delta\nu_{\mathrm{IH}}$. This was also the case for other oxide glasses, such as borate, germanate and aluminosilicate glasses, but the effect of macroanions ($GeO_{6/2}^{2-}$, $AlO_{n/2}^{(n-3)-}$, and $BO_{4/2}^{-}$) should be con-

sidered. The formation of macroanions leads to a decrease in local network flexibility by consuming NBOs and increasing the interpolyhedra linkage. Consequently, it was concluded that the inhomogeneous broadening of $Eu^{3+}$ fluorescence for oxide glasses increases with decreasing the local flexibility of glass network.

In Chapter 4, the inhomogeneous broadening was investigated for the glasses which contains doubly bonded oxygens (DBO), i.e., phosphate glasses. The linewidth for these glasses was smaller than any other oxide glasses dealt with in this thesis and increased with a decrease of the amount of DBO estimated by PSB. Moreover, it was found that $Eu^{3+}$ ions in borophosphate glasses are preferentially surrounded by NBOs of $PO_{4/2}$ tetrahedra even in the glass with 5 mol% of $P_2O_5$ due to the local charge compensation by NBOs.

Through the discussions of the last two chapters, it was revealed that the inhomogeneous linewidth of $Eu^{3+}$ fluorescence is significantly related with the local flexibility of glass network. Both NBO concentration in matrix and the degree of interpolyhedra linkages surrounding $Eu^{3+}$ ions are associated with the flexibility of local glass network.

In Chapter 5, the local vibrational state around RE ions in fluoride glasses were investigated and the effect towards the upconversion fluorescence of $Er^{3+}$ was discussed. The upconversion efficiency increased in the order of decreasing the phonon energy, $\hbar\omega$, associated with the multiphonon relaxation of RE ions, which was calculated from the PSB of $Eu^{3+}$. Further, it was found that $\hbar\omega$ was not in agreement with the IR-active maximum phonon energy of glass matrix. As demonstrated by molecular dynamic simulation, it is considered that this lack of agreement is due to the participation of RE ions in the local vibration mode. The local modification of glass structure around RE ions can also contribute to the mismatch, which was demonstrated by the result of Mössbauer spectroscopy.

In Chapter 6, $Sm^{2+}$-doped heavy metal fluoride glasses were synthesized and persistent spectral hole burning (HB) was observed even at room temperature, which is the highest temperature observed among glass materials. In this system, photochemical process is likely to be dominant because of the absence of anti-hole adjacent to the hole. It was mentioned that PSB intensity can be one of useful useful parameters for choosing host materials for HB because the hole width is directly related with the electron-phonon coupling strength.

# Bibliography


[1] H. Scholze, *Glass: Nature, Structure, and Properties*, Springer-Verlag, New York, 1991.

[2] M. Poulain, "Fluoride glass composition and processing"; pp. 1–35 in *Fluoride glass fiber optics*. Edited by I. D. Aggarwal and G. Lu, Academic press, San Diego, 1991.

[3] J. Lucas, "Fluoride glasses," *J. Mater. Sci.*, **24** 1–13 (1989).

[4] J. Lucas, "Rare earths in fluoride glasses," *J. Less-Common Met.*, **112** 27–40 (1985).

[5] C. M. Baldwin, R. M. Almedia, and J. D. Mackenzie, "Halide glasses," *J. Non-Cryst. Solids*, **43** 309–344 (1981).

[6] J. E. Marion and M. J. Weber, "Phosphate laser glasses," *Eur. J. Solid State Inorg. Chem.*, **28** 271–287 (1991).

[7] M. J. Weber, "Science and technology of laser glass," *J. Non-Cryst. Solids*, **123** 208–222 (1990).

[8] E. Snitzer, "Rare earth fiber lasers," *J. Less-Common Met.*, **148** 45–58 (1989).

[9] T. Izumitani and H. Toratani, "Laser glass" (in Japanese), *Solid State Phys.*, **18**[5] 287–296 (1983).

[10] H. Toratani and K. Hirao, "Rare earth doped upconversion glass lasers" (in Japanese), *Oyo Buturi*, **61**[1] 43–46 (1992).

[11] S. Tanabe, K. Hirao, and H. Toratani, "Rare earth containing upconversion laser glasses" (in Japanese), *Solid State Phys.*, **27**[3] 186–196 (1992).

[12] F. M. Durville, E. G. Behrens, and R. C. Powell, "Laser-induced refractive-index gratings in Eu-doped glasses," *Phys. Rev. B* **34**[6] 4213–4220 (1986).

[13] E. G. Behrens and R. C. Powell,"Characteristics of laser-induced gratings in $Pr^{3+}$- and $Eu^{3+}$-doped silicate glasses," *J. Opt. Soc. Am. B* **7**[8] 1437–1444 (1990).

[14] V. F. French, R. C. Powell, D. H. Blackburn, and D. C. Cranmer, "Refractive index gratings in rare-earth-doped alkaline earth glasses," *J. Appl. Phys.*, **69**[2] 913–917 (1991).

[15] M. M. Broer, A. J. Bruce, and W. H. Grodkiewicz, "Photoinduced refractive-index changes in several $Eu^{3+}$, $Pr^{3+}$, and $Er^{3+}$-doped oxide glasses," *Phys. Rev. B* **45**[13] 7077–7083 (1992).

[16] R. M. Macfarlane and R. M. Shelby, "Measurement of optical dephasing of $Eu^{3+}$ and $Pr^{3+}$ doped silicate glasses by spectral holeburning," *Opt. Commun.*, **45**[1] 46–51 (1983).

[17] K. Hirao, S. Todoroki, K. Tanaka, N. Soga, T. Izumitani, A. Kurita, and T. Kushida, "High temperature persistent spectral hole burning of $Sm^{2+}$ in fluorohafnate glasses," *J. Non-Cryst. Solids*, **152**[2–3] 267–269 (1993).

[18] W. D. Kingery, H. K. Bowen, and D. R. Uhlmann, *Introduction to ceramics*, p. 96. Wiley, New York, 1976.

[19] B. M. J. Smets and D. M. Krol, "Group III Ions in sodium silicate glass. Part 1. X-Ray photoelectron spectroscopy study," *Phys. Chem. Glasses*, **25**[5] 113–118 (1984).

[20] D. M. Krol and B. M. J. Smets, "Group III Ions in sodium silicate glass. Part 2. Raman study," *Phys. Chem. Glasses*, **25**[5] 113–125 (1984).

[21] C. M. Baldwin and J. D. Mackenzie, "Fundamental condition for glass formation in fluoride systems," *J. Am. Ceram. Soc.*, **62**[9–10] 537-538 (1979).

[22] M. J. Weber, "Recent optical studies of the local environment of rare earth ions in glass"; in *Proc. 4th Int. Conf. on Ultrastructure Processing of Ceramics, Glasses, and Composites*. Edited by R. D. Uhlmann, S. H. Risbud, M. C. Weinberg, and D. R. Ulrich, Wiley, New York, 1990. in press.

[23] M. J. Weber, "Laser spectroscopy of glasses," *Ceramic Bulletin*, **64**[11] 1439–1443 (1985).

[24] P. K. Gallagher, C. R. Kurkjian, and P. M. Bridenbaugh,"Absorption and fluorescence

of trivalent europium in borate glasses," *Phys. Chem. Glasses*, **6**[3] 95–103 (1965).

[25] C. R. Kurkjian, P. K. Gallagher, W. R. Sinclar and P. M. Bridenbaugh, "The absorption and fluorescence spectra of trivalent europium in silicate glasses," *Phys. Chem. Glasses*, **4**[6] 239–246 (1963).

[26] S. J. Gurman, R. J. Newport, M. Oversluizen, and E. J. Tarbox, "An extended X-ray absorption fine structure study of the rare earth sites in a neodymium doped glass" *Phys. Chem. Glasses*, **33**[1] 30–32 (1992).

[27] M. A. Marcus and A. Polman, "Local structure around Er in silica and sodium silicate glasses," *J. Non-Cryst. Solids*, **136** 260–215 (1991).

[28] E. M. Larson, F. W. Lytle, P. G. Eller, R. B. Greegor, and M. P. Eastman, "XAS study of lanthanide specification in borosilicate glass," *J. Non-Cryst. Solids*, **116** 57–62 (1990).

## Chapter 1
## Local vibrational state around $Eu^{3+}$ ions in several oxide glasses

[29] P. McMillan, "Structural studies of silicate glasses and melts—applications and limitations of Raman spectroscopy," *Am. Mineral.*, **69** 622–644 (1984).

[30] D. W. Matson, S. K. Sharma, and J. A. Philpotts, "The structure of high-silica alkali silicate glasses. A Raman spectroscopic investigation," *J. Non-Cryst. Solids*, **58** 323–352 (1983).

[31] J. R. Sweet and W. B. White, "Study of sodium silicate glass and liquids by infrared reflectance spectroscopy," *Phys. Chem. Glasses*, **10**[6] 246–251 (1969).

[32] J. R. Ferraro and M. H. Manghnani, "Infrared absorption spectra of sodium silicate glasses at high pressures," *J. Appl. Phys.*, **43**[11] 4595–4599 (1972).

[33] H. Verweij and J. H. J. M. Buster, "The structure of lithium, sodium and potassium germanate glasses, studied by Raman scattering," *J. Non-Cryst. Solids*, **34** 81–99 (1979).

[34] M. K. Murthy and E. M. Kirby, "Infra-red spectra of alkali-germanate glasses," *Phys. Chem. Glasses*, **5**[5] 144–146 (1964).

[35] C. Nelson, D. R. Tallant, and J. A. Shelnutt, "Raman spectroscopic study of scandium in sodium silicate glasses," *J. Non-Cryst. Solids*, **68** 87–97 (1984).

[36] A. J. G. Ellison and P. C. Hess, "Lanthanides in silicate glasses: a vibrational spectroscopic study," *J. Geophys. Res. B* **95**[10] 15717–15726 (1990).

[37] A. J. G. Ellison and P. C. Hess, "Vibrational spectra of high-silica glasses system $K_2O$–$SiO_2$–$La_2O_3$," *J. Non-Cryst. Solids*, **127** 247–258 (1991).

[38] D. A. McKeown, F. L. Galeener, and G. E. Brown Jr, "Raman studies of Al coordination in silica-rich sodium aluminosilicate glasses and some related minerals," *J. Non-Cryst. Solids*, **68** 361–378 (1984).

[39] P. Tarte, "Infra-red spectra of inorganic aluminates and characteristic vibrational frequencies of $AlO_4$ tetrahedra and $AlO_6$ octahedra," *Spectrochim. Acta*, **23A** 2127–2143 (1967).

[40] F. M. Durville, E. G. Behrens, and R. C. Powell, "Relationship between laser-induced gratings and vibrational properties of Eu-doped glasses," *Phys. Rev. B* **35**[8] 4109–4112 (1987).

[41] V. K. Zakharov, I. V. Kovaleva, V. P. Kolobkov, and L. F. Nikolaev, "Vibronic spectra of $Eu^{3+}$ ions in inorganic glasses," *Opt. Spectrosc. (USSR)*, **42**[5] 532–536 (1977).

[42] H. Toratani, T. Izumitani, and H. Kuroda, "Compositional dependence of nonradiative decay rate in Nd laser glasses," *J. Non-Cryst. Solids*, **52** 303–313 (1982).

[43] D. W. Hall, S. A. Brawer, and M. J. Weber, "Vibronic spectra of $Gd^{3+}$ in metaphosphate glasses: comparison with Raman and infrared spectra," *Phys. Rev. B* **25**[4] 2828–2837 (1982).

[44] V. P. Kolobkov, S. P. Lun'kin, I. N. Morozova, A. N. Chikovskii, P. G. Beltadze, and G. G. Mshvelidze, "Vibronic spectra of rare-earth activated silicophosphate and germanophosphate glasses," *J. Appl. Spectrosc.*, **49** 706–709 (1988).

[45] S. Tanabe, S. Todoroki, K. Hirao, and N. Soga, "Phonon sideband of $Eu^{3+}$ in sodium borate glasses," *J. Non-Cryst. Solids*, **122** 59–65 (1990).

[46] T. Miyakawa and D. L. Dexter, "Phonon

sidebands, multiphonon relaxation of excited states, and phonon-assisted energy transfer between ions in solids," *Phys. Rev. B* **1**[7] 2961–2969 (1970).

[47] S. Hüfner, *Optical Spectra of Transparent Rare Earth Compounds*, Academic press, New York, 1978, p. 36.

[48] S. Todoroki, unpublished result.

[49] M. Stavola, L. Isganitis, and M. G. Sceats, "Cooperative vibronic spectra involving rare earth ions and water molecules in hydrated salts and dilute aqueous solutions," *J. Chem. Phys.*, **74**[8] 4428–4241 (1981).

[50] M. Tanaka and T. Kushida, "*J*-Mixing effect on vibronic spectra of $Eu^{3+}$ ions," *J. Alloys Comps.*, in print; *or* in *RARE EARTH, Materials of the 21st century, Extended Abstracts for RARE EARTHS '92 in Kyoto.* p.536. Edited by G. Adachi and H. Nagai.

[51] S. Todoroki, S. Tanabe, K. Hirao, and N. Soga, "Phonon sideband spectra and local structure around $Eu^{3+}$ ions in sodium silicate glasses," *J. Non-Cryst. Solids*, **136** 213–218 (1991).

[52] R. Dupree, D. Holland, P. W. McMillan, and R. F. Pettifer, "The structure of soda-silica glasses: a MAS NMR study," *J. Non-Cryst. Solids*, **68** 399–410 (1984).

[53] H. Maekawa, T. Maekawa, K. Kawamura, and T. Yokokawa, "The structural groups of alkali silicate glasses determined from $^{29}Si$ MAS-NMR," *J. Non-Cryst. Solids*, **127** 53–64 (1991).

[54] K. Arai, H. Namikawa, K. Kumata, T. Honda, Y. Ishii, and T. Handa, "Aluminum or phosphorus co-doping effects on the fluorescence and structural properties of neodymium-doped silica glass," *J. Appl. Phys.*, **59**[10] 3430–3436 (1986).

## Chapter 2
## Mössbauer spectroscopy of $^{151}$Eu in several oxide glasses

[55] C. R. Kurkjian, "Mössbauer spectroscopy in inorganic glasses," *J. Non-Cryst. Solids*, **3** 157–194 (1970).

[56] M. D. Dyar, "A review of Mössbauer data on inorganic glasses: the effects of composition on iron valency and coordination," *Am. Mineral.*, **70** 304–316 (1985).

[57] S. S. Sekhon and R. Kamal, "The applications of Mössbauer spectroscopy to the study of inorganic oxide glasses," *Phys. Chem. Glasses*, **29** 157–167 (1988).

[58] G. Tomandl, "Mössbauer effect in glasses"; pp. 273–312. in *Glass science and technology*, vol. 4B, Edited by R. D. Uhlmann and N. J. Kreidl Academic press, San Diego, 1990.

[59] M. F. Taragin and J. C. Eisenstein, "Mössbauer-effect study of europium in glass," *Phys. Rev. B* **2**[9] 3490–3494 (1970).

[60] M. F. Taragin and J. C. Eisenstein, "Mössbauer-effect study of europium in $Eu_2O_3$ and in a silicate glass," *J. Non-Cryst. Solids*, **11** 395–396 (1973).

[61] J. M. D. Coey, A. McEvoy, and M. W. Shafer, "Mössbauer study of europium in fluorozirconate glass," *J. Non-Cryst. Solids*, **43** 387–392 (1981).

[62] M. Winterer, E. Mörsen, B. D. Mosel, and W. Müller-Warmuth, "Paramagnetic hyperfine structure in $^{151}$Eu Mössbauer spectra of $Eu^{2+}$ ions in borate glasses," *J. Phys. C: Solid State Phys.*, **20** 5389–5399 (1987).

[63] S. Tanabe, K. Hirao, and N. Soga, "Mössbauer spectroscopy of $Eu^{3+}$ in oxide crystals and glasses," *J. Non-Cryst. Solids*, **113** 178–184 (1989).

[64] S. Musić, Z. Bajs, K. Furić, and V. Mohaček, "Mössbauer and vibrational spectra of sodium borosilicate glasses containing europium or tin ions," *J. Mater. Sci. Lett.*, **10** 889–892 (1991).

[65] C. M. P. Barton and N. N. Greenwood, "Europium-151 Mössbauer spectroscopy"; pp. 395–446 in *Mössbauer Effect Data Index*, Edited by J. D. Stevens and V. E. Stevens, Plenum, New York, 1973.

[66] G. M. Kalvius, G. K. Shenoy, G. J. Ehnholm, T. E. Katila, O. V. Lounasmaa, and P. Reivari, "Quadrupole moment of the 21.6-keV state of $^{151}$Eu," *Phys. Rev.*, **187**[4] 1503–1505 (1969).

[67] J. A. Duffy and M. D. Ingram, "Optical basicity—IV: Influence of electronegativity on the Lewis basicity and solvent properties of molten oxyanion salts and glasses," *J. inorg. nucl. Chem*, **37** 1203–1206 (1975).

[68] J. A. Duffy and M. D. Ingram, "An interpretation of glass chemistry in terms of the optical basicity concept," *J. Non-Cryst. Solids*, **21** 373–410 (1976).

[69] J. A. Duffy, "A common optical basicity

scale for oxide and fluoride glasses," *J. Non-Cryst. Solids*, **109** 35–39 (1989).

[70] J. A. Duffy and M. D. Ingram, "Comments on the application of optical basicity to glass," *J. Non-Cryst. Solids*, **144** 76–80 (1992).

[71] P. J. Bray and J. G. O'Keefe, "Nuclear magnetic investigations of the structure of alkali borate glasses," *Phys. Chem. Glasses*, **4**[2] 37–46 (1963).

[72] K. Kamiya, T. Yoko, Y. Itoh, and S. Sakka, "X-Ray diffraction study of $Na_2O$–$GeO_2$ melts," *J. Non-Cryst. Solids*, **79** 285–294 (1986).

## Chapter 3
## Origin of inhomogeneous linewidth of $Eu^{3+}$ fluorescence I.
— Silicate, germanate, aluminosilicate, and borate system

[73] N. Soga, K. Hirao, M. Yoshimoto, and H. Yamamoto, "Effects of densification on fluorescence spectra and glass structure of $Eu^{3+}$-doped borate glasses," *J. Appl. Phys.*, **63**[9] 4451–4454 (1988).

[74] J. R. Morgan, E. P. Chock, W. D. Hopewell, M. A. El-sayed, and R. Orbach, "Origins of homogeneous and inhomogeneous line width of the $^5D_0$–$^7F_0$ transition of $Eu^{3+}$ in amorphous solids," *J. Phys. Chem.*, **85**[7] 747–751 (1981).

[75] G. Nishimura and T. Kushida, "Luminescence studies in $Ca(PO_3)_2$:$Eu^{3+}$ glass by laser-induced fluorescence line-narrowing technique. I. Optical transition mechanism of the $^5D_0$–$^7F_0$ line," *J. Phys. Soc. Jpn.*, **60**[2] 683–694 (1991).

[76] J. Dexpert-Ghys, B. Piriou, N. Jacquet-Francillion, and C. Somberet, "Europium site selective spectroscopy of aluminoborosilicate glasses: structural approach and influence of phosphorus on the environment of the lanthanide," *J. Non-Cryst. Solids*, **125** 117–128 (1990).

[77] T. F. Belliveau and D. J. Simkin, "On the coordination environment of rare earth ions in oxide glasses, calcium titanosilicate and sodium aluminosilicate glasses," *J. Non-Cryst. Solids*, **110** 127–141 (1989).

[78] X. Gang and R. C. Powell, "Site-selection spectroscopy and energy transfer studies of $Eu^{3+}$ ions in glass hosts," *J. Appl. Phys.*, **57**[4] 1299–1304 (1985).

[79] G. Boulon, M. Bouderbala, and J. Sériot, "Site selection using laser-induced fluorescence spectroscopy of the $Eu^{3+}$ probe ions in oxide glass hosts: a review and some new results," *J. Less-Common Met.*, **112** 41–66 (1985).

[80] J. Hegarty, W. M. Yen, M. J. Weber, and D. H. Blackburn, "Laser-induced fluorescence line narrowing of $Eu^{3+}$ in lithium borate glass," *J. Luminescence*, **18/19** 657–660 (1979).

[81] P. Avouris, A. Campion, and M. A. El-sayed, "Variations in homogeneous fluorescence linewidth and electron-phonon coupling within an inhomogeneous spectral profile," *J. Chem. Phys.*, **67**[7] 3397–3398 (1977).

[82] N. Motegi and S. Shionoya, "Excitation migration among inhomogeneously broadened levels of $Eu^{3+}$ ions," *J. Luminescence*, **8** 1–17 (1973).

## Chapter 4
## Origin of inhomogeneous linewidth of $Eu^{3+}$ fluorescence II.
— Phosphate and borophosphate system

[83] S. W. Martin, "Review of the structures of phosphate glasses," *Eur. J. Solid State Inorg. Chem.*, **28** 163–205 (1991).

[84] R. K. Brow, R. J. Kirkpatrick, and G. L. Turner, "The short range structure of sodium phosphate glasses I. MAS NMR studies," *J. Non-Cryst. Solids*, **116** 39–45 (1990).

[85] M. Tatsumisago, T. Kowada, and T. Minami, "Structure of rapidly quenched lithium phosphate glasses," *Phys. Chem. Glasses*, **29**[2] 63–66 (1988).

[86] Y. H. Yun and P. J. Bray, "Nuclear magnetic resonance studies of the glasses in the system $K_2O$–$B_2O_3$–$P_2O_5$," *J. Non-Cryst. Solids*, **30** 45–60 (1978).

[87] M. Scagliotti, M. Villa, and G. Chiodelli, "Short range order in the network of the borophosphate glasses: Raman results," *J. Non-Cryst. Solids*, **93** 350–360 (1987).

[88] M. Villa, M. Scagliotti, and G. Chiodelli, "Short range order in the network of the borophosphate glasses: A $^{31}P$ NMR-MAS

(Magic Angle Spinning) study," *J. Non-Cryst. Solids*, **94** 101–121 (1987).

[89] A. Osaka, M. Ikeda, and K. Takahashi, "Network structure of borophosphate glasses (Part 2) Raman spectra of potassium borophosphate glasses," *Nippon Seramikkusu Kyokai Gakujutsu Ronbunshi*, **96**[5] 521–524 (1988).

[90] A. Rulmont, R. Cahay, M. Liegeois-duyckaerts, and P. Tarte, "Vibrational spectroscopy of phosphates: some general correlations between structure and spectra," *Eur. J. Solid State Inorg. Chem.*, **28** 207–219 (1991).

[91] E. I. Kamitsos, M. A. Karakassides, and G. D. Chryssikos, "Vibrational spectra of magnesium-sodium-borate glasses. 2. Raman and mid-infrared investigation of the network structure," *J. Phys. Chem.*, **91** 1073–1079 (1987).

## Chapter 5
## Local vibrational state of $Er^{3+}$ ions in up-conversion fluoride glasses

[92] D. C. Yeh, W. A. Sibley, M. Suscavage, and M. G. Drexhage, "Multiphonon relaxation and infrared-to-visible conversion of $Er^{3+}$ and $Yb^{3+}$ ions in barium-thorium fluoride glass," *J. Appl. Phys.*, **62**[1] 266–275 (1987).

[93] S. Tanabe, S. Yoshii, K. Hirao, and N. Soga, "Upconversion properties, multiphonon relaxation, and local environment of rare-earth ions in fluorophosphate glasses," *Phys. Rev. B* **45**[9] 4620–4625 (1992).

[94] S. Tanabe, K. Hirao, and N. Soga, "Upconversion fluorescences of $TeO_2$- and $Ga_2O_3$-based oxide glasses containing $Er^{3+}$," *J. Non-Cryst. Solids*, **122** 79–82 (1990).

[95] J. Y. Allain, M. Monerie, and H. Poignant, "Narrow linewidth tunable CW and Q-switched 0.98$\mu$m operation of erbium-doped fluorozirconate fibre laser," *Electron Lett.*, **25** 1082–1083 (1989).

[96] J. Y. Allain, M. Monerie, and H. Poignant, "Room temperature CW tunable green upconversion holmium fibre laser," *Electron Lett.*, **26**[4] 261–262 (1990).

[97] R. G. Smart, J. N. Carter, A. C. Tropper, D. C. Hanna, S. T. Davey, S. F. Carter, and D. Szebesta, "CW room temperature operation of praseodymium-doped fluorozirconate glass fibre lasers in the blue-green, green and red spectral regions," *Opt. Commun.*, **86**[3–4] 337–40 (1991).

[98] K. Hirao, S. Todoroki, and N. Soga, "CW room temperature upconversion lasing in $Er^{3+}$-doped fluoride glass fiber," *J. Non-Cryst. Solids*, **143** 40–45 (1992).

[99] F. K. Fong, S. L. Naberhuis, and M. M. Miller, "Theory of radiationless relaxation of rare-earth ions in crystals," *J. Chem. Phys.*, **56**[8] 4020–4027 (1972).

[100] Hirao and N. Soga, "Heat capacity and chemical bond strength of oxide glasses," *Nippon Seramikkusu Kyoukai Gakujutsu Ronbunshi*, **97**[3] 359–364 (1989).

[101] K. Kawamura, *Pasokon bunshi simulation — Bunshi dōrikigaku jikken nyuumon* (in Japanese), (Kaibundo, Tokyo, 1990).

[102] R. Coupé, D. Louër, J. Lucas, and A. J. Leonard, "X-ray scattering studies of glasses in the system $ZrF_4$–$BaF_2$," *J. Am. Ceram. Soc.*, **66**[7] 523–529 (1983).

[103] A. Lecoq and M. Poulain, "Lanthanum fluorozirconate glasses," *J. Non-Cryst. Solids*, **34** 101–110 (1979).

[104] Q. Xu, K. Kawamura, and T. Yokokawa, "Molecular dynamic calculations for boron oxide and sodium borate glasses," *J. Non-Cryst. Solids*, **104** 261–272 (1988).

[105] Q. Xu, K. Kawamura, and T. Yokokawa, "Molecular dynamics investigation of $Na_2O$–$B_2O_3$ glasses — A comparison with X-ray diffraction studies —," *Nippon Seramikkusu Kyoukai Gakujutsu Ronbunshi*, **97**[11] 1416–1419 (1989).

[106] H. Ogawa, Y. Shiraishi, K. Kawamura, and T. Yokokawa, "Molecular dynamics study on the shear viscosity of molten $Na_2O{\cdot}2SiO_2$," *J. Non-Cryst. Solids*, **119** 151–158 (1990).

[107] K. Kawamura,"A molecular dynamic simulation of $Na_2O{\cdot}SiO_2$ – $K_2O{\cdot}SiO_2$ melts — effect of basic cell size," *Molecular Simulation*, **6** 245–255 (1991).

[108] O. Greis and J. M. Haschke, "Rare earth fluoride"; pp. 387–460 in *Handbook on the physics and chemistry of rare earths vol. 5*, Edited by K. A. Gschneidner, Jr. and L. Eyring, North-Holland Publishing Company, Amsterdam, 1882.

[109] P. R. Papiernik, D. Mercurio et B. Frit, "Structure du Tétrafluorure de Zirconium,

$ZrF_4$ $\alpha$" (in French), *Acta Cryst.* B**38** 2347–2353 (1982).

[110] B. Mehlhorn und R. Hoppe, "Neue hexafluorozirkonate(IV): $BaZrF_6$, $PbZrF_6$, $EuZrF_6$, $SrZrF_6$" (in German), *Z. anorg. allg. Chem.*, **425** 180–188 (1976).

[111] R. W. G. Wyckoff, *Crystal structures*, p. 241. Interscience Publishers, New York, 1963.

[112] A. Zalkin and D. H. Templeton, "Refinement of the crystal structure of lanthanum trifluoride with neutron diffraction data," *Acta Cryst.* B**41** 91–93 (1985).

[113] O. Greis und T. Petzel, "Ein beitrag zur strukturchemie der selten-erd-trifluoride," *Z. anorg. allg. Chem.*, **403** 1–21 (1974).

[114] A. K. Cheetham and N. Norman, "The structures of yttrium and bismuth trifluorides by neutron diffraction," *Acta Chem. Scand.*, A**28** 55–60 (1974).

[115] T. Hashi and Y. Takahashi, "Anomalous behaviours of Raman heterodyne signals in $Pr^{3+}$:$LaF_3$" (in Japanese), *Solid State Phys.*, **27**[1] 71–82 (1992).

## Chapter 6
## Spectral hole burning in $Sm^{2+}$-doped fluoride glasses

[116] W. E. Moerner, *Persistent spectral hole-burning: science and applications*, pp. 1–15 Springer-Verlag, Berlin, 1988.

[117] K. Sawada, K. Kominami, and M. Iwamoto, "High temperature photochemical hole burning of tetrasodium 5,10,15,20-tetra(4-sulfonatophenyl)phorphin in polyvinylalcohol," *Japan. J. Appl. Phys.* **27**[7] L1304–1306 (1988).

[118] A. Furusawa, K. Horie, K. Kuroki, and I. Mita, "Photochemical hole burning of tetraphenylporphin in phenoxy resin at 4.2–80K," *J. Appl. Phys.* **66**[12] 6041–6047 (1989).

[119] H. Suzuki, T. Shimada, T. Nishi, and H. Hiratsuka, "Fast and efficient photon-gated burning of persistent spectral holes in donor-acceptor electron transfer systems," *Jpn. J. Appl. Phys.* **29**[7] L1146–1149 (1990).

[120] R. M. Macfarlane and R. M. Shelby, "Persistent spectral hole-burning in inorganic materials"; pp. 127–151 in *Persistent spectral hole-burning: science and applications*, Edited by W. E. Moerner, Springer-Verlag, Berlin, 1988.

[121] R. M. Macfarlane and J. -C. Vial, "Photon-gated spectral hole burning in $LiGa_5O_8$:$Co^{2+}$," *Phys. Rev. B* **34**[1] 1–4 (1986).

[122] A. Szabo and R. Kaarli, "Optical hole burning and spectral diffusion in ruby," *Phys. Rev. B* **44**[22] 12307–12313 (1991).

[123] N. E. Rigby and N. B. Manson, "Spectral hole burning in emerald," *J. Opt. Soc. Am. B* **9**[5] 775–778 (1992).

[124] A. Winnacker, R. M. Shelby, and R. M. Macfarlane, "Photon-gated hole burning: a new mechanism using two-step photoionization," *Opt. Lett.*, **10**[7] 350–352 (1985).

[125] R. J. Danby, K. Holliday, and N. B. Manson, "Transient and photon-gated persistent spectral holeburning in $CaSO_4$:Sm," *J. Luminescence*, **42** 83-88 (1992).

[126] C. Wei, S. Huang, and J. Yu, "Two-photon hole burning and fluorescence-line-narrowing studies on $BaFCl_{0.5}Br_{0.5}$:$Sm^{2+}$ at 77K," *J. Luminescence* **43** 161–166 (1989).

[127] L. Zhang, J. Yu, and S. Huang, "Fluorescence line narrowing and inhomogeneous broadening of $Sm^{2+}$ in $BaFCl_xBr_{1-x}$," *J. Luminescence* **45** 301–303 (1990).

[128] A. Oppenländer, F. Madeore, J.-C. Vial, and J.-P. Chaminade, "Spectral hole burning at 183K in a chemically disordered rare-earth compound," *J. Luminescence* **50** 1–6 (1991).

[129] C. Wei, K. Holliday, A. J. Meixner, M. Croci, and U. P. Wild, "A spectral hole burning study of $BaFCl_{0.5}Br_{0.5}$:$Sm^{2+}$," *J. Luminescence* **50** 89–100 (1991).

[130] K. Holliday, C. Wei, M. Croci, and U. P. Wild, "Spectral hole-burning measurements of optical dephasing between 2–300K in $Sm^{2+}$ doped substitutionally disordered microcrystals," *J. Luminescence* **53** 227–230 (1992).

[131] R. Jaaniso and H. Bill, "Room temperature persistent spectral hole burning in Sm-doped $SrFCl_{1/2}Br_{1/2}$ mixed crystals," *Europhys. Lett.* **16**[6] 569–574 (1991).

[132] G. Zhenan, "d-f and f-f transition bands of praseodymium and samarium ions in silica glasses," *J. Non-Cryst. Solids* **80** 429–434 (1986).

[133] R. M. Macfarlane and R. M. Shelby, "Ho-

mogeneous line broadening of optical transitions of ions and molecules in glasses," *J. Luminescence*, **36** 179–207 (1987).

[134] R. Cases, D. L. Griscom, and D. C. Tran, "Radiation effects in $ZrF_4$ based glasses. I. electron spin resonance," *J. Non-Cryst. Solids* **72** 51–63 (1985).

## Acknowledgments

The present thesis has been carried out under the direction of Professor Naohiro Soga at Faculty of Engineering in Kyoto University.

The author wishes to express his sincere gratitude to Professor Naohiro Soga for his continuous encouragement and valuable advice all through the duration of the present work. The author also indebted to Prof. Kazuyuki Hirao at Faculty of Engineering in Kyoto University and Dr. Setsuhisa Tanabe at College of Liberal Arts & Sciences in Kyoto University, for their informative discussion and helpful advice. The profitable suggestions from Prof. Teiichi Hanada, Dr. Kazuki Nakanishi, Dr. Katsuhisa Tanaka and Dr. Zuyi Zhang are also gratefully acknowledged. Hearty thanks are made to Mr. Hironori Kaji, Mr. Yasuhiko Benino and all the students of Soga's Lab. for their collaboration.

The author wishes to thank Prof. Yasuto Isozumi and Dr. Rintaro Katano, Institute for Chemical Research, for the Mössbauer effect measurements, Prof. Katsuyuki Kawamura, Hokkaido University, for offering excellent softwares for molecular dynamic simulation, and Dr. Tetsuro Izumitani, Hoya Corporation, Prof. Hiroyuki Nasu and Dr. Jun Matsuoka, Mie University, for their valuable advice. The author also thanks Mr. Hiroyoshi Minakuchi, Simadzu Corporation, for preparing reduced glass samples, and Prof. Takashi Kushida and Dr. Atusi Kurita, Osaka University, for low-temperature spectroscopic measurements.

The author express his sincere gratitude to his parents, Dr. Riichi Todoroki and Mrs. Chie Todoroki for their understanding and encouragement.

Shin-ichi Todoroki

## Papaers concerning the works at Kyoto Univ.

95/01/22 Dr. S. Todoroki

- Doctoral thesis (Studies on Local Structure around Rare Earth Ions in Glasses, [20])

  **Chapter1** [2], [3], [9], [12], [17]
  **Chapter2** [14], [15]
  **Chapter3** [11]
  **Chapter4** [8], [19]
  **Chapter5** [5], [6], [7], [10]
  **Chapter6** [13], [16]

- Molecular Dynamic simulation: [1], [4]
- Holuburning in oxide glasses: [18]

## References


[1] N. Soga, K. Hirao, and S. Todoroki. Prediction of glass forming tendency by molecular dynamics simulation. In *Proc. 15th Int. Congr. Glass*, Vol. 4, pp. 52–57, Leningrad, Jul. 1989.

[2] S. Tanabe, S. Todoroki, K. Hirao, and N. Soga. Phonon sideband of $Eu^{3+}$ in sodium borate glasses. *J. Non-Cryst. Solids*, Vol. 122, No. 1, pp. 59–65, 1990.

[3] S. Todoroki, S. Tanabe, K. Hirao, and N. Soga. Phonon sideband spectra and local structure of $Eu^{3+}$ in sodium silicate glasses. *J. Non-Cryst. Solids*, Vol. 136, No. 3, pp. 213–218, 1991.

[4] K. Hirao, S. Todoroki, and N. Soga. A study on the prediction of glass forming region by using molecular dynamics simulation. *Rep. Asahi Glass Found.*, Vol. 59, pp. 27–35, 1991. (in Japanese).

[5] K. Hirao, S. Todoroki, and N. Soga. CW room temperature operation of erbium-doped fluorozirconate glass fiber laser. *J. Non-Cryst. Solids*, Vol. 143, No. 1, pp. 40–45, 1992.

[6] S. Todoroki, K. Hirao, S. Tanabe, and N. Soga. The local structure around rare earth ions in indium and lead based fluoride glasses with high upconversion efficiency. *J. Non-Cryst. Solids*, Vol. 143, No. 1, pp. 46–51, 1992.

[7] K. Hirao, S. Todoroki, S. Tanabe, and N. Soga. Study of $Er^{3+}$-doped upconversion glass. In L. David Pye, W. C. LaCourse, and H. J. Stevens, editors, *The Physics of Non-crystalline Solids, Proc. 7th. Int. Conf. Physics of Non-Crystalline Solids*, pp. 611–616, Cambridge, Aug. 1992. Taylor & Francis, London, UK.

[8] S. Todoroki, K. Hirao, and N. Soga. Fluorescence properties of $Eu^{3+}$ ions doped in several oxide glasses. *J. Soc. Mat. Sci., Japan*, Vol. 41, No. 464, pp. 583–587, 1992. (in Japanese).

[9] S. Tanabe and S. Todoroki. Analyses of local structure of rare earth ions in glasses by phonon sideband spectra. *New Glass*, Vol. 7, No. 3, pp. 189–195, 1992. (in Japanese).

[10] K. Hirao, S. Todoroki, and N. Soga. A study of upconversion laser glasses and their molecular design simulations for fluorozirconate glass. In *Boletin de la sociedad Espan ola de ceramica y vidrio (Proceedings of the XVI International Congress on Glass)*, Vol. 3, pp. 121–126, Madrid, 1992.

[11] S. Todoroki, K. Hirao, and N.Soga. Origin of inhomogeneous linewidth of fluorescence spectra of $Eu^{3+}$ in several oxide glasses. *J. Appl. Phys.*, Vol. 72, No. 12, pp. 5853–5860, 1992.

[12] S. Todoroki, K. Hirao, and N. Soga. Phonon sideband spectra and local structure around $Eu^{3+}$ ions in sodium germanate glasses. *J. Alloys Comps.*, Vol. 193, pp. 207–209, 1993.

[13] K. Hirao, S. Todoroki, K. Tanaka, N. Soga, T. Izumitani, A. Kurita, and T. Kusida. High temperature persistent spectral hole burning of $Sm^{2+}$ in fluorohafnate glasses. *J. Non-cryst. Solids*, Vol. 152, No. 2,3, pp. 267–269, 1993.

[14] S. Todoroki, K. Hirao, and N. Soga. A study of the structure around $Eu^{3+}$ ions in oxide glasses using Mössbauer spectroscopy. *Nucl. Instr. and Meth. B*, Vol. 76, No. 1–4, pp. 76–77, 1993.

[15] S. Tanabe, T. Ohyagi, S. Todoroki, T. Hanada, and N. Soga. Relation between the $\Omega_6$ intensity parameter of $Er^{3+}$ ions and the $^{151}$Eu isomer shift in oxide glasses. *J. Appl. Phys.*, Vol. 73, No. 12, pp. 8451–8454, 1993.

[16] K. Hirao, S. Todoroki, and N. Soga. Room temperature persistent spectral hole burning of $Sm^{2+}$ in fluorohafnate glasses. *J. Lumin.*, Vol. 55, No. 4, pp. 217–219, 1993.

[17] S. Todoroki, K. Hirao, and N. Soga. Phonon sideband spectra and local structure around $Eu^{3+}$ ions in aluminosilicate glasses. *J. Ceram. Soc. Japan*, Vol. 101, No. 9, pp. 1065–1067, 1993.

[18] K. Hirao, S. Todoroki, D. H. Cho, and N. Soga. Room-temperature persistent hole burning of $Sm^{2+}$ in oxide glasses. *Opt. lett.*, Vol. 18, No. 19, pp. 1586–1587, 1993.

[19] K. Hirao, S. Todoroki, and N. Soga. Origin of inhomogeneous linewidth of $Eu^{3+}$ fluoresence in phosphate and borophosphate glasses. *J. Non-cryst. Solids*, Vol. 175, No. 2,3, pp. 263–269, 1994.

[20] S. Todoroki. *Studies on local structure around rare earth ions in glasses.* PhD thesis, Kyoto Univ., 3 1993. No. 1285.

---

Abstracts are available at http://www.geocities.com/Tokyo/1406/p_paper.html .